UNCERTAINTIES IN RESERVOIR LIMIT TEST RESULTS: EFFECT OF INPUT PARAMETERS

A THESIS SUBMITTED TO
THE GRADUATE SCHOOL OF NATURAL AND APPLIED SCIENCES
OF
MIDDLE EAST TECHNICAL UNIVERSITY

GÜL ALTINBAY

IN PARTIAL FULFILLMENT OF THE REQUIREMENTS
FOR
THE DEGREE OF MASTER OF SCIENCE
IN
PETROLEUM AND NATURAL GAS ENGINEERING

SEPTEMBER 2013

Approval of the thesis:

UNCERTAINTIES IN RESERVOIR LIMIT TEST RESULTS:
EFFECT OF INPUT PARAMETERS

submitted by **GÜL ALTINBAY** in partial fulfillment of the requirements for **the Degree Of Master Of Science In Petroleum And Natural Gas Engineering Department, Middle East Technical University** by,

Prof. Dr. Canan Özgen
Dean, Graduate School of **Natural and Applied Sciences** _____

Prof. Dr. Mahmut Parlaktuna
Head of Department, **Petroleum And Natural Gas Engineering Dept.** _____

Prof. Dr. Serhat Akın
Supervisor, **Petroleum And Natural Gas Engineering Dept. METU** _____

Examining Committee Members:

Prof. Dr. Mahmut Parlaktuna
Petroleum And Natural Gas Engineering., METU _____

Prof. Dr. Serhat Akın
Petroleum And Natural Gas Engineering Dept., METU _____

Prof. Dr. Nurkan Karahanoğlu
Geology Engineering Dept., METU _____

Msc. Demet Çelebioğlu
TPAO, ANKARA _____

Msc. Deniz Yıldırım
TPAO, ANKARA _____

DATE: 04. September 2013

I hereby declare that all information in this document has been obtained and presented in accordance with academic rules and ethical conduct. I also declare that, as required by these rules and conduct, I have fully cited and referenced all material and results that are not original to this work.

Name, Last name: GÜL ALTINBAY

Signature :

ABSTRACT

UNCERTAINTIES IN RESERVOIR LIMIT TEST RESULTS: EFFECT OF INPUT PARAMETERS

Altınbay Gül
M.S., Department of Petroleum and Natural Gas Engineering
Supervisor : Prof. Dr. Serhat Akın

September 2013, 128 pages

Reservoir parameters from the well test data are essential for reservoir management. Especially the identification the presence of the reservoir boundaries is important for an appraisal well testing. Providing reserve estimation, identifying new well locations and well placement and avoiding dry holes are some important outcomes. However more work on precision of the input data is needed before using the calculated well test parameters. Lots of ambiguity in the results obtained from well tests should be considered because these input data is inevitably subject to estimation errors. When used in well test interpretation, each of them also brings its own source of errors.

In this thesis, uncertainties caused by input parameters (rock properties and fluid properties) and measured data (flow rate and pressure) is discussed rigorously. By using the determined input parameters an experimental design is constructed. To reduce the errors and increase the confidence intervals, some remedies are used such as analyses procedure (use of deconvolution), design of well tests (longer build up times and more than one build up period after sufficient flow period). After running the cases of the experimental design, the results are used to develop a linear predictive model to conduct sensitivity analysis. A real field example is presented to illustrate such errors and the applied remedies to field application.

Keywords: reservoir limit test, uncertainties, input parameters.

ÖZ

REZERVUAR SINIR TEST SONUÇLARINDAKİ BELİRSİZLİKLER: GİRDİ PARAMETRELERİNİN ETKİSİ

Altınbay Gül
Yüksek Lisans, Petrol ve Doğal Gaz Mühendisliği Bölümü
Tez Yöneticisi: Prof Dr. Serhat Akın

Eylül 2013, 128 sayfa

Kuyu test verilerinden elde edilen rezervuar parametreleri rezervuar yönetimi için gereklidir. Kuyu test değerlendirmesi, özellikle rezervuar sınırlarının varlığının belirlenmesi için çok önemlidir. Yeni kuyu yerleri verebilme, kuyu yerleşimini belirleme ve kuru kuyulardan kaçınarak, rezerv tahminini doğru bir şekilde hesaplanması sağlanır. Test parametrelerini hesaplamada kullanmadan önce, girdi verilerinin büyük bir hassasiyetle belirlenmesi gereklidir. Girdi verilerinin hataları kaçınılmaz bir konu olduğu için, bu hataların sınır testlerinden elde edilen sonuçların belirsizliğine katkı sağladığı göz ardı edilmemelidir. Kuyu testleri yorumlanırken, girdi parametrelerinin her birinin kendi hata kaynağını getirdiği bilinmelidir.

Bu tezde, rezervuar kayaç ve akışkan özellikleri gibi girdi parametrelerden kaynaklanan ayrıca basınç ve debi gibi kaydedilen veriden kaynaklı belirsizlikler dikkatli bir şekilde tartışılmıştır. Bu verilerle deneysel dizayn tasarlanmıştır. Hataları en aza indirmek ve güvenlik sınırlarını arttırmak için, birden fazla kapamalar, yeterli akış sonrası uzun süreli kapamalar ve bunların yeterli olmadığı yerlerde deconvolüsyon yöntemi kullanılmıştır. Deneysel dizayndan elde edilen örneklerin kullanılmasıyla elde edilen sonuçlar tahmini model oluşturmakta kullanılmış ve hassasiyet analizi yapılmıştır. Böylece gerçek saha verileri ile bu verilerdeki hataların belirlenmesi ve belirlenmesinde kullanılan yöntemler anlatılmıştır.

Anahtar Kelimeler: rezervuar sınır testleri, belirsizlikler, girdi parametreleri.

ACKNOWLEDGEMENTS

I am sincerely grateful to my supervisor Prof. Dr. Serhat Akın for his valuable suggestions, guidance and support. He has always been accessible and willing to help throughout my work.

I would like to thank related TPAO authorities for allowing me to use the data of B.E Field which enabled me to complete this study. I also offer my regards to TPAO Production Department Management for their understanding and consideration during my thesis-writing period.

My special thanks also go to Murat Fatih Tuğan for encouraging me at the very beginning of this study. Murat Fatih Tuğan generously shared with me his ideas and adviced me to advance in this research. He provided their guidance, countless suggestions, and editing that enabled me to complete this study.

Moreover, I wish to thank Murat Demir, Sertuğ Evin, Volkan Üstün, Demet Çelebioğlu and Deniz Yıldırım; the time we spent together has always been a great business experience for me through the years at TPAO.

I am heartily thankful to Mustafa Erkin Gözel, Ceyda Çetinkaya and Melike Özkaya Türkmen for his kind company on working till late hours at the office.

I owe many thanks to my dear friends Armağan and Hakan Kuru for their motivation, which was invaluable to me. This tough period became smooth and rewarding for me.

On a personal note, I am heartily thankful to my husband Hasan, my little sisters Çiğdem and Arife, and my parents for their patience, understanding and caring support which has been my source of strength and inspiration.

TABLE OF CONTENTS

LIST OF TABLES

TABLES

LIST OF FIGURES

FIGURES

NOMENCLATURE

Abbreviations

cp	: Centipoise
CPU	: Central Processing Unit Time
DOE	: Design of Experiment
IARF	: Infinite Acting Radial Flow
MDH	: Miller-Dynes-Hutchinson
mD	: milliDarcy
ppm	: parts per million
PVT	: Pressure Volume Temperature
RMSE	: Root Mean Square Error
sup	: Superposition
TVD	: True Vertical Depth
XPT	: Pressure Express

Greek Symbols

a	: Coefficient of variables in metamodel
Δ	: Difference
ε	: Error term of metamodel
Ø	: Porosity, %
ρ	: Specific gravity
μ	: Viscosity, cp

Latin Symbols

A	: Area, ft^3
B	: Formation Volume Factor, rb/stb or rcf/scf
c	: Compressibility, 1/psi
C	: Wellbore Storage Coefficient
D	: Depth, m
d	: Distance to boundary, ft
e	: Base of natural logarithm
E	. East Boundary, ft

F : Formation factor
g : Metamodel function
h : Thickness, m
k : Permeability, mD
k : Number of space filling design variable
ln : Natural logarithm
I : Resistivity index
L : Distance of core plug, ft
L : Distance to boundary, ft
L : Disrepancy
m' : Slope of pressure derivative curve
n : Number of simulation case
n : Saturation exponent
N : North boundary, ft
P : Pressure, psi
q : Rate, m^3/day
r : Wellbore radius, inch
r_i : Radius of ivestigation, ft
R : Universal gas constant, 8.314 J/mol K
R^2 : Correlation coefficient
R : Resistivity, ohm
Rt : True formation resistivity, ohm
s : Skin
S : Salinity, ppm
S : Saturation, %
S : South boundary, ft
T : Temperature, ˚C
t : Time, min or hr
x : Input variable of metamodel
V : Volume, ft^3
W : West Boundary, ft
y : Output variable of metamodel

Subscription

den : Density log
f : Formation
g : Gas phase
i : Initial
o : Oil phase
p : Production

sf	: Sand face
s	: Sonic log
sh	: Shale
t	: Total
w	: Water phase
w	: Wellbore
wa	: Equivalent wellbore radius
wf	: Well flow

CHAPTER 1

INTRODUCTION

Well test is the first operation conducted to get detailed information about the reservoir after drilling a well. Information obtained from a well test is used in managing the reservoir. Therefore, a clear understanding and analyzing the well test data is crucial. Thus can allow reducing uncertainty in reserve estimate, improving recovery efficiencies through improved completion practices and well placement, reducing completion costs and identifying new locations avoiding dry holes (El-Hawary, Mahgoub, & Sayyouh, 1999; Houze, Viturat, & Fjaere, 2011). For example, skin obtained from well test is used for completion design. Suitable completion design reduces the cost and increase the productivity. Detecting boundaries is the main benefit of reservoir limit tests. By defining the distances to the boundaries, reservoir manager can avoid the dry holes and make better well placement. Furthermore, the obtained boundary distances can be used to calculate the closure of the reservoir, hence calculating the reservoir volume. Investment that is made to develop the field is related to magnitude of the reserve.

Well tests are the primary tools that reveal the model and the flow parameters of an oil/gas reservoir. The shape of the pressure and pressure derivative curves obtained from recorded data during well test is used to identify model of reservoir with integrated geological, geophysical and petrophysical information. By magnifying the pressure changes, derivative curve can also provide easy recognition of pattern for flow periods. The correct definition of reservoir model improve the overall accuracy, so the relevant reservoir parameters. Those parameters belong to a specific reservoir model are the calculated values from the input parameters which are fluid parameters, rock properties and measurements of pressure and rate. It is inevitable that these input data are subject to uncertainties. Thus calculated parameters are also subject to uncertainty. Therefore more work is needed before using the results of the well test analysis to identify the reservoir model and parameters (El-Hawary et al., 1999).

To analyze the reservoir model, interpretation engineers input some known parameters such as well radius, net pay thickness, porosity, water saturation, compressibility of formation and reservoir fluids, formation volume factor, density, viscosity and rate measurements and pressure records vs. time. Using known parameters provides to calculate the unknown parameters such as wellbore storage coefficient, skin factor, reservoir permeability and distance to boundaries. Parameters involved in well test whether it is input or calculated in

other words “known” or “unknown” are related to each other and affect the pressure transient analysis. To better recognition of these parameters, sensitivity to the input values have to be analyzed. Since understanding the relation between them gives the more precise result of the well test analysis.

Other essential is the arbitrarily long ideal production and shut in period to estimate reservoir properties because the reservoir properties obtained by pressure transient analysis are directly proportional to the time range of well tests. Those longer duration well tests are subcategorized as reservoir limit tests and the time needed for these tests may vary between hours to months according to reservoir parameters. As short duration well tests reveal parameters belong to wellbore and near wellbore flow, longer duration tests may reveal information regarding the boundaries. However, conducting a test in long production and shut in period cannot be feasible due to operational aspects such as hole stability and cost of the operation. If the formation that operator want to test is loose, long shut in periods cause ruining the hole. Thus make drilling and workover operations difficult. In addition to this, longer test means longer operation time and so increase the cost of the rig rent and labor. However operator wants to drill with fewer problems and minimize cost while gathering as much information as possible about the tested formation. To overcome this problem, a new method named Deconvolution is introduced in 2004 by von Schroter. Deconvolution is an algorithm that empowers the well test analysis to get more information even it is a short test. By using consecutive build ups, boundaries can be identified. In this study, deconvolution method is used to detect the boundaries of the reservoir.

In this thesis, we will analyze the uncertainties in reservoir parameters obtained by reservoir limit test; the causes of the errors and remedies for them. First of all variables and error margins that affect the well test results are investigated from the published literature data. Error margins are applied to the B.E. field input parameters in gas well test analysis. By using the error intervals, an experimental design is conducted to create possible scenarios. For all scenarios, deconvolved data is matched to the model of the reservoir. Results are collected to make a linear predictive model by using least square method. Finally, sensitivity analyses are conducted to find out the most important parameters that affect the well test results.

CHAPTER-2

LITERATURE REVIEW

2.1 History of Well Test Analysis: From Straight Lines to Deconvolution

Looking back at the history of well test analysis in the oil industry, it is possible to identify different periods in Table 2.1 during which particular analysis techniques dominated and specific types of information prevailed (A. C. Gringarten, 2008).

Table 2.1 History of the Well Test Analysis

Date	Interpretation Method	Tools	Emphasis
50's	Straight lines	Laplace Transform	Homogeneous Reservoir Behavior
Late 60's Early 70's	Pressure Type Curve Analysis	Green's Functions	Near Wellbore Effects
Late 70's	Type Curves with Independent Variables	Integrated Methodology Stehfest Algorithm	Double Porosity Behavior
Early 80's	Derivatives	Computerised Analysis	Heterogeneous Reservoir Behavior and Boundaries
90's		Computer Aided Analysis Downhole Rate Measurements Integration with Interpretation Models from other Data	Multilayered Reservoir
Early 00's		Deconvolution	Enhanced Radius of Investigation Boundaries

Matthews and Russell (1967) and Earlougher (1977) described the well test analysis methods prevailing during 1950's and 1960's. Miller, Dyes, and Jr. (1950) and Horner (1951) developed techniques based on straight lines that apply to middle time semilog data or to simple boundary effects at late times. While Miller-Dynes-Hutchinson (MDH) plot is a graph of the pressure as a function of logarithm of time, Horne introduced Horner time to use semilog analysis for any flow period by taking into account the superposition effects. However, well test analysis only revealed the reservoir permeability, average reservoir pressure, drainage area and productivity index. To gain information about the near well bore

effects, Ramey Jr (1970) emphasized the early time and introduce type curve matching. It consisted a log-log plot of the pressure response vs time on a tracer paper. By sliding your data on this plot, same size in both plots can be caught. Than relative positions (the match points) give the permeability, skin and wellbore storage values.

In the late 70's and beginning of 80's, type curve matching is developed by A. Gringarten, Burgess, Viturat, Pelissier, and Aubry (1981) to identify more complex well behaviors. Thus make well test analysis more useful as a reservoir description tool.

With type curve match and specialized plots, well test analysis was a manual process until 1983. D. Bourdet, Whittle, Douglas, and Pirard (1983) introduced derivative curves which is the slope of the pressure data displayed on the log-log plot. Well test analysis became a valuable reservoir characterization tool with the Bourdet Derivative. Bourdet derivative make possible to (A. C. Gringarten, 2008):

- understand and recognize heterogeneous reservoir behaviors such as double permeability and composite
- identify partial penetration or limited entry and other near wellbore effects
- analyze horizontal wells
- handle a wide range of boundary effects

Analytical models are useful when a perfectly constant production is achieved however during well test, rates vary in time, and producing responses are very noisy so that shut in periods are focused. von Schroeter, Hollaender, and Gringarten (2004) introduced deconvolution algorithm to solve such problems. Deconvolution algorithm is used to

- remove the wellbore storage effects
- converts variable rate pressure data into a constant rate single drawdown with a duration equal to the total duration of the test
- detect boundaries by using consecutive build ups

Deconvolution algorithm extended the power of the well test analysis in understanding reservoir boundaries.

2.2 Uncertainty Evaluation

Data collection and management are very important before analyzing the pressure responses, because uncertainty in well test analysis arises from the input data. Incomplete reservoir description from reservoir limit test interpretation with the lack of available data, or less precise data increases the risks while taking decisions to develop the field. Evaluation and quantification of such uncertainties is important to reduce the risks and improve making decisions.

To quantify uncertainty, right methodology has to be applied in order to take the right decisions for field development. There are many methodologies that can overcome different sources of uncertainties. Statistical behavior of uncertainty and the status of uncertainty should be identified well to choose and apply the proper methodology.

2.2.1 Different Statistical Behaviors of Uncertainty

Zabalza-Mezghani, Manceau, Feraille, and Jourdan (2004), define three different statistical behaviors that can be used to classify the uncertainties;

Deterministic uncertainties:
That occurs when parameter has a continuous uncertainty range. In other words, parameter may alter between a minimum and a maximum value. This includes for instance uncertainty on any mean property such as porosity, permeability, fluid saturation, compressibility, correlation length for a geostatistiscal model, upscaling coefficient between arithmetic and harmonic laws, horizontal well length, etc.

Discrete uncertainties:
That occurs when parameter can take only a finite number of discrete values. This includes for instance an uncertainty on a few possible depositional scenarios, the boolean behavior of a fault which is conductive or not, or the optimal number of new production infill wells to be implemented.

Stochastic uncertainties:
That corresponds to an uncertainty which does not have a smooth behavior on production responses. For example a small incrimination of the parameter value may lead to completely different results in terms of production profiles. That corresponds to an uncertainty which can take infinity of equiprobable discrete values. For instance, infinity of equiprobable structural maps, fracture maps, geostatistical realizations, and history matched models, etc.

Input data that is used in the interpretation of the well test is the complex physical behavior of a heterogeneous media. In addition to this, each input data has own range vary between a minimum and maximum value. Therefore, statistical behavior of the well test input data corresponds to the deterministic uncertainty. Experimental design, one of the known methods to handle deterministic uncertainties, is well suited to evaluate the impact of uncertain parameters on well test results.

2.2.2 Design of Experiment

The (statistical) design of experiment (DOE) is defined as an efficient procedure for planning the experiments so that the data obtained from experiment can be analyzed to yield valid and objective conclusion (Siomina & Ahlinder, 2008).

Design of experiments techniques enable designers to determine simultaneously the individual and interactive effects of many factors that could affect the output results in any design. DOE also provides a full insight of interaction between design elements; therefore,

helping turn any standard design into a robust one. Simply put, DOE helps to pin point the sensitive parts and sensitive areas in your designs that cause problems in Yield.

To efficiently analyze the output of the simulations, the experimental design should have the following desirable characteristics(Cioppa & Lucas, 2007).

- Approximate orthogonality of the input variables
- Space-filling, that is, the collection of experimental cases should be a representative subset of the points in the hypercube of explanatory variables
- Ability to examine many variables effectively
- Flexibility in analyzing and estimating as many effects, interactions, and threshold as possible
- Ease in generating the design
- Ability to gracefully handle premature experiment termination

2.2.2.1 Space Filling Design

Space-filling designs are useful for modeling systems that are deterministic or near-deterministic. Sensitivity studies of computer experiments are one such deterministic model systems. Such experiments can be very detailed involving many input variables with complicated interrelationships. A goal of designed experiments on these systems is to find a simpler empirical model that adequately predicts the behavior of the system over limited ranges of the factors (Institute, 2008).

Physical experiments are complicated by noise due to unsystematic effect of uncontrolled factors and bias due to systematic effect of controlled factors. Therefore classical experimental design uses replication to control noise and randomization to control bias (Santner, Williams, & Notz, 2003). However in computer experiments, noise and bias do not occur, so replication and randomization are undesirable because repeating the same run yields the same result. To overcome this problem, there are two objectives (Institute, 2008):

- The first objective is to prevent replicate points by spreading the design points out to the maximum distance possible between any two points. In other words, spread the design points out as far from each other as possible consistent with staying inside the experimental boundaries.
- The second objective is to space the points uniformly over the region of interest.

The following methods are implemented for these types of designs (Institute, 2008):

The Sphere-Packing method emphasizes spread of points by maximizes the minimum distance between pairs of design points.

The Latin Hypercube method maximizes the minimum distance between design points but requires even spacing of the levels of each factor. This method is a compromise between spread of points and uniform spacing.

The Uniform method mimics the uniform probability distribution. This method minimizes the discrepancy between the design points (which have an empirical uniform distribution) and a theoretical uniform distribution.

To choose the most suitable method, a comparison has to make between Sphere Packing, Latin Hypercube and Uniform methods (SAS Institute, 2008). Figure 2.1 from the JMP Design of Experiment Guide, the design diagnostics for three eight-run space-filling designs are shown. The minimum distance from each point to its closest neighbor and the discrepancy value of the each design are listed. For a good design, while minimum distance from each point to its closest neighbor must be high, the discrepancy must be as small as possible. In sphere packing design, the minimum distances are the highest however the discrepancy is also high. In Uniform design, discrepancy took the minimum value, however the minimum distances took the smallest values. In Latin Hypercube Design, discrepancy and minimum distances has optimal values. Therefore, the best method chosen for the diagnostic of the well test design is the Space Filling Latin Hypercube Design.

Design Diagnostics - Sphere Packing

Run	ScaledX1	ScaledX2	Minimum Distance	Nearest Point
1	0.00000	1.00000	0.518	2
2	0.50000	0.86603	0.518	1
3	0.86603	0.50000	0.518	4
4	1.00000	1.00000	0.518	3
5	1.00000	0.00000	0.518	6
6	0.50000	0.13397	0.518	5
7	0.00000	0.00000	0.518	8
8	0.13397	0.50000	0.518	7

discrepancy = 0.0469

Design Diagnostics - Latin Hypercube

Run	ScaledX1	ScaledX2	Minimum Distance	Nearest Point
1	0.57143	0.71429	0.404	6
2	0.85714	0.42857	0.404	1
3	1.00000	0.85714	0.452	1
4	0.00000	0.14286	0.452	5
5	0.42857	0.28571	0.404	7
6	0.28571	1.00000	0.404	1
7	0.14286	0.57143	0.404	5
8	0.71429	0.00000	0.404	5

discrepancy = 0.0092

Design Diagnostics - Uniform

Run	ScaledX1	ScaledX2	Minimum Distance	Nearest Point
1	0.43909	0.68509	0.276	6
2	0.69031	0.93093	0.351	1
3	0.07393	0.19080	0.346	6
4	0.81410	0.56585	0.282	7
5	0.56496	0.06460	0.44	7
6	0.31491	0.43909	0.276	1
7	0.93092	0.30959	0.282	4
8	0.18696	0.81304	0.283	1

discrepancy = 0.0046

Figure 2.1 Comparison of Three Eight-Run Space-Filling Designs (Institute, 2008)

2.2.2.2 Latin Hypercube

In the original concept of Latin hypercube sampling introduced by McKay, Beckman, and Conover (1979), the pairing was done by associating a random permutation of the first n integers with each input variable. Latin hypercube sampling selects *n* different values from each of *k* variables $X_i, \ldots X_k$ in the following manner. The range of each variable is divided into *n* strata on the basis of equal probability. One value from each interval is selected at random with respect to the probability density in the interval. The *n* values thus obtained for X_1 are paired in a random manner the *n* values of X_2. These *n* pairs are combined in a random manner with the *n* values of X_3 to form *n* triplets, and so on, until *n* *k*-tuplets are formed. These *n* *k*-tuplets are the same as the *n* *k*-dimensional input vectors. This is the Latin hypercube sample. It is convenient to think of this sample as forming an ($n \times k$) matrix of input where the i^{th} row contains specific values of each of the *k* input variables to be used on the i^{th} run of the computer model (Wyss & Jorgensen, 1998).

2.2.2.3 Meta-Model Construction

A model contains k continuous input variables that we wish to explore with n computational experiments over a region. The model generates a vector of output responses denoted as **y**. Let the i^{th} input variable be denoted as x_i, with representing the n × k input design matrix and y_j representing an output response from the simulation. To understand the model, a meta-model has to be built to quantify the relationship between the input variables ($x_1, x_2, \ldots, x_k$) and the output measures ($y_1, y_2, \ldots\ldots, y_n$). A meta-model is a relatively simple function, g, compared with the original model, which is constructed given an experimental design and the corresponding responses. A good meta-model is one in which the differences between the meta-model and the simulation output are small. The simplest and most commonly used meta-models is one in which g is a linear combination of the inputs (Cioppa & Lucas, 2007),

$$g(x) = a_0 + \sum_{i=1}^{k} (a_i x_i) \tag{2.1}$$

The number of run, n must satisfy the following condition,

$$n > k + 1 \tag{2.2}$$

When estimating the coefficients in equation 1.1, the precision of the estimates can be adversely affected by collinearity among the input variables (Ryan, 2008). Therefore, a linear meta-model may not sufficiently characterize the response surface. Unfortunately, it takes many more observations to estimate meta-models with curvilinear and interaction terms. In such a case, meta-model, g includes quadratic and bilinear interaction effects and also the linear term (Cioppa & Lucas, 2007),

$$g(x) = a_0 + \sum_{i=1}^{k}(a_i x_i) + \sum_{j=1}^{k}(a_j x_j^2) + \sum_{i=1}^{k}\sum_{j>1} a_{i,j}\, x_i x_j \tag{2.3}$$

The number of run, n must satisfy the following condition,

$$n > \left[k + k + \binom{k}{2} + 1\right] \tag{2.4}$$

2.3 Uncertainty Evaluation in Well Test Analysis

2.3.1 Previous Works

Uncertainty in well test analysis is an issue which a few publications have addressed it. There is a sharp contrast with other areas of petroleum. First, Horne (1994) distinguished the thorough overview of uncertainty sources of the well test interpretation. After this work the given uncertainty sources are;

- Physical error in the pressure data (noise, drift, time shift and temperature effect).
- Errors in the flow rate measurement (measured both surface and down hole).
- Ambiguity in response (Matching several different models with apparently equal verisimilitude).
- Ill-posedness of parameter estimation for a given reservoir model.
- Uncertainty in fluid and rock properties.

Horne discussed the impact of the first four sources. However even the first four of them can be easily overcome, well test result could never be any more accurate than the input parameters such as fluid and rock properties (Azi, Gbo, & Gringarten, 2008). Unfortunately, well test results are presently reported as unique values also with accurate precision. For example, distances to boundaries are often reported with a resolution of a tenth of a foot, skin with two decimal digits, and permeabilities greater than 100 mD within 0.1 mD, i.e. with resolutions better than 0.1%, which is utterly ridiculous (Azi et al., 2008).

After Horne introduced those uncertainty sources, Spivey and Pursell (1998) conducted a detailed study and provided a thorough review of static data used in the well test interpretation of oil and gas reservoirs. They first distinguished the uncertainties in input parameters, by using the papers published by Rosepiler (1982), McCain Jr. (1991), W. D. McCain, Voneiff, Hunt, and Semmelbeck (1993), Piper, WD, and Corredor (1993) and Aly, Hunt, Pursell, and McCain (1997).

El-Hawary et al. (1999) emphasized the data management to improve well test results. According to El-Hawary, source of error and the uncertainty on solution was due to the

improper well test design and inaccurate data entry. He concluded that by understanding the concept of the variable dependency and the impact of the input data errors on well test results, the analysts cannot avoid the unnecessary expense.

Gbo (1999) recommended using the probability density functions for static data. To estimate the quantitative impact of each type of uncertainty, he used Monte Carlo simulations. In this manner, he presented their cumulative effect on well test results as a probability density function.

Khasanov, Khabibullin, and Krasnov (2004) studied the uncertainty originated from both the ill-posedness of parameter estimation for a given reservoir model and errors in input data. He described the objective function which measures the difference between model and data. The objective function provides optimal solution with a whole range of solutions instead of a single value.

Azi et al. (2008) introduced the statistical information on the combined effect of potential sources of errors on well test results by providing uncertainty ranges derived from a number of different tests in different reservoirs. He found that the permeability-thickness product kh is usually known within 15%; the permeability k, within 20%; the wellbore storage constant C, within 20%; the skin factor S, within ±0.3; and distances, within 25% range.

CHAPTER-3

THEORY

3.1 Diffusion Equation

Diffusivity equation describes how the pressure reacts in time as a function of the local pressure gradient around an elementary piece of rock. It is derived from combination of Darcy'Law, the law of conservation of mass and the slightly compressible fluid equation with assuming the following aspects (Houze et al., 2011).

- Darcy's Law applies.
- Gravity effects are ignored.
- Reservoir and fluid properties are independent of pressure.
- Single phase and slightly compressible fluid flow.
- Isotropic and homogeneous reservoir.

3.1.1 Darcy's Law

Darcy (1856) studied the pressure loss due to the flow of water in sand by conducting experiment shown in Fig. 3.1.

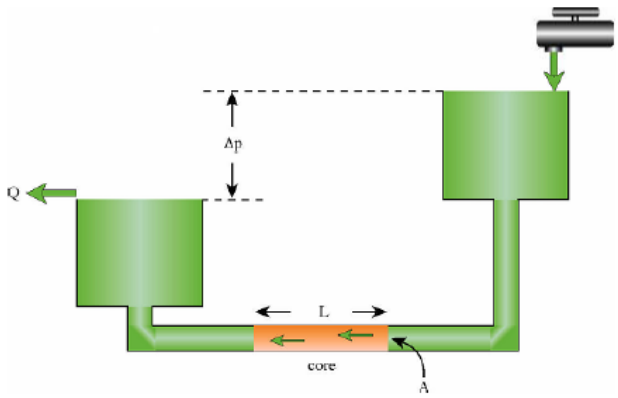

Figure 3.1 Darcy Experiment (Houze et al., 2011)

In this experiment, Darcy propose an empirical flow law by establishing a linear relationship between the pressure gradient across a horizontal section of porous medium and the flow rate

of fluid through same section. By considering all parameters constant, Darcy's law states that pressure drop for a distance ($\Delta P/L$) is;

- proportional to the flow rate density (q/A)
- proportional to the fluid viscosity (μ)
- inversely proportional to the reservoir permeability (k)

In field units, this empirical formula would be written:

$$\frac{\Delta p}{L} = -887.2\frac{q\mu}{kA} \tag{3.1}$$

The Differential form of Darcy's law can be written for linear flow in linear coordinates and for radial flow in cylindrical coordinates;

Linear flow;

$$\frac{\partial p}{\partial x} = -887.2\frac{q_x\mu}{k_xA} \tag{3.2}$$

Radial Flow;

$$r\frac{\Delta p}{\partial r} = -141.2\frac{q\mu}{kh} \tag{3.3}$$

It is the fundamental law for dynamic data analysis. It is used for determining the pressure gradient at the sandface when the well is flowing and no flow or inflow boundary according to the pressure gradient.

3.1.2 Conservation of mass;

Lavoisier (1785) stated that mass of a closed system will remain constant. The law implies that mass can neither be created nor lost.

$$Mass_{in} - Mass_{out} = Accumulation = Mass_{after} - Mass_{before} \tag{3.4}$$

Considering the flow in the x direction through an area A, between x and x+δx and between time *t* and $t + t\delta$ (1 bbl/day=0,23394 ft^3/hr).

$$[0.23394\rho q_x\delta t]_x - [0.23394\rho q_x\delta t]_{x+\delta x} = [\rho\emptyset A\delta x]_{t+\delta t} - [0.23394\rho q_x\delta t]_t \tag{3.5}$$

Differential form:

$$-0.23394\frac{\partial \rho q_x}{\partial x} = A\frac{\partial \rho \emptyset}{\partial t} \tag{3.6}$$

Darcy's Law in x direction:

$$q_x = -\frac{k_X A}{887.2\mu}\frac{\partial p}{\partial x} \tag{3.7}$$

Combining of the Darcy's law with the conservation of mass law:

$$0.23394\frac{\partial}{\partial x}\left[\frac{k_X A\rho}{887.2\mu}\frac{\partial p}{\partial x}\right] = A\frac{\partial \rho \emptyset}{\partial t} \tag{3.8}$$

$$\frac{\partial \rho \emptyset}{\partial t} = 0.0002637 k_X \frac{\partial}{\partial x}\left[\frac{\rho}{\mu}\frac{\partial p}{\partial x}\right] \tag{3.9}$$

First member of the equation can be expressed as the following to focus on slightly compressible fluids:

$$\frac{\partial(\rho\emptyset)}{\partial t} = \frac{\partial(\rho\emptyset)}{\partial p}\frac{\partial p}{\partial t} = \left[p\frac{\partial \emptyset}{\partial p} + \emptyset\frac{\partial \rho}{\partial p}\right]\frac{\partial p}{\partial t} = \rho\emptyset\left[\frac{1}{\emptyset}\frac{\partial \emptyset}{\partial p} + \frac{1}{\rho}\frac{\partial \rho}{\partial p}\right]\frac{\partial p}{\partial t} \tag{3.10}$$

New differential form:

$$0.0002637\frac{k_x}{\rho\emptyset}\frac{\partial}{\partial x}\left[\frac{\rho}{\mu}\frac{\partial p}{\partial x}\right] = \left[\frac{1}{\emptyset}\frac{\partial \emptyset}{\partial p} + \frac{1}{\rho}\frac{\partial \rho}{\partial p}\right]\frac{\partial p}{\partial t} \tag{3.11}$$

3.1.3 Compressibility

Formation compressibility:

$$c_f = \frac{1}{\emptyset}\frac{\partial \emptyset}{\partial p} \tag{3.12}$$

Fluid compressibility:

$$c_{fluid} = \frac{1}{\rho}\frac{\partial \rho}{\partial p} \tag{3.13}$$

$$c_t = c_f + c_{fluid} = \left[\frac{1}{\emptyset}\frac{\partial \emptyset}{\partial p} + \frac{1}{\rho}\frac{\partial \rho}{\partial p}\right] \tag{3.14}$$

By inserting the compressibility terms to the RHS of the differential equation:

$$\frac{\partial p}{\partial t} = 0.0002637 \frac{k_x}{\rho \emptyset [c_f + c_{fluid}]} \frac{\partial}{\partial x} \left[\frac{\rho}{\mu} \frac{\partial p}{\partial x}\right] \tag{3.15}$$

By considering:

$$\frac{\partial}{\partial x} \left[\frac{\rho}{\mu} \frac{\partial p}{\partial x}\right] \approx \frac{\rho}{\mu} \frac{\partial^2 p}{\partial x^2} \tag{3.16}$$

Final form of the diffusion equation in x direction:

$$\frac{\partial p}{\partial t} = 0.0002637 \frac{k_x}{\mu \emptyset c_t} \frac{\partial^2 p}{\partial x^2} \tag{3.17}$$

Radial solution of diffusivity equation is used for production or injection wells.

$$\frac{\partial p}{\partial t} = 0.0002637 \frac{k_x}{\mu \emptyset c_t} \frac{1}{r} \left[\frac{\partial}{\partial r} \left(r \frac{\partial p}{\partial r}\right)\right] \tag{3.18}$$

3.2 Superposition

3.2.1 Superposition in time

The diffusivity equation is used to get linear solutions of the well test analysis. To analyze the behavior of well with changing rate, several pressure responses can be added to the diffusivity equation (Van Everdingen & Hurst, 1949). It is called the superposition principle.

During well test, it is difficult to maintain a constant flow rate. Hence, pressure transient analysis deals with the buildup data rather than drawdown data. However with the principle of superposition, it is possible to convert complex production histories to a single constant rate response (Houze et al., 2011).

Figure 3.2 displays that a build up from t_p to $\Delta t + t_p$ after a single drawdown t_p is actually equal to the sum of the production with same rate during $\Delta t + t_p$ and the injection with same rate from t_p to $\Delta t + t_p$.

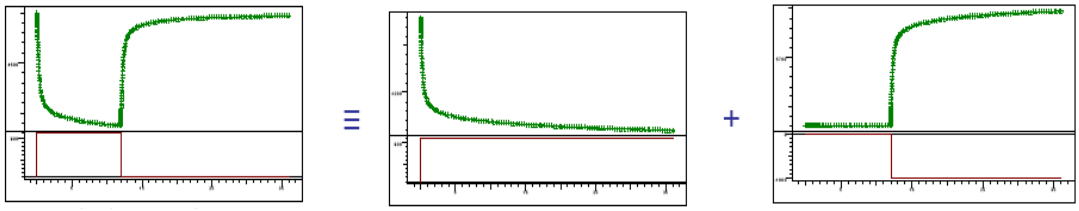

Figure 3.2 Simple Superposition (Houze et al., 2011)

3.2.2 Superposition in space (image wells);

Another way to solve and model a diffusion problem is "image wells" method. As seen in Figure 3.3, by imaging a well at distance 2L from the real well with exactly same properties, a boundary can be created at a distance L from the real well. At any point between the two well two pressure changes can be defined: (1) pressure change due to the real well response and (2) pressure change due to the image well which is symmetric to the real well with respect to defined boundary. The sum of two pressure changes of wells will honor the diffusion equation.

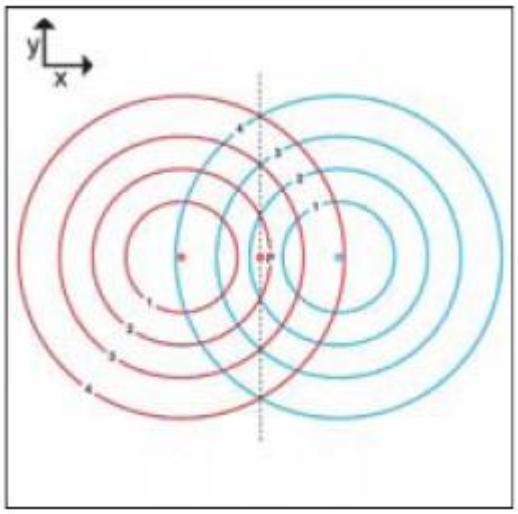

Figure 3.3 Representation of Image Wells (Houze et al., 2011)

3.3 Bourdet derivative;

Bourdet proposed an interpretation method for well test based on the pressure derivative with respect to natural logarithm of time (Bourdet, 2002). In other words, "the Bourdet Derivative is the slope of the semilog plot displayed on the log log plot" (Houze et al., 2011 pp.73). By considering very early time to last data, derivative curve describes the well and flow behavior in the reservoir (especially infinite acting radial behavior), reservoir and boundary models. "Use of the derivative of pressure vs. time is mathematically satisfying because the derivative is directly represented in one term of the diffusivity equation, which is the

governing equation for the models of transient pressure behavior used in well test analysis" (Bourdet et al., 1989 pp.293). Thus, pressure derivative exaggerate the small phenomena of reservoir behavior. Figure 3.4 and Figure 3.5 demonstrate respectively semilog plot and the log-log plot.

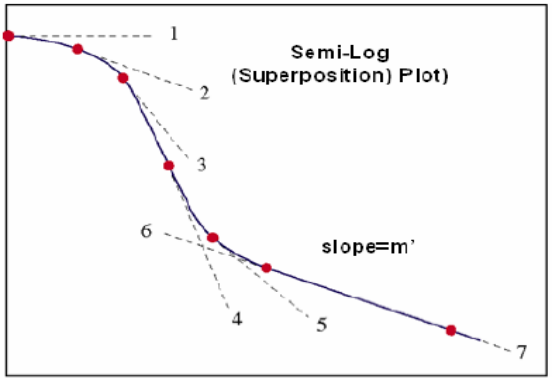

Figure 3.4 Semilog Plot (Houze et al., 2011)

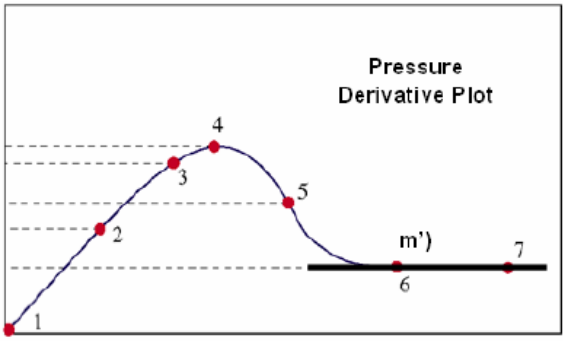

Figure 3.5 Bourdet Derivative, Log-Log Plot (Houze et al., 2011)

Bourdet derivative can be analyzed easily by dividing into three parts: (1) early time when a pressure transient gives the near wellbore effects, (2) middle time when pressure transient moved into bulk formation, (3) late time when the radius of investigation reached the boundaries.

3.4 Early Time Behavior

3.4.1 Wellbore Storage:

During a well test, well is opened and shut by valve which is not exactly placed at the sandface level. Sometimes it is located on surface. Therefore, fluid volume between the located valve and the sandface level act as cushion and pressure at sandface cannot be transmitted to the gauge. This is called wellbore storage.
Van Everdingen and Hurst (1949) represented wellbore storage by compressibility of fluid c_w in the wellbore volume V_w.

$$C = V_w c_w \tag{3.18}$$

On the plot of Δp vs Δt, from the straight line slope m, the wellbore coefficient is estimated by Van Everdingen and Hurst (1949).

$$C = \frac{qB}{24m} \tag{3.19}$$

Earlougher (1977) defined wellbore storage which is related to the rise of the fluid level in the wellbore.

$$C = 144\frac{A}{\rho} \tag{3.20}$$

The sandface and the surface rate relationship are formulated by following equation;

$$q_{sf} = qB + 24C\frac{\partial p}{\partial t} \tag{3.21}$$

Wellbore storage is an undesirable effect because it masks the early part of pressure response and delays the pressure response of reservoir. For drawdown, wellbore storage ends when sandface flow rate reaches the surface flow rate. For buildup, wellbore storage ends when reservoir stops flowing into well after shut in.

Figure 3.6 illustrates that the surface and the sandface flow rates are not equal at the time of shut in or opening to flow.

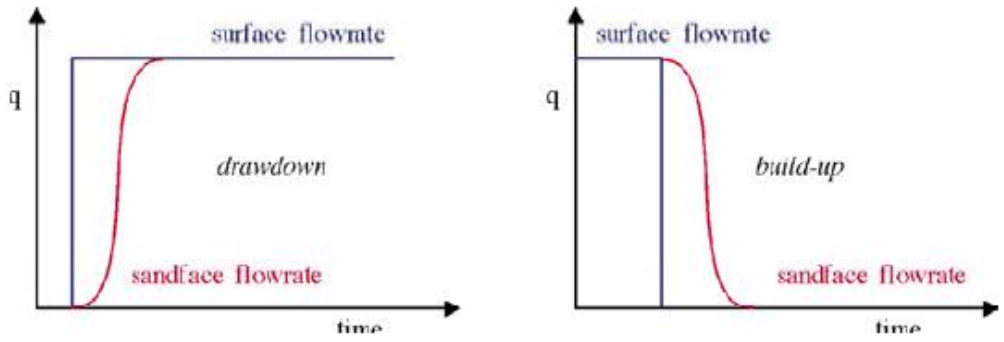

Figure 3.6 Sandface and Surface Flow rates vs. Time (Houze et al., 2011)

At the beginning of the Bourdet derivative curve, unit slope straight line can be positioned on log-log plot.

$$\Delta p = C\Delta t \tag{3.22}$$

For multirate solution:

$$\sup(\Delta t) \approx \ln(\Delta t) \tag{3.23}$$

Derivative:

$$\Delta p' = \Delta t \frac{dC\Delta t}{\Delta t} = C\Delta t \tag{3.24}$$

Wellbore storage model can be constant or changing. However most seen model is the changing wellbore storage which is related to changing compressibility of fluid.

3.4.2 Skin

Van Everdingen and Hurst (1949) defines the skin as a dimensionless parameter it characterizes the well as a damaged or stimulated.

$$S = \frac{kh}{141.2qB\mu}\Delta p_{skin} \tag{3.25}$$

Skin is constant when additional pressure drop is proportional to the sandface rate. However, it may not be constant during production depending on time and rate. Over long period of flow and times, wells get damaged and skin increasing.

In case of a damage well due to cement job or drilling/completion fluid invasion, permeability around the well decreases, causing pressure drop during fluid flow into well. The skin is positive.

In case of a stimulated well, permeability is improved with acid or frac operation. Thus reduce the pressure drop. The skin is then negative.

Skin can also be modeled by the notion of equivalent radius. Brons and Marting (1961) defined the equivalent wellbore radius with no pressure loss around the well.

$$S = -ln\left(\frac{r_{wa}}{r_w}\right) \tag{3.26}$$

$$r_{wa} = r_w e^{-S} \tag{3.27}$$

As shown in Figure 3.7, when the skin is negative, equivalent wellbore radius will be larger than wellbore radius and when the skin is positive, equivalent wellbore radius will be smaller than wellbore radius.

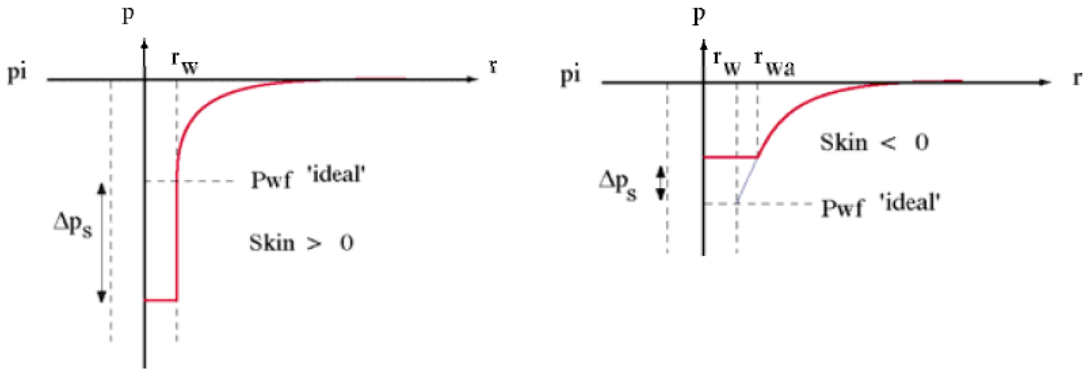

Figure 3.7 Skin and Equivalent Wellbore Radius (Houze et al., 2011)

3.5 Middle Time Behavior;

3.5.1 Infinite Acting Radial Flow;

When the well produces at a constant rate, as shown in Figure 3.8, flow lines behave as a radial geometry around the well. After production establishment, infinite acting radial flow occurs.

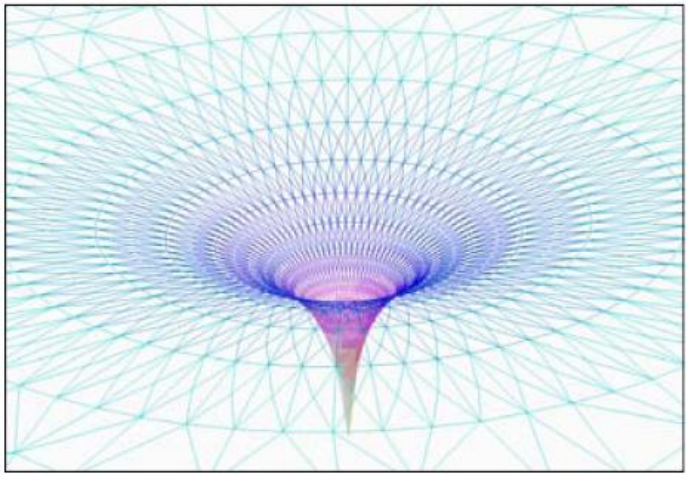

Figure 3.8 Radial Geometry Around the Well (Houze et al., 2011)

Miller et al. (1950) characterized IARF by linearity between the pressure change and logarithm of the elapsed time. By a plot (called MDH) of pressure vs the logarithm of time, a straight line can be drawn through the points when all wellbore storage effects end. From the slope of this straight line, the reservoir permeability thickness product is estimated.

For:

$$t \geq \frac{379200\emptyset\mu c_t r_w^2}{k} \tag{3.28}$$

Permeability thickness product and skin formulation where m is the slope of straight line and the location of the straight line is characterized by the straight line pressure at 1 hour ($\Delta p_{1\,hr}$) (Miller et al., 1950).

$$kh = 162.6\frac{qB\mu}{m} \tag{3.29}$$

$$\Delta p = 162.6\frac{qB\mu}{m}\left[\log \Delta t + log\frac{k}{\emptyset\mu c_t r_w^2} - 3.23 + 0.87S\right] \tag{3.30}$$

$$S = 1.151\left[\frac{\Delta p_{1\,hr}}{m} - \log\frac{k}{\emptyset\mu c_t r_w^2} + 3.23\right] \tag{3.31}$$

For Bourdet derivative, the pressure derivative stabilized to a level which is equal to the slope of MDH plot straight line.

Approximation for IARF in a case of multirate pressure response and the superposition time, $\sup(\Delta t)$.

$$\Delta p = m'\sup(\Delta t) \tag{3.32}$$

where $m'$is the slope of the semi log straight line.

Derivative when IARF occurs:

$$\Delta p' = \frac{d\Delta p}{dsup(\Delta t)} = m' \tag{3.33}$$

Identifying the IARF from derivative curve is easy and straight forward rather than the MDH plot where sometimes this straight line cannot be seen. Because pressure derivative acts as magnifying glass of the semi log behavior, Type curve match is easy to position with a unit slope line on wellbore storage and the a horizontal line on infinite acting radial flow response.

In this reservoir limit test study; boundary models of reservoir will only be discussed. The other middle time well and reservoir model are out of scope of this study.

3.6 Late Time Behavior: Boundaries

Generally in well tests, after pressure dominated by infinite acting radial flow, the analysis will end there and the infinite acting radial flow will be the final behavior. However, if the reservoir is small enough and the reservoir limit test is long enough, boundaries can be detected.

A boundary can be defined as a surface positioned at a distance from the tested well where a change in the flowing property occurs (Houze et al., 2011). There are two main boundary elements which are constant pressure and no flow boundaries.

3.6.1 Constant pressure boundaries, Steady State;

It is a surface, which provides pressure support to keep the pressure at reservoir initial pressure. If the constant pressure boundary is detected, the well bottom hole pressure profile becomes constant and steady state regime is observed (Bourdet, 2002).

$$[p]_{\sum} = p_i \tag{3.34}$$

Figure 3.9 shows the pressure profile from well to the constant pressure boundary where fluid flux occurs to keep the pressure constant.

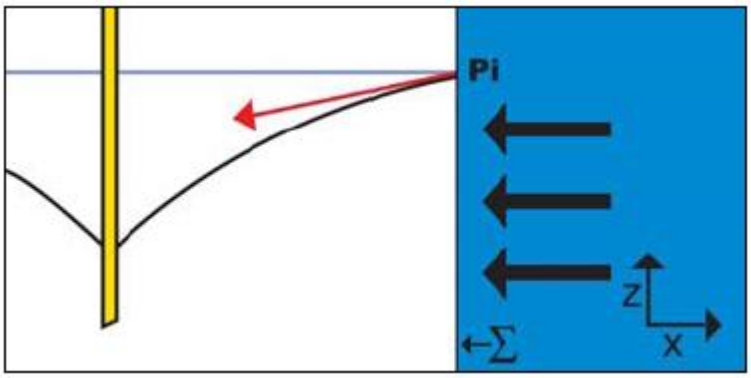

Figure 3.9 Fluid Flux from a Constant Pressure Boundary (Houze et al., 2011)

It is possible to model the constant pressure boundary by an injection image well, which has the same rate but the opposite sign, -q. In reality, it is observed for wells near a gas cap or active water drive.

3.6.2 No flow Boundaries;

No flow boundary can be formulated with Darcy's equation by applying zero rate to the boundary surface (Houze et al., 2011).

$$\left[\frac{\partial p}{\partial n}\right]_{\sum} = 0 \tag{3.35}$$

The cross sectional illustration of pressure profile from well to the no flow boundary is given in Figure 3.10.

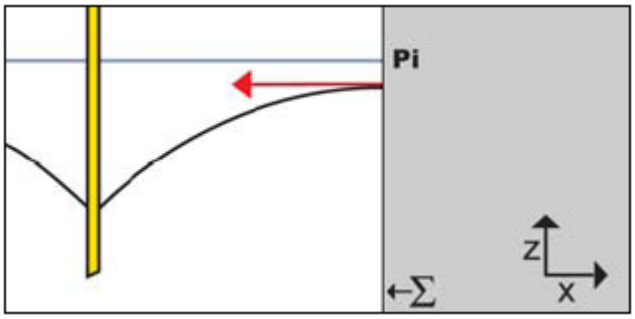

Figure 3.10 Pressure Profile Near A No Flow Boundary (Houze et al., 2011)

3.6.2.1 A Single Sealing Fault

Single sealing fault is the basic model for no flow boundary. In the ground plan, a given value of pressure drop due to a boundary at different times is represented with the circles in Figure 3.11.

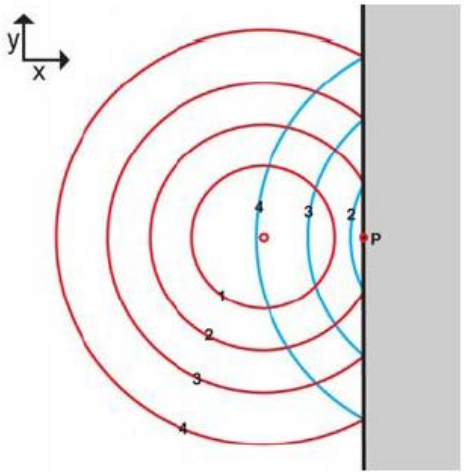

Figure 3.11 In the ground plan, pressure drop for a single sealing fault (Houze et al., 2011)

While the well is producing, it causes a pressure drop which diffuses within the reservoir (red circles). Until boundary detection, infinite acting radial flow continues. Once the boundary is detected, pressure support will cease and additional pressure drop occurs (blue circles). This pressure drop affects the pressure profile which is picked up by the gauge in the well and the boundary can be detected by analyzing this profile (Houze et al., 2011).

When the boundary is detected, gauge record the pressure response that behave half of the actual reservoir than infinite acting reservoir response. Therefore the speed of the pressure drop is twice faster than the infinite reservoir. It is also same for the image well method which adds one more wells to the infinite reservoir system, so production of two well causes a doubling of the speed of pressure drop.

For semilog analysis, both drawdown (MDH plot) and the build up (Horner plot), infinite acting radial flow is characterized by the first straight line. After sealing fault is detected, the pressure response deviates to another straight line with twice the slope of infinite acting radial flow line. The distance to boundary can be found by the following equation with the time of intercept between those straight lines.

$$L = 0.01217\sqrt{\frac{k\Delta t_{int}}{\emptyset\pi c_t}} \tag{3.36}$$

For log-log analysis, infinite acting radial flow is characterized by flat level after wellbore storage and well effects end. After sealing fault is detected, the Bourdet derivative deviates upwards and then stabilizes to a second flat level which is the original infinite acting radial flow. Again the distance to boundary can be found by the above formula replacing Δt_{int} with the midpoint of transition time Δt_x between first and the last original infinite acting flow (Larsen, 1983).
Some limitations while analyzing the pressure transient test to detect the boundaries are proposed as follows (Houze et al., 2011):

In case of a poor data quality: Nonlinear regression may fail and boundary can be corrected manually by using the governing group, t/r^2. If the boundary distance is multiplied by two, the boundary time can be multiplied by four.

In case of nearby boundaries, there is not enough time to establish a flat level for infinite acting radial flow. This results in a higher position of flat level which causes a small value determination for permeability thickness product. In case of afar boundaries, there is enough time to establish a flat level but not enough time to detect the boundary and infinite acting radial flow continues.

In case of a short production time before shut in, the Bourdet derivative may be distorted and thus create a temporary down trend before boundary detected.

In addition to those, doubling the slope is rarely seen on real data. If slope is less than double, single sealing fault is the easiest one among boundary models to associate the time and distance. Before doubling the slope, the second or the third boundary detection is more likely. For a long reservoir limit test, the forth boundary can be detected for a closed reservoir.

3.6.1.2 Closed System, Pseudo Steady State;

When the reservoir limit test is long enough or the reservoir is small enough, reservoir can be modeled as a closed system. During the production period, it is characterized by linear depletion and during the shut in period, it is characterized by pressure stabilization to an average reservoir pressure which is lower than initial pressure of the reservoir.

For drawdown, infinite acting radial flow ends when the boundary is detected and deviates to reach a new flow regime called pseudo steady state where flowing pressure is a linear function of the elapsed time (Bourdet, 2002).

The circular and the rectangular closed systems as illustrated in Figure 3.12, are the main reservoir models.

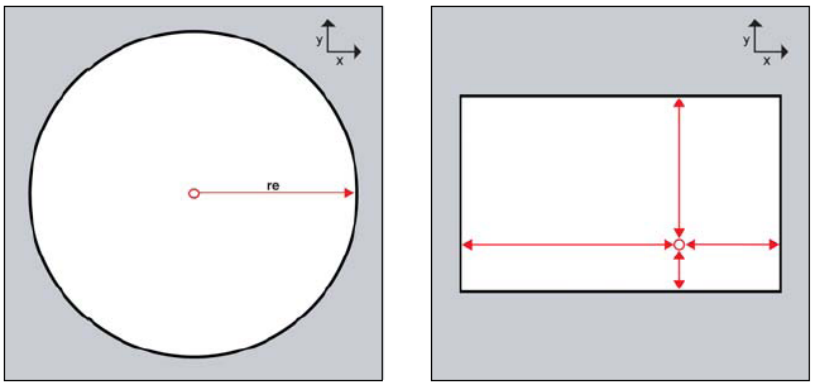

Figure 3.12 Circular and Rectangular Reservoir (Houze et al., 2011)

A well is centered in a reservoir of circular shape with radius r_e is the simplest closed system model. It is not only used to model the closed system but also a well drainage area which is the part of the reservoir drained by well centered in that part. It is defined with the following relationship (W. J. Lee, 1982).

$$r_i = \sqrt{\frac{kt}{948\emptyset\mu c_t}} \tag{3.37}$$

Another practical closed system model is the rectangular reservoir. In such a case four boundaries can be easily located at any distance by image wells.

For semilog analysis, the curve deviates to an infinite slope during production period, whereas curve tends to stabilize at average reservoir pressure during shut in periods.

For log-log analysis, during production period, pseudo steady state flow will be represented with a late time unit slope for the circular and the rectangular models. During the shut in

period Bourdet derivative will dive towards zero due to stabilization at average reservoir pressure as shown in Figure 3.13.

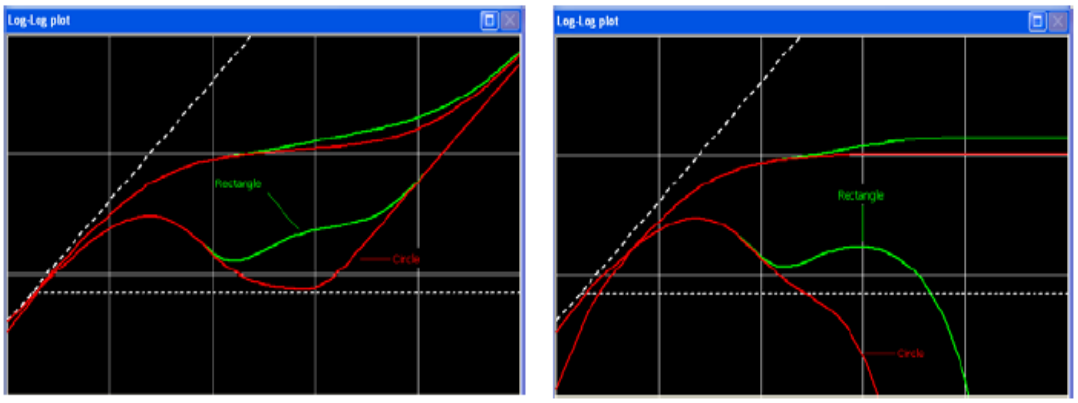

Figure 3.13 Log-Log Analysis of Drawdown and Build up Test for Circular and Rectangular Reservoirs (Houze et al., 2011)

CHAPTER-4

STATEMENT OF PROBLEM AND SCOPE

The objective of this study is to determine how errors of the input parameters affect the results of the analyses of reservoir limit tests. In order to estimate the output parameters of a well test, reservoir model identification is the first step and this can be handled by using pressure and pressure derivative curves. Before evaluating the pressure and pressure derivative curves, parameters of the base case will be entered for initialization. Pressure and flow rate values will be loaded. Quality control and quality assurance of the pressure and flow rate data will be checked. Pressure record from the upper and lower gauges will be compared after extracting the derivative curves of both gauges. Measured flow rate will be checked by comparing the all pressure build up curves. However, the match points on these curves are strongly related to input parameters which subject to uncertainty.

These input parameters will be divided into two main categories and the effects of uncertainties in these parameters will be analyzed in detail. The first category is the fluid parameters such as; viscosity, fluid compressibility, formation volume factor and flow rate and the second one is petrophysical parameters such as; porosity, net pay thickness, formation compressibility and saturations.

All variables that affect the well test results will be determined from the logs, gas samples and correlations and PVT analysis. Their error range will be found from the published literature. Error ranges will be applied to the input parameters to determine the minimum and maximum values to create a predictive model. By using the minimum and the maximum values of input parameters, the optimum design of experiment will be constructed by using SAS' JMP Software free trial version 10 (can be downloaded at http://www.jmp.com/uk/landing/adwords.shtml?gclid=CO_s1_34x7kCFW_HtAod2woAQg) in order to evaluate the variables that cover the whole space. Characteristics of the design will be evaluated to check the quality of the design of experiment. The cases obtained from the design of experiment will be conducted for the closed boundary model constructed with the base case parameters. For each case, model will be matched with the manually and also by using the improvement option of the Saphir Module. By using the results of the each case, a linear predictive model will be constructed with least squares method in JMP which is a statistical analysis program. Results will be plotted for screening purposes. The effect of the input parameters to the reservoir parameters will be evaluated. Finally, sensitivity analysis will be conducted to seek which parameter has the greater impact on well test results.

CHAPTER-5

SOURCE OF THE ERROR IN INPUT PARAMETERS

In order to handle the uncertainties in input parameters, a good knowledge about the data sources is the prerequisite. In each sub-chapter, firstly, the sources of each parameter will be discussed. Henceforward, the effect of error in input parameters on the result of well test is mentioned.

5.1. Fluid Parameters

Fluid parameters include viscosity, fluid compressibility and formation volume factor. Those are directly related to the composition of the formation fluid. Properties of these formation fluids were actually determined million years ago, at the time of burial and the formation or migration of hydrocarbons. Today, we only try to estimate these properties, either by experiments or correlations. The first and best way to estimate a fluid property is to take representative fluid samples and carry out some laboratory measurements. On the other hand there may be some technical impossibilities to take fluid samples or there may be some problems during the experiments. In such situations, correlations can be used to obtain the fluid property data. Although, correlations are based on many years' experience, these will only stay as estimates and will only converge to real data. Hence usage of real laboratory data is always preferred.

5.1.1. Viscosity

Viscosity is defined as a measure of the fluid's internal resistance to flow. Gas viscosity increases with pressure. It also increases with temperature, whereas liquid viscosity decreases (Danesh, 1998). A. Lee, González, and Eakin (1966) proposed a correlation using the gas molecular weight and gas density at prevailing pressure and temperature. For gases with gravity less than 1, correlation give result to within %2 at low pressure and to within 4 % at high pressure when the gas gravity is less than one. For retrograde gases with gravities over 1.5, correlations gives low estimates by up to 20% (W. McCain, 1990).

Viscosity is one of the fluid input parameter for well test interpretation. It is used in the calculation of the drainage area, skin factor and also distance to boundary. Sensitivity of the viscosity is opposite of the permeability because it always appears as a ratio (k/μ). The affected parameters are expressed by following formulas;

Radius of investigation;

$$r_i = \sqrt{\frac{kt}{948\emptyset\mu c_t}} \tag{5.1}$$

Skin;

$$S = 1.151\left[\frac{\Delta p_{1\,hr}}{m} - \log\frac{k}{\emptyset\mu c_t r_w^2} + 3.23\right] \tag{5.2}$$

$$r_{wa} = r_w e^{-S} \tag{5.3}$$

Distance to boundaries;

$$L = 0.01217\sqrt{\frac{k\Delta t_{int}}{\emptyset\pi c_t}} \tag{5.4}$$

5.1.2. Fluid Compressibility

Gas compressibility is a function of pressure and z factor. It is calculated from following equation;

$$C_g = \frac{1}{p} - \frac{1}{z}\frac{\partial z}{\partial p} \tag{5.5}$$

This equation is accurate for low pressures. In such a case, pressure is dominant term and the error of z factor and its derivative is negligible.

Standing and Katz (1942) presented a gas compressibility factor chart as a function of Ppr and Tpr. McCain Jr. (1991) do not recommend the use of this chart for pseudo reduced temperatures Tpr less than 1.4 and the pseudo reduced pressure within the range 0.4< Ppr< 3.

Water compressibility is calculated from temperature (T in °F), pressure (P in psi) and salinity (S in mg/L) values by using the following equation (Osif, 1988). Hence this equation is only valid for salinities below than 200,000 mg/L, pressures between 1000 and 20,000 psi and temperatures between 200 and °270 F.

$$C_w = \frac{1}{(7.033p + 0.5415S - 537T + 403300)} \tag{5.6}$$

Pressure and temperature must be considered for accurate results of gas compressibility and salinity must be considered for water compressibility. Those results are used for calculating the total compressibility with following equation during well test analysis.

$$C_t = C_f + S_w C_w + S_o C_o + S_g C_g \tag{5.7}$$

And total compressibility affects the drainage area, skin factor and distance to boundary.

5.1.3. Formation Volume Factor

Formation volume factor is actual volume occupied by a certain amount of gas at reservoir condition, divided by the volume occupied by the same amount of gas at standard condition.

Gas formation volume factor can be expressed by following equation in ft^3/scf unit;

$$B_g = 0.02827 \frac{zT}{P} \tag{5.8}$$

For the given temperature and pressure, accuracy of the gas formation volume factor is directly related to the accuracy of the used z factor value.

Those aspects must be considered while calculating gas formation volume factor. Accurate formation volume factor as an input for well test affect the permeability and the wellbore storage coefficient.

Wellbore storage coefficient from the unit slope of the log- log plot;

$$C = \frac{qB}{24m} \tag{5.9}$$

Permeability;

$$kh = 162.6 \frac{qB\mu}{m} \tag{5.10}$$

Permeability also affects the drainage area, skin factor and distance to boundaries.

5.1.4. Spesific gravity

Inadequate water gravity and the specific gas gravity data can lead to errors in the fluid parameter measurements when correlations are used in Saphir Module.

Specific gas gravity is calculated from composition of the gas. It can be also defined by the user without entering composition of the gas. In both cases, specific gravity brings its own error because Saphir determines the Z factor, viscosity, compressibility and the formation volume factor with Dranchuk, Lee et al., and Internal correlations by using the specific gravity of gas (A. Lee et al., 1966).

Separator gas samples taken from a particular well in a year is used for specific gas gravity measurements. The results show that the individual gas volume measurements are about % 0.8, the median error %0.9 and the average error %1.3. The error extends from %0 to %11 (Stoin & Sullivan, 1965).

Water gravity is calculated from salinity of the water. It can be also defined by the user without entering salinity of the water. In both cases, water gravity brings its own error because Saphir determines the solution gas/water ratio, viscosity, compressibility and the formation volume factor with the correlations Katz, Gould, Dodson and Standing and Van-Wingen-Frick by using the water gravity.

All formation waters contain dissolved solids, primarily sodium chloride (NaCI) but the quantity of the ions changes every formation. Salinity is usually between 200 ppm to 300,000 ppm (McCain Jr., 1991). Also variation of water salinity is observed in most of the fields. Sources of the water salinity data are produced water (if field produces water) and oil base mud-core data. According to a study conducted by McCoy, Jr., and Fisher (1997), for a sandstone gas reservoir, calculated salinity from a produced water is 11307 ppm with a standard deviation 625 ppm and repeated salinity calculation from oil base mud-core data produce about 10% error.

Since there is no production sample and core data, spontaneous-potential (SP) and resistivity-log calculations are conducted to find brine resistivity, Rw. Unfortunately quantitative SP-log interpretation are not reliable (McCoy et al., 1997).

5.2. Petrophysical Parameters

Petrophysical parameters are the chemical and physical properties of porous media and their contained fluid in particular of reservoir rock. As for petrophysical parameters, there are two ways to obtain; the experimental data and the data obtained from correlations. Again, the experimental data, and the log measurements are more accurate compared to data obtained from correlations. However petrophysical parameters strongly depend on type of the geological heterogeneity of rocks. Three different types of heterogeneity can be defined in sandstones (different depositional units in the same reservoir, lateral and multiple reservoirs apparently “blanket” sands, shale “breaks” of indeterminate aerial extends) and two types in carbonate reservoirs (lateral discontinuities in pay zones, very erratic – sometimes vugular and fractural porosity) (Siemek & Nagy, 2004).

Petrophysical parameters that are calculated from logs are also affected by such heterogeneities. To overcome the uncertainty and obtain consistence results, multiwell normalization i.e., consistent and comparative multiwell log analysis process that uses the histograms, cross plots and depth based logs (Aly et al., 1997). It should be also integrated, calibrated and correlated with the core data. However it must be considered that the core data can indicate properties of few cubic inches, while the log data can indicate properties of few cubic meters. Hence, by using those properties, the well test analysis can indicate properties of few acres.

Although, log tools directly measure the resistivity, density; the parameters we are interested in the indirectly measured ones, i.e. calculated by combining direct measurements and some constants/variables by the help of correlations. Hence, the results will involve some uncertainty and the extent of this uncertainty depends on the closeness of these constants/variables selected to their real value.

5.2.1. Porosity

Porosity is the fundamental property of the reservoir rock. Porosity can be calculated from sonic log, density log, and neutron log. However, each tool brings its own limitations while logging (environmentally) and interpretation.

From sonic log, porosity is calculated by equations;

Wyllie Time- average;

$$\emptyset_s = \left(\frac{\Delta t_{log} - \Delta t_{matrix}}{\Delta t_f - \Delta t_{matrix}}\right) \tag{5.11}$$

Raymer-Hunt-Gardner;

$$\emptyset_s = \frac{5}{8} \times \left(\frac{\Delta t_{log} - \Delta t_{matrix}}{\Delta t_{log}}\right) \tag{5.12}$$

For unconsolidated formations;

$$\emptyset_s = \left(\frac{\Delta t_{log} - \Delta t_{matrix}}{\Delta t_f - \Delta t_{matrix}}\right) \times \frac{1}{C_p} \tag{5.13}$$

With;

$$C_p = \left(\frac{\Delta t_{sh} \times C}{100}\right) \tag{5.14}$$

Enlarged borehole, formation fractures, improper centralization and excessive logging speed cause signal attenuation resulting in cycle skipping or transient time spikes to higher values. While interpretation, equations requires a formation matrix transit time which varies with lithology. The choice of equation depends on formation whether it is uncompacted or unconsolidated formation.

From density log porosity is calculated with the following formula;

$$\emptyset_{den} = \left(\frac{\rho_{ma} - \rho_b}{\rho_{ma} - \rho_f}\right) \tag{5.15}$$

While logging the well, borehole enlargement causes higher porosity measurement than the actual porosity due to the sensor pad losing contact with the borehole wall. Porosity calculated from density log depends on the choice of matrix density, which varies with lithology and fluid density, which varies with fluid type and salinity.

Rather than density porosity, neutron porosity is less affected from enlarged boreholes. However pressure and temperature have the greatest effect on porosity calculated from neutron log. Neutron porosity may be read directly on log curve. If matrix is something other than that used in running the log, the porosity reading on log curve will not be correct (Bateman, 1986).

To obtain better results, both the environmental and the interpretation effects must be considered for porosity calculation from logs. In addition to this, if there is ambiguity in lithology prediction, combination of porosity log devices should be run into the wellbore together to create cross plot for accurate porosity results.

Due to aforementioned ambiguities, porosity is inevitably subject to measurement and estimation errors. Those errors affect the well test interpretation and the calculated parameters such as; skin, distance to boundaries, radius of investigation and the drainage area. For illustration how affect porosity to the well test result, following formulas is used;

Radius of investigation;

$$r_i = \sqrt{\frac{kt}{948\emptyset\mu c_t}} \tag{5.16}$$

Similarly the drainage area ($A = \pi r_i^2$) is indirectly affected by the porosity.

Skin factor;

$$S = 1.151\left[\frac{\Delta p_{1\,hr}}{m} - \log\frac{k}{\emptyset\mu c_t r_w^2} + 3.23\right] \tag{5.17}$$

Distance to boundary;

$$L = 0.01217\sqrt{\frac{k\Delta t_{int}}{\emptyset\mu c_t}} \tag{5.18}$$

5.2.2. Net Pay Thickness

Net pay thickness, in terms of reservoir engineering point of view, can be defined as a thickness of formation from where oil and gas produced. Not all of the reservoir thickness is the net pay thickness because some nonproductive shale beds or tight units of formation can reduce the reservoir thickness. Net pay thickness is calculated from the coring techniques and logs by using porosity, shale and water saturation cut off. For both techniques be used for net pay thickness estimation, log and core intervals must be long enough to enclose whole productive zone.

While log is used for net pay thickness estimation, it brings their own limitations because log process causes different range of uncertainties in net pay thickness estimation. Using the wrong cut off values and underestimating the impermeable beds cause wrong interpretation of net pay thickness. To overcome such uncertainty pre-interpretation diligence such as log quality assurance, log to log depth alignments, borehole environmental corrections and repair of data in intervals where logs are invalid because of stress induced borehole breakouts should be employed. W. D. McCain et al. (1993) gave the impact of these remedies on net pay calculation in Table 5.1.

Table 5.1 Effect of Not Properly Applying Pre-Interpretation Activities (W. D. McCain et al., 1993)

Pre-Interpretation Log Analysis Work	Potential Range of Impact on Net Pay Calculations If Only Normal Diligence is Applied
Log To Log Depth Alignment	±25%
Borehole Size, Salinity and Invasion Effects	±15%
Enlarged Borehole and Mud Weight Effects	±25%
Neutron Environmental Effects	±5%

Table 5.1 Effect of Not Properly Applying Pre-Interpretation Activities (W. D. McCain et al., 1993) (Continued)

Borehole Curvature	±0.5%
Borehole Rugosity	0% to 200%
Log Normalization	10% to +15%
Combined Effects	120%

To reduce the error, applying such techniques while calculating net pay thickness is required because net pay thickness has significant impact on the result of the calculated reservoir parameters directly or indirectly (Zahoor & Khan, 2012).

Permeability calculated from the well test analysis is directly affected by the net pay thickness. Permeability can be determined by using the following equation (Lee, Rollins and Spivey, 2003).

$$kh = 162.6\frac{qB\mu}{m} \tag{5.19}$$

Furthermore the radius of investigation, i.e., the distance from the well to which the pressure transient has moved can be estimated (J. Lee, Rollins, & Spivey, 2003) with the following equation by using the permeability calculated for determined net pay thickness.

$$r_i = \sqrt{\frac{kt}{948\emptyset\mu c_t}} \tag{5.20}$$

Similarly the drainage area ($A = \pi r_i^2$) is indirectly affected by the net pay thickness.

The influence of net pay thickness on skin and the effective wellbore radius can be analyzed by the following equations.

$$S = 1.151\left[\frac{\Delta p_{1\,hr}}{m} - \log\frac{k}{\emptyset\mu c_t r_w^2} + 3.23\right] \tag{5.21}$$

5.2.4. Fluid Saturations

Fluid saturation is defined as the fraction of the pore volume occupied by a given fluid volume. Fluid saturation estimation is fairly complex and subject to high degree of uncertainty. Fluid saturation can be determined directly by measured the volume of gas, oil and water of a core sample and indirectly through capillary pressure measurement or log interpretation. Generally, mud filtrate has flushed the saturated fluids from rock sample and

the saturation results from this technique cannot be representative of the reservoir rock. Therefore saturations are usually estimated from electrical resistivity logs.

There are many techniques to find the fluid saturations from logs. In clean formation rock resistivity and the fluid saturation is proposed by Archie with an empirical equation in 1942;

$$F = \emptyset^{-m} \tag{5.22}$$

$$I = \frac{R_t}{F \times R_w} = \frac{R_t}{R_o} \tag{5.23}$$

$$S_{w=} I^{-1/n} \tag{5.24}$$

Porosity is obtained from a core or a porosity log (sonic, neutron or density). Formation factor is calculated from Equation 5.22 using cementation exponent m obtained from laboratory or resistivity measurements. Resistivity index (I) is calculated from Equation 5.23 using true formation resistivity (Rt) obtained from an appropriate resistivity device, formation factor F as calculated from Equation 5.22 and water resistivity (Rw) obtained from a water recovery nearby zone or calculated from the SP log. Finally using Equation 5.24 Sw is calculated from resistivity index and saturation exponent (n) obtained from laboratory measurements by testing samples (Pickett, 1966).

To calculate water saturation, accurate values of formation factor and saturation exponent are required. In addition to those, according to Waxman and Smits (1968) and Waxman and Thomas (1974), cation exchange capacity must be calculated if illite present, since resistivity logs are effected by illite. Furthermore, the major source of error is on water saturation is porosity. The possible error in water saturation arises to % 100 at porosities less than five percent (Rosepiler, 1982).

Figure 5 1 shows that for shaley sands with %30 porosity, error in water saturation is between %25 and %10 (Mahgoub, Daoud, & El-Tayeb, 2008).

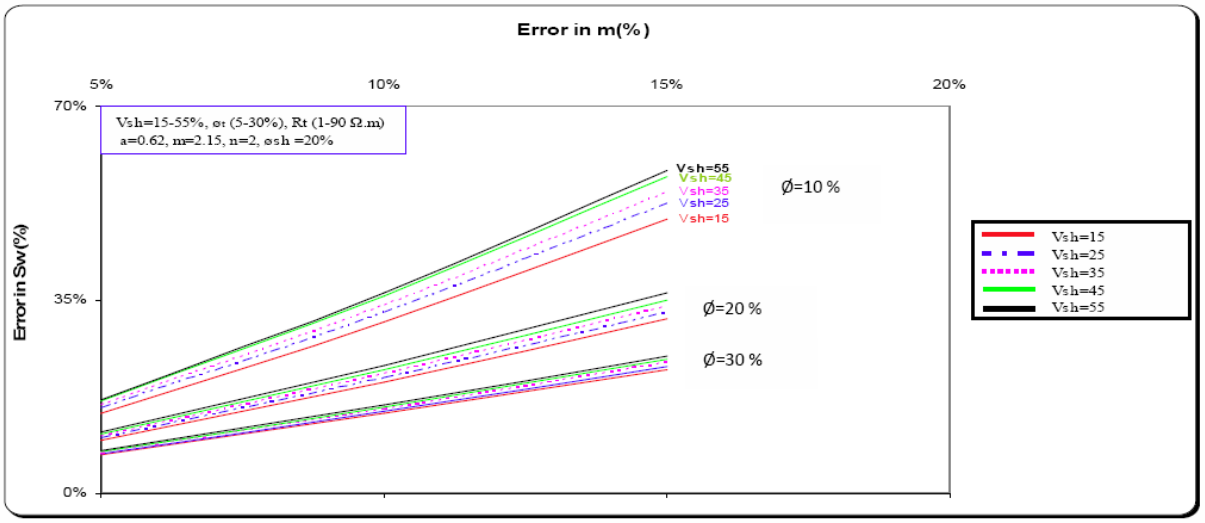

Figure 5 1 Sw Error Analaysis Chart for Waxman & Smith Model (Mahgoub et al., 2008)

The accurate determination of the water saturation as an input value for well test interpretation is important because the accuracy of the total compressibility estimate depends on the accuracy of the log derived fluid saturations. Total compressibility affects the result of the well test interpretation.

$$C_t = C_f + S_w C_w + S_o C_o + S_g C_g \tag{5.25}$$

5.2.5. Formation Compressibility

Compressibility is defined as the fractional change in pore volume of the rock with a unit change in pressure (Ahmed, 2006). It can be expressed in terms of porosity. The formation compressibility is defined mathematically by;

$$c_f = c_p = \frac{1}{\emptyset}\frac{\partial \emptyset}{\partial P} = \frac{1}{V_p}\frac{\Delta V_P}{\Delta P} \tag{5.26}$$

Several authors studied on formation compressibility with various parameters including the porosity. For example, Hall (1953) correlated the pore compressibility with porosity with the following relationship:

$$c_f = \left(\frac{1.782}{\emptyset^{0.432}}\right) \times 10^{-6} \tag{5.27}$$

Newman (1973) used 79 samples for consolidated sandstone and limestone to develop a correlation between porosity and the formation compressibility by defining different constants for limestone and sandstone.

$$c_f = \frac{a}{(1 + cb\emptyset)} \tag{5.28}$$

where a=97.32*10^-6, b=0.699993, c=79.8181 for sandstones and a=0.8535, b=1.075, c=2.202*10^-6 for limestones.

It is obvious that compressibility is directly related to porosity and pressure. With the correct use of these parameters the closeness of constants/variables selected to their real value is important to reduce the error of formation compressibility.

Formation compressibility is also calculated in the laboratory using core plugs by changing the overburden pressure on core plug while holding the pore pressure constant. Without considering the selection of constant and variables for a typical formation, laboratory determination allows to obtain accurate result.

Formation compressibility as an input value for well test analysis is used to compute the total compressibility with log derived saturations and the fluid compressibility. The accuracy of the total compressibility depends on the accuracy of those petro physical parameters.

$$C_t = C_f + S_w C_w + S_o C_o + S_g C_g \tag{5.29}$$

5.3. Errors in Pressure and Rate Measurements

5.3.1. Pressure Data Error

Pressure data errors can be caused by various factors such as noise, drift, temperature effects and time shifts. This study addresses the impact of noise and drift since other issues do not have significant effects on results.

Archer et.al. (2002) introduced a uniformly distributed noise into the pressure data. They found that the resulting permeability and skin factor estimates are approximately normally distributed, hence validates that the results from cases with pressure error are normally distributed. This phenomenon was also observed by Horne (1994).

Gauge drift is the instability of the pressure measurement gauges with increasing time. This is caused by fatigue of the electronic component of the sensing material in the gauges. Especially, strain gauges are susceptible to drift problems (Houze et al., 2011). This problem is more common in long term well test that are designed to reveal boundary distances, i.e. reservoir limit tests. Moreover, gauge drift problem may also be observed in data obtained from permanent downhole gauges (PDG). This problem can be identified by comparing the data obtained from the multiple downhole gauges used during the test.

5.3.2. Flow Rate Errors

As for the flow rate parameter, there are several ways to obtain such data. Almost all of them rely on the volume calculations per time; however, the volume calculation procedures may vary. Orifice meters, turbine meters are the examples for the sources of flow rate data. In this study, only the accuracy of flow rate measurement devices will be discussed. The sources of errors associated with using each device are out of scope of this study. Moreover, importance of reducing the uncertainty in flow rates and introducing the correctly smoothed flow rates to the test data will be discussed.

Archer et al. (2002) states that flow rate noise (i.e., errors) relatively do not affect the results of well test analysis. Besides it is worth to note that the permeability estimate increases with the noise in flow rate date within tolerable limits. However the associated confidence intervals broaden with increasing noise.

CHAPTER-6

FIELD OVERVIEW

6.1 General Geological Overview of the Field

B.E-1 well is located on the southern part of the Black Sea, on the Turkey's territorial waters. It is on Akçakoca - Ereğli offshore area. B.E Structure has been identified on 2D seismic surveys conducted during 1991, 2004 and 2005 years. In the area, the first economic well was A-1, tested natural gas in September 2004 which is approximately 10 kms to southeast of B.E Structure (Figure 6.1). The last promising gas well, A-3 was tested by the end of 2006. B.E-1 well is located 6 kms to A-3 well.

The possible hydrocarbon system identified in the Western Black Sea focuses primarily on deep sea turbiditic deposits of Middle and Lower Eocene aged Kusuri Formation that is the primary gas reservoir target of B.E-1. Target depth was at TVD: 1800 m ± 200 m however measured depth is 1936 m in Middle-Lower Eocene Formation which is mainly sandstone with shale and siltstone.

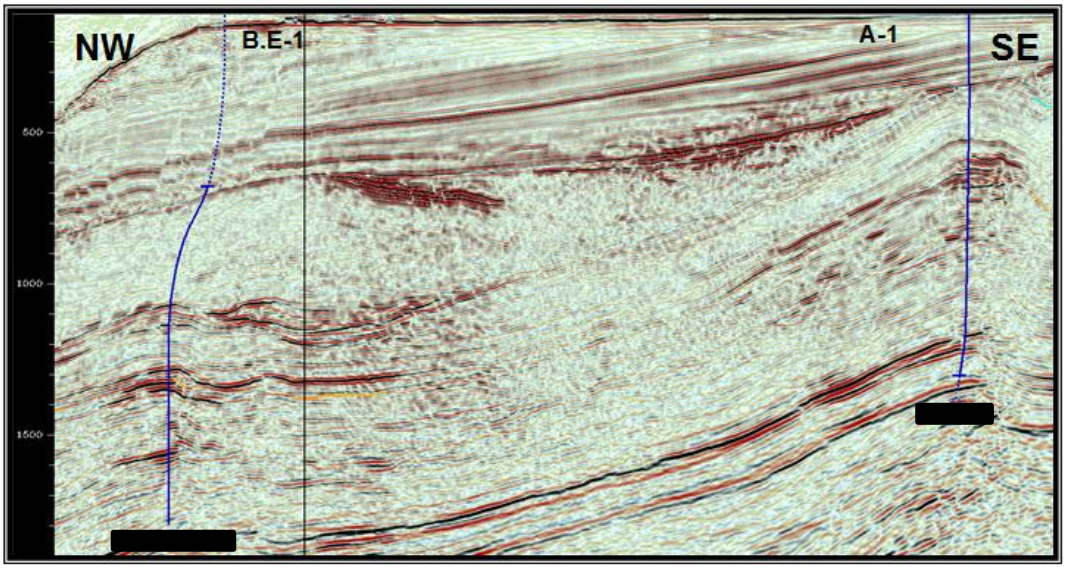

Figure 6.1 B.E-1 and A-1 Well Projection On Seismic Cross Section

Productive part of the K formation is mainly sandstone with shale and siltstone. Therefore the correlations and the constant values used to find petrophysical properties such as

porosity, saturations and formation compressibility were chosen according to sandstone. Stratigraphic section is summarized below and shown in Figure 6.3.

Middle Eocene (S Member of K formation): 1128 m to 1452 m TVD

Marl: Cream-light beige-dirty white coloured, with soft, thin carbonate and lignite ıntercalations.
Sandstone/Siltstone/Marl/Mudstone interbedding:
Sandstone: Brown-dark beige coloured of volcanic materials.
Sıltstone: Grey-light cream coloured, softly, carbonated.
Marl: Cream coloured, soft.
Tuff: Light yellow coloured, porous.

Lower Eocene (A Member of K Formation): 1452 m to 2198 m TVD

Marl/Mudstone/Sandstone interbedding:
Marl: Cream coloured, soft
Mudstone: Beige coloured
Sandstone: Grey coloured, soft, calcareous cement, marl and mudstone intercalations.
Sandstone: Beige, light grey coloured, soft, calcareous cement, marl and mudstone intercalations.
Sandstone: Brown-dark beige coloured of volcanic materials. Shale: Grey coloured, soft and silty.

Formation compressibility of the sandstone was determined as 3.14E-06 1/psi by using the Nemann's correlation mentioned in Chapter-5. 5% error is applied and the input range of the formation compressibility is between 2.99E-06 1/psi and 3.32E-06 1/psi.

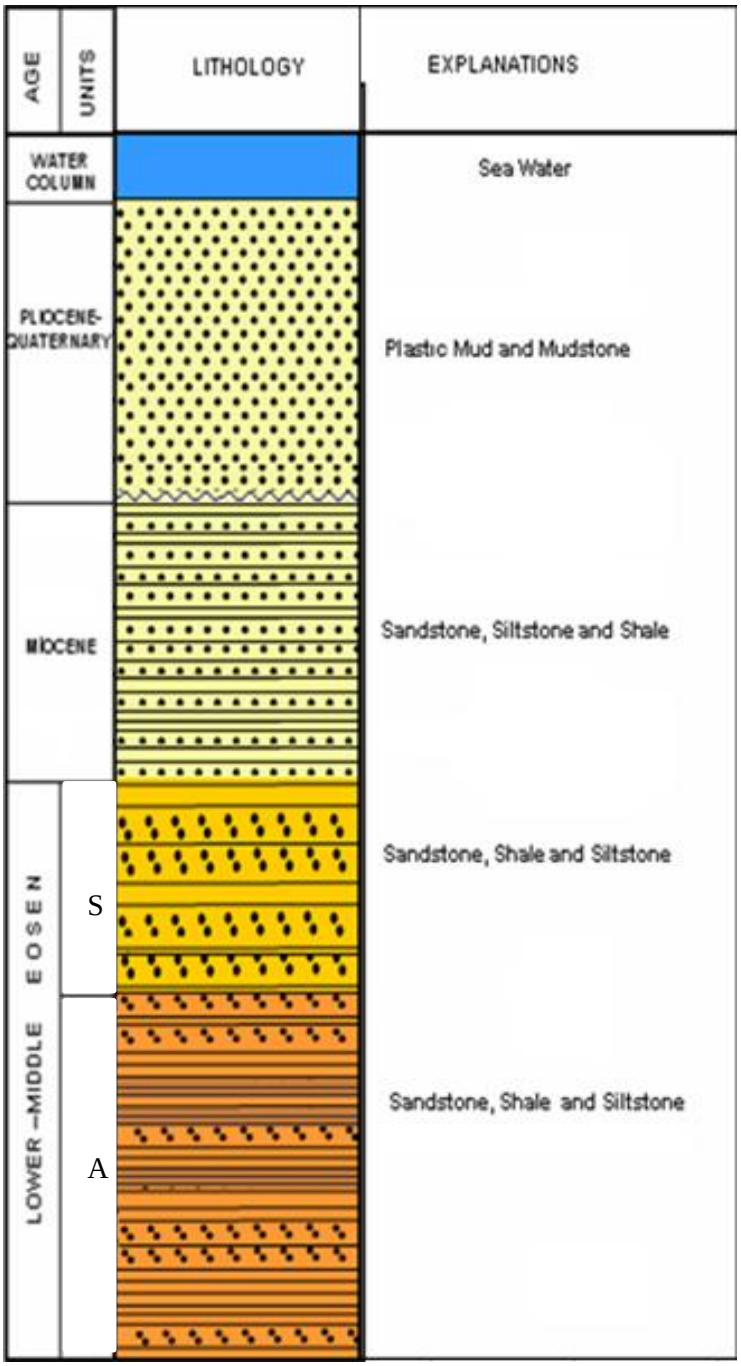

Figure 6.2 Stratigraphic Column of B.E-1

Stratigraphic contour map and the fault around the well are shown in the Figure 6.3. This map shows that it is a limited reservoir. There is no information how far it is extended through the northwest. Therefore the modulus of the reservoir extension through the west and northwest is the most uncertain information. After well test interpretation, extension through the west and northwest part will be tried to determine.

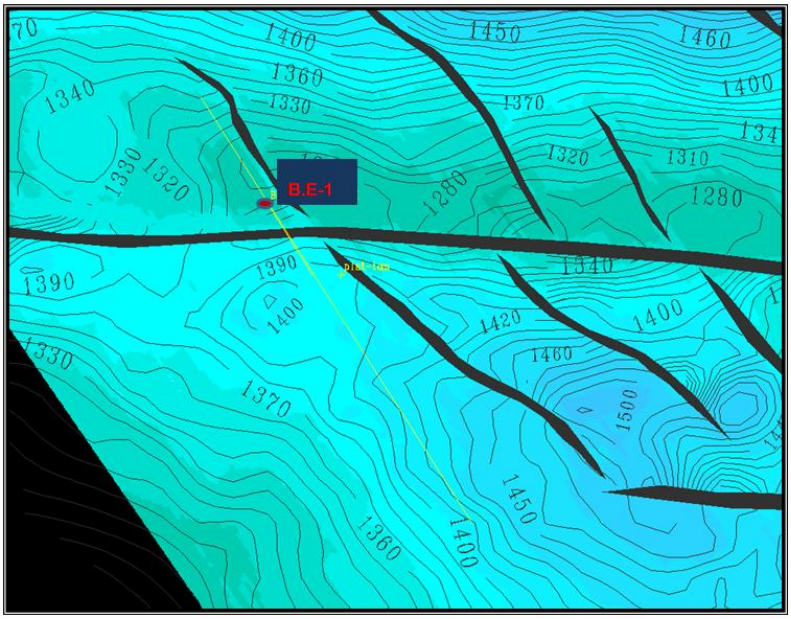

Figure 6.3 Structural Map of B.E and Faults

6.2 Operational Overview of the Well

B.E-1 well was drilled in 2007 and is located on the south-southwestern part of the Black Sea on Turkey's territorial water.

During the drilling operation of B.E-1 well, gas shows from A Formation were observed, and log (Figure 6.6 and Figure 6.7) and XPT interpretation (Figure 6.5 and Table 6.3) supported these gas shows. Identified gas zone from the log and XPT data is 1453.5-1490.5 m. The tested interval does not mean the net pay thickness.

7" production casing was run to the hole. Inner diameter of the 7" casing is 6.17". If it was an openhole test, there could be an uncertainty in the well diameter due to borehole enlargements. However it was a cased hole and there is no uncertainty in diameter of the tested interval. Therefore well diameter (6.17") is a single input value.

After setting the quantum packer, the interval of 1453.5-1490.5 m in A Formation was perforated with TCP guns and tested at 26-29 October 2007 (Figure 6.4). Gas test was conducted between 1453.5-1490.5 m in A Formation. After the gas test, a PX plug was set into the X nipple at 1428 m. to isolate this zone. An RBP packer was set at 1365 m. and 3 m. sand was placed on RBP packer. Two cement plugs were set at between 325-425 m. and 1196-1296 m until the production period.

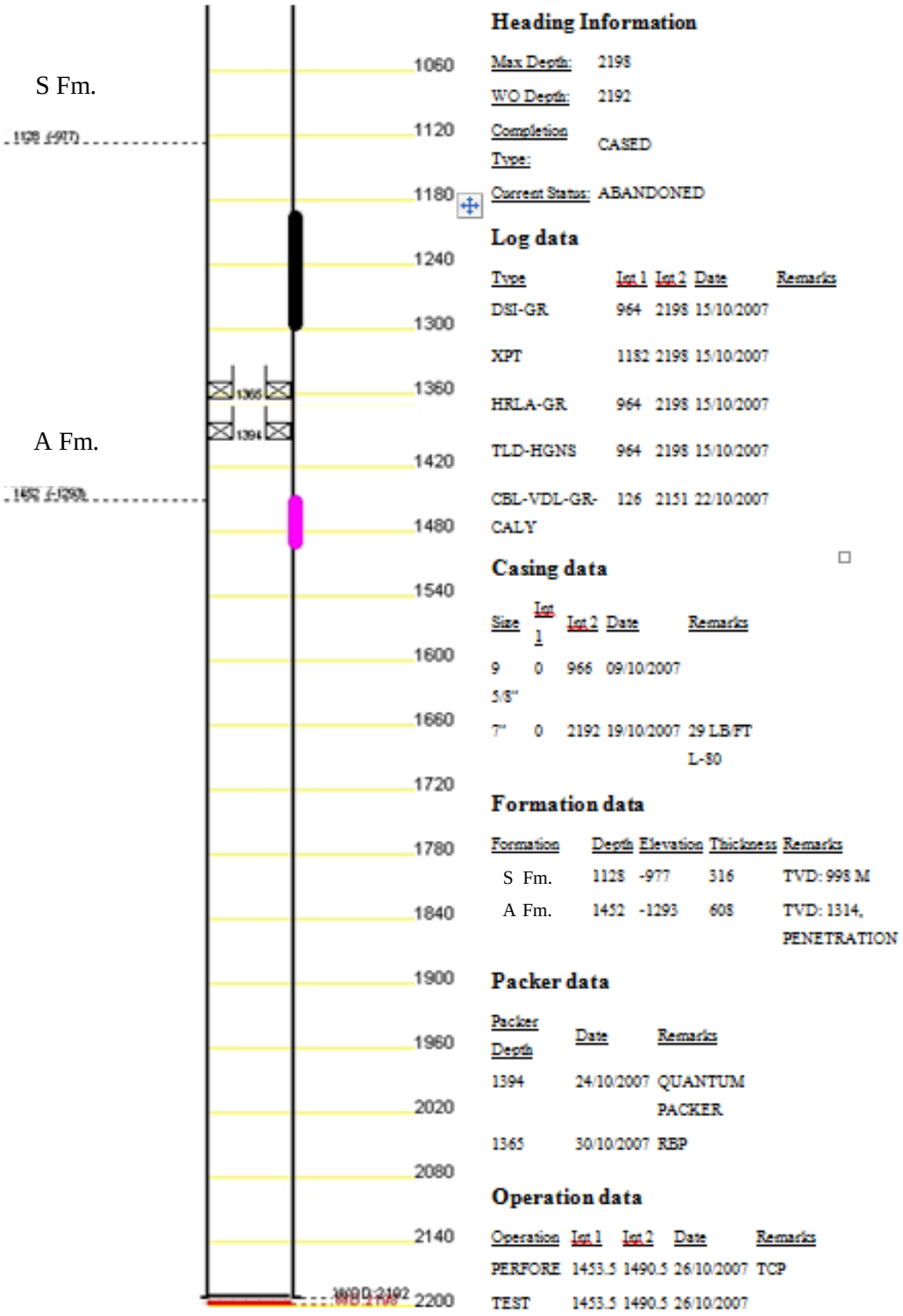

Figure 6.4 Well Sketch and Operation History of B.E-1

Measured gas pressure and gas flow rate values used in well test interpretation are given in Table 6.1. Gas analysis results and gas properties of B.E-1 well performed by Çayağzı Natural Gas Process Facilities are given in Table 6.2.

Table 6.1 Gas Flow Test of B.E-1

Choke	Duration (hr)	Wellhead Pressure (psig)	Bottom hole Pressure (psia)	Gas Rate (m3/day)	Condensate/ Gas Ratio (stb/MMscf)	Water/Gas Ratio (stb/MMscf)
1453.5-1490.5 m. interval was perforated						
20/64”	0.03	609			0	
32/64”	0.52	1604			0	
24/64”	1.12	1632	2009		0	
Shut-in	4.0	1860	2043.7	-	-	-
20/64”	0.03	1836	2040		0	0
24/64”	7.0	1741	2012.3	202600	0	0
Shut-in	11.2	1855	2038.4	-	-	-
20/64”	0.08	1807	2007		0	0
28/64”	19.0	1681	1986.5	246700	0	0
Shut-in	23.0	1839	2025.7	-	-	-

For the test interpretation, rate and the pressure values on Table 6.1 are used as input. Also for calculation of the fluid properties such as; viscosity, gas formation volume factor, gas compressibility and specific gravity, gas compositions shown in Table 6.2 is used. In Saphir Modul, viscosity, gas compressibility, and gas formation volume factor are determined from specific gravity of gas. Specific gravity determined from the gas composition is 0.5579. For specific gas gravity measurements, the error extends from 0% to 11% (Stoin & Sullivan, 1965). The corresponding specific gas gravity range used in well test interpretation is between 0.5536 and 0.61369.

Table 6.2 Gas Analysis Results of B.E-1

Composition	Mol %
C_1	99.105
C_2	0.223
C_3	0.006
i-C_4	0.006
n-C_4	0.000
i-C_5	0.001
n-C_5	0.000
n-C_6	0.007
H_2	0.000
H_2S	0.000
N_2	0.638

Table 6.2 Gas Analysis Results of B.E-1 (Continued)

CO_2	0.013
Mol. Weight, g/mol	16.2
Specific Gravity (Air=1)	0.5579
Critical Pressure, psia	666.0
Critical Temperature °R	343.2
Inferior Calorific Value, kcal/Sm^3	8090
Superior Calorific Value, kcal/Sm^3	8595

XPT measurements are conducted from the Middle Eocene (S Member of K formation) between 1182 m and 1452 m and Lower Eocene (A Member of K Formation) between 1452 m and 1934 m. However identified gas zone from the log and XPT data is between 1453.5-1490.5 m. This all thickness is not the net productive sandstone due to shaly bands. Thickness used in well test interpretation will be determined from the Density-Neutron, Resistivity Logs and XPT results. As shown in the Table 6.3, gas intake from the two productive zone is highlighted with red. First one is a 1 m productive zone between 1454 m and 1455 m. Second zone is 7 m between 1483 m and 1490 m. Totally 8 m productive sands exist in Lower Eocene A Member of K Formation.

In Figure 6.6, drawdowns mobilities (md/cp) are plotted versus depth. In the lower zones of the A Member of K Formation, there is gas intake (Table 6.3). However the drawdown mobilities in the lower zones shown in Figure 6.6 are very low. High values of drawdown motilities are observed between 1454 to 1455 m and 1483 to1490 m that are the productive zones.

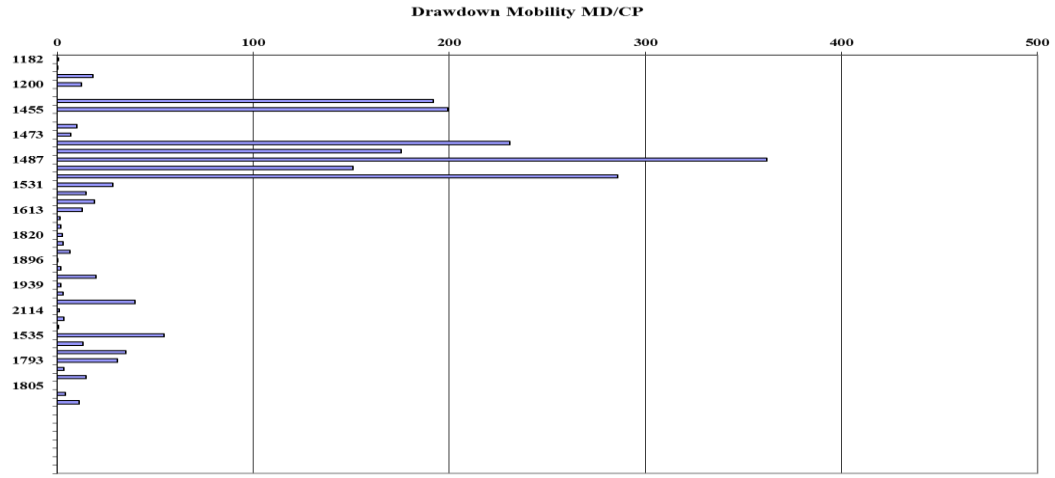

Figure 6.5 Drawdown Mobility (md/cp) vs. TVD Graph of XPT Pressure Results

Table 6.3 XPT Log Results

TEST	DEPTH	TVD	Drawdown Mobility MD/CP	Last read build-up Prs (PSIA)	TEST TYPE	Fluid Intake
1	**1182**	1047	0.80			LOST SEAL
2	**1187**	1052	0.10			DRY TEST
3	**1198**	1062	18.00			Manuel 5 cc
4	**1200**	1064	12.20			DRY TEST
5	**1232**	1095				LOST SEAL
6	**1454**	1317	191.70	6.71	AA sands	Smart 10cc
7	**1455**	1317	199.40		AA sands	Smart 5cc
8	**1456**	1318				DRY TEST
9	**1468**	1330	10.00			DRY TEST
10	**1473**	1335	6.90			DRY TEST
11	**1483**	1345	230.80	0.06	A sands	Smart 5cc
12	**1485**	1347	175.50	0.48	A sands	Smart 5 10
13	**1487**	1349	362.00	0.07	A sands	Smart 5 10
14	**1488**	1350	151.00	0.13	A sands	Smart 5 10
15	**1490**	1352	286.00		A sands	Smart 5 10
16	**1531**	1393	28.40			smart 5 5
17	**1543**	1405	14.50			smart 5 6
18	**1610**	1472	18.90			smart 5 7
19	**1613**	1475	12.70			Smart 5
20	**1676**	1538	1.50			LOST SEAL, Washout
21	**1787**	1649	1.80			Smart 5 5
22	**1820**	1681	2.60			Manuel 10 10
23	**1833**	1695	2.80			DRY TEST
24	**1853**	1715	6.40			Smart 5cc
25	**1896**	1758	0.40			Smart 5 5
26	**1903**	1765	1.90			Smart 5 5
27	**1904**	1765	19.70			Manuel 0 5 10 10 partial build up
28	**1939**	1801	1.90			Smart 5 6
29	**2049**	1911	3.10			e
30	**2100**	1962	39.5			Manuel 5 10 10 partial build up
31	**2114**	1976	0.90			Manuel 5 5
32	**2143**	2004	3.50			Manuel 5 5 0 5
33	**2161**	2023	0.80			Manuel 5 5 0 5 Supercharged
34	**1535**	1397	54.50			Manual 10 10
35	**1537**	1399	13.00			Manuel 10 10 DRY
36	**1548**	1410	34.90			Manual 10 10 cant penetrate mc
37	**1793**	1655	30.60			Manual 10 10 cant penetrate mc
38	**1797**	1659	3.40			Manual 10 10
39	**1799**	1661	14.60			Manuel 5 10 10 partial build up
40	**1805**	1667	0.4			Manual 0 5 0 5
41	**1811**	1673	4.10			Manual 10 10

Density-Neutron and Gama Ray logs were taken from the Middle Eocene (S Member of Kusuri formation) between 1128 m and 1452 m and Lower Eocene (A Member of Kusuri Formation) between 1452 m and 2198 m. Figure 6.6 shows only the part which includes the

depth between 1450 m. and 1500 m. Those logs also support the results of the XPT measurements. Anomalies from the Neutron-Density Log show that there are productive zones where Gama Ray also shows less shaley formation. First one is between 1454 m and 1455 m and the second zone is between 1482 m and 1491 m. However, Neutron-Density log gives 2 meter more thickness than XPT measurement results.

From this interval average porosity value is determined as 27% from the Density-Neutron log. Porosity values for each depth vary between 24% and 30%.

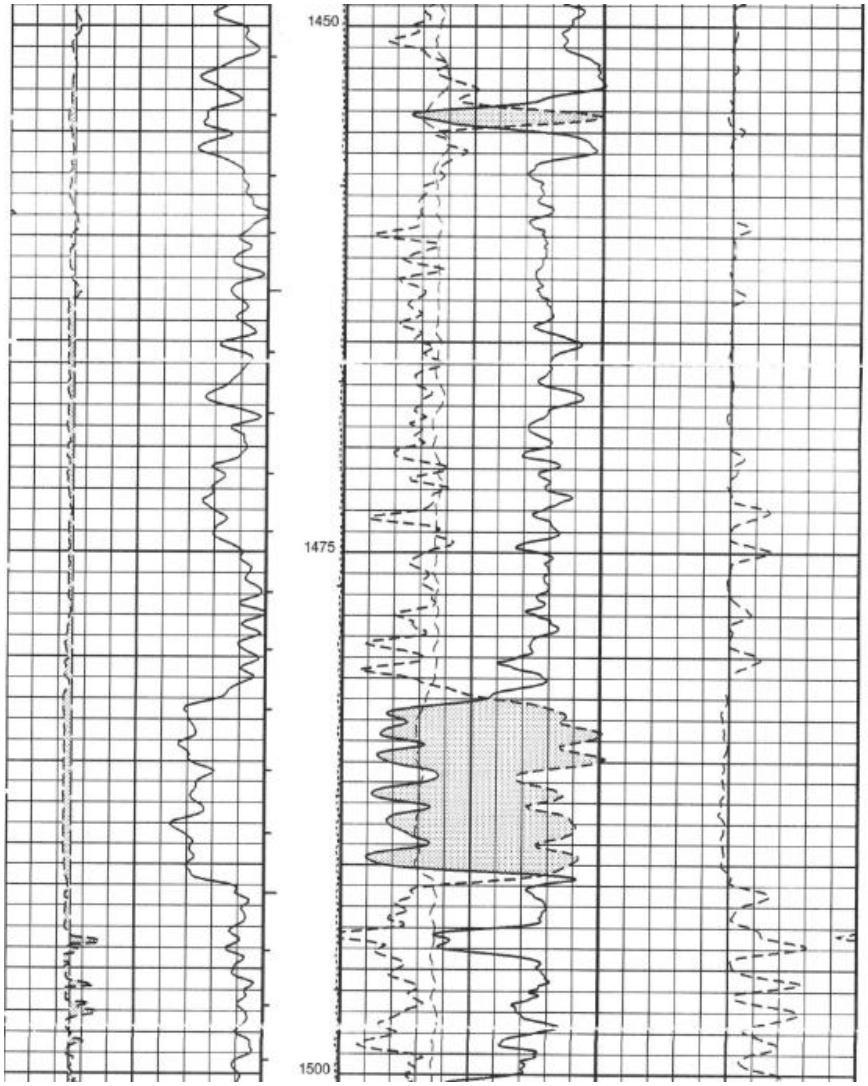

Figure 6.6 Gama Ray and Density-Neutron Log of A Member

Resistivity and Gama Ray logs were taken from the Middle Eocene (S Member of K formation) between 1128 m and 1452 m and Lower Eocene (A Member of K Formation) between 1452 m and 2198 m. Figure 6.7 shows only the part which includes the depth between 1450 m. and 1500 m. Those logs also support the results of the XPT measurements and Neutron-Density log. Anomalies from the Resistivity Log also show that there are

productive zones where resistivity of the formation increases. First one is between 1454 m and 1455 m and the second zone is between 1482 m and 1491 m. Density-Neutron, Resistivity and Gama Ray logs show the same result. However XPT shows 8 m thickness of the productive zones. In well test interpretation, by applying 10% percent error the net thickness range determined between 8 m and 10 m.

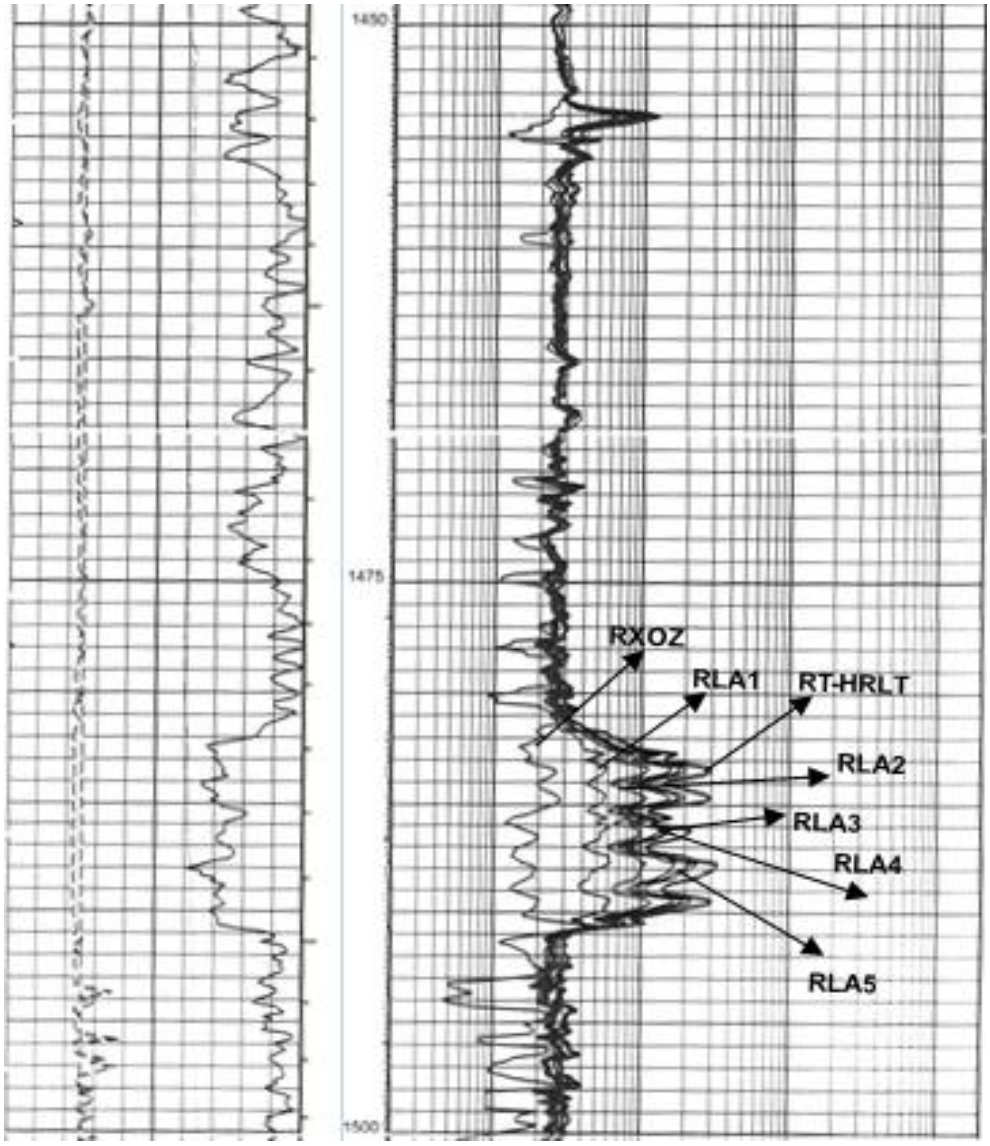

Figure 6.7 Gama Ray and Resistivity Logs of A Member

From Resistivity logs, water saturation was determined as 30%. For shaley sands with 30% porosity, error in water saturation is between %25 and %10 (Mahgoub et al., 2008). By applying 25% error, input range of the water saturation is determined between 22.5% and 37.5%. Unfortunately the most uncertain value is the water saturation therefore the most effected input parameter will be the water saturation.

Another uncertain value is the salinity of water. There is no water production during the well test. Core from the productive formation was not taken due to operational cost. However in well test analysis, specific gravity of water, water formation volume factor and water compressibility are calculated by using the salinity of the formation water. Therefore it is an essential value for a well test analysis. Analogy from the nearest fields was conducted to estimate an accurate value of the formation water salinity. The nearest field is located about 6 km to B.E Field. The furthest field from the B.E field is located 20 km. The salinities of the nearest fields mentioned at the beginning of the chapter alter between 18000 ppm and 40000 ppm. This range is used as an input value of formation water salinity.

CHAPTER-7

METHODOLOGY

In Chapter-5, sources of the error in input parameters were defined and error percentages of the fluid and petrophysical parameters were given from the reference literature. In Chapter-6, all input values used in well test interpretation were defined and range of variables used in this study was determined.

Design of experiment will be conducted with the determined range of the input parameters by using Space Filling Latin Hypercube Design. Ortogonality and the space filling properties of the experimental design will be used to evaluate whether it is a proper design or not.

Then, loading the data, initialization and model fit will be mentioned to analyze the well test. Deconvolution method is applied to the model before the run of the cases obtained from experimental design.

Finally, in the last part, a dimensionless model will be constructed from the results of the runs for screening processes and to make sensitivity analysis. Those screening processes and sensitivity analysis will give the parameters which have a greater effect on the reservoir limit test interpretation results.

7.1 Design of Experiment

Table 7.1 gives the input variables and their range used in well test interpretation runs. There are 6 input parameters which have uncertainty ranges. These parameters are net thickness, porosity, formation compressibility, specific gravity of gas, water salinity and water saturation. Since tested fluid is compressible, viscosity, fluid compressibility and formation volume factor is calculated from correlations by using gas density according to instant pressure. Minimum, actual and maximum values of each parameter are given in the Table 7.1. If factorial design is constructed to consider all possibilities, the number of cases is equal to 3^6 (729 cases). However, such a design gives a large number of cases and does not cover the whole range of each variable. In other words, it uses only maximum, middle and minimum values of input variable instead of the whole space of interval for each input variables.

Table 7.1 Input Variables and Their Range Used in Well Test Interpretation

Input Variables	Error in %	Minimum Value	Actual Value	Maximum Value
Well Diameter (rw), inch			6.17	
Net thickness (h), m	10	8.1	9	9.9
Porosity (Ø), %	12	23.76	27	30.24
Formation Compressibility (Cf). 1/psi	5	2.99E-06	3.14E-06	3.32E-06
Specific Gravity of Gas (ρ)	10	0.5536	0.5579	0.61369
Water Salinity (S), ppm	Analogy	18000	29000	40000
Water Saturation (Sw), %	25	22.5	30	37.5

7.1.1 Space Filling Latin Hypercube Design

In order to decrease the number of cases and cover whole space created by the interval of the input variables, Space Filling Design is used and to obtain maximum uniformity (JMP Guide, 2008). Latin Hypercube Sampling Method is chosen to construct experimental design.

JMP software is used to prepare the Space Filling Latin Hypercube Design which was explained in Chapter-2. While entering the minimum and the maximum values of the input, they are defined as continuous variables in the JMP software. In each interval of the input variable, a random number is selected so that probability of each interval is equal to one cover the case number. While preparing the Space Filling Latin Hypercube Design, two important characteristic of design, space filling properties and orthogonality, should be evaluated whether it is a proper design or not (JMP Guide, 2008).

To check space filling property, discrepancy and Euclidean maximum and minimum distance are examined. Discrepancy shows the integrated difference between the design points of each variable and whether those design points are distributed uniformly or not. Discrepancy changes between 0 and 1. If the discrepancy closes to zero, design is prepared with perfect space filling property. If the discrepancy is close to 1, design is prepared with too few or too many data (JMP Guide, 2008).

Minimum case number is calculated as 7 from the Eqn. 2.2. Therefore selected case numbers started with minimum 10. Table 7.2 shows the design case number and the corresponding discrepancy values. Although minimum case number is 7, first case number with 10 shows that it is not sufficient since the discrepancy number is close to 1. And keep trying with 10 number increments up to reach 100 number of case.

It can be seen in Table 7.2 that as the number of cases increases, the discrepancy values decrease. After 50 case number, there is not much difference in discrepancy. Therefore 50

trials are chosen as case number which proves that it has the better space filling property with a less discrepancy number.

Table 7. 2 Design Case Number and the Corresponding Discrepancy Values

Case Number	Discrepancy
10	0.861
20	0.294
30	0.0167
40	0.0108
50	0.0085
60	0.0067
70	0.0058
80	0.0062
90	0.005
100	0.0041

JMP software normalizes the variables between 0 and 1, and normalized range is divided into number of cases intervals. The design points are chosen randomly in each interval and then points are converted back to their original range. Discrepancy changes with each design due to random selection of design points. To overcome this problem, 10 designs with case number 50 are prepared. The discrepancy values of trial and the corresponding trial values are given in Table 7.3. Discrepancy values vary between 0.0083 and 0.0101. The smallest discrepancy number which is 0.0083 is chosen as experimental design for this study.

Table 7. 3 Discrepancy of each trial

Trial	Discrepancy
1	0.009
2	0.0088
3	0.0087
4	0.0091
5	0.0083
6	0.0101
7	0.0084
8	0.0086
9	0.0093
10	0.0092

In Latin Hypercube Design, almost equal number of variables are selected from the divided intervals. For example, porosity value differs between the 23.76 and 30.24 and for this case interval is divided by 8. Nearly 7 or 8 cases were chosen for each interval. Therefore

distribution of the variables seems like a uniform distribution (Figure 7.1). The other distributions of the input variables are given in Appendix A.

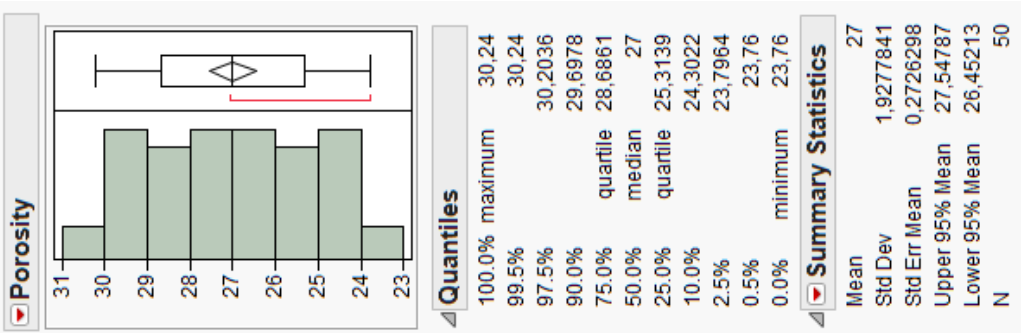

Figure 7.1 Porosity Distribution of Experimental Design

Correlation coefficients are also determined to check whether design parameters were distributed independently or not. Table 7.4 shows that correlation coefficients between variables are close to zero. This means that the experimental design is nearly orthogonal.

Table 7. 4 Correlation Coefficients between all Variables

Variables	Net Thickness	Porosity	Formation Compressibility	Gas Density	Water Salinity	Water Saturation
Net Thickness	-	-0.0731	0.0255	-0.0045	-0.0333	-0.0178
Porosity	-0.0731	-	-0.1244	-0.0365	-0.0119	0.0292
Formation Compressibility	0.0255	-0.1244	-	-0.0120	0.0602	0.0289
Gas Density	-0.0045	-0.0365	-0.0120	-	-0.0127	-0.0100
Water Salinity	-0.0333	-0.0119	0.0602	-0.0127	-	0.0539
Water Saturation	-0.0178	0.0292	0.0289	-0.0100	0.0539	-

Scatter plot matrix and projected distributions of the variables are also examined to check the space filling property of the design. Scatter plot matrix is given in Figure 7.2. Projected distribution of net thickness and porosity is given in Figure 7.3. Other projected distributions between the variables are given Appendix B.

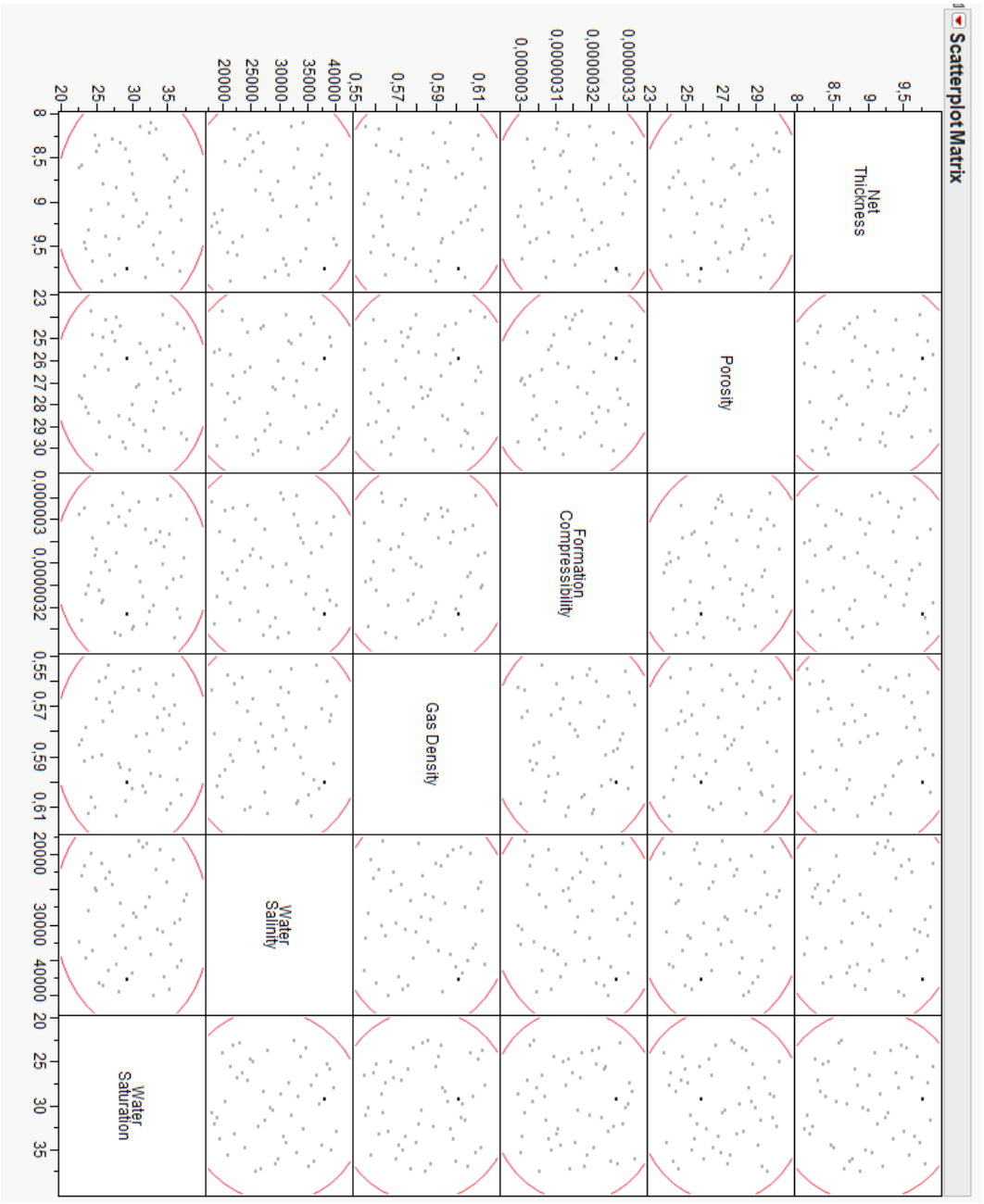

Figure 7.2 Scattered Plot Matrix of Variables

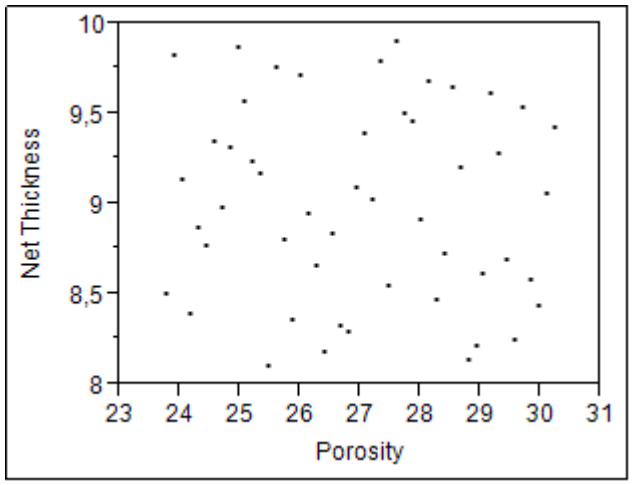

Figure 7.3 Projected Distribution of Net Thickness vs Permeability

Distribution of the Euclidean maximum and minimum distance of the normalized design points are given in Figure 7.4. Distances vary between 0.6552 and 0.702. Distances between the points are so close, meaning that the design of experiment is good enough.

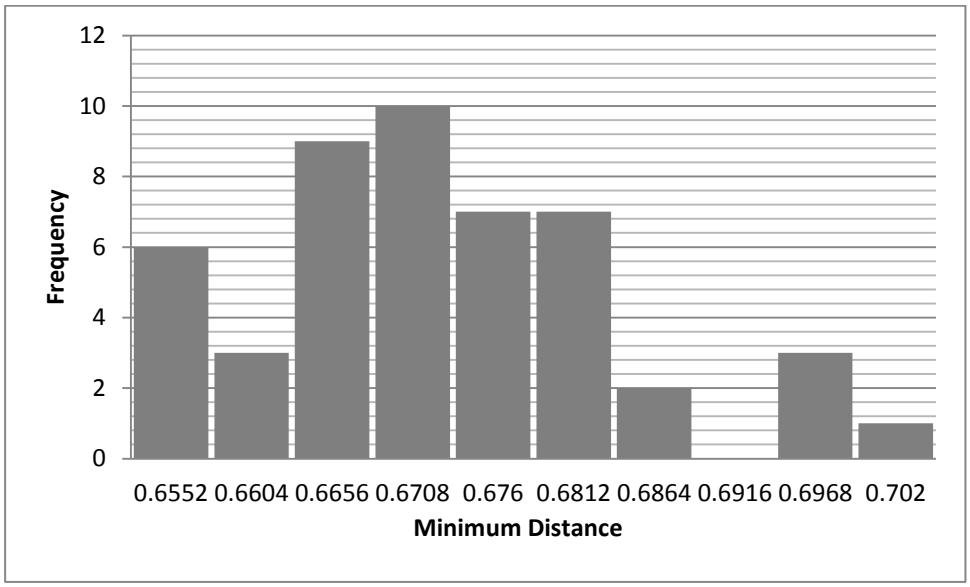

Figure 7.4 Euclidean Maximum Minimum Distance Distribution

After analyzing the discrepancy values of trials, the correlation coefficients between variables, the projected distribution of the variables and Euclidean minimum maximum distance distribution, it can be concluded that the prepared experimental design with 50 cases guarantee the space filling property and the orthogonality. Space Filling Latin Hypercube Design points are given in Appendix C.

7.2 Reservoir Limit Test Interpretation

The Saphir Module of the Ecrin Software is used for the reservoir limit test interpretation.

7.2.1 Initialization

The main options to set up the interpretation process such as type of the fluid and the type of the test must be selected. For this study, the reference fluid is gas and the gas rates were recorded. Oil and water rates are not available because there is no oil and water production during the test. The type of the test conducted for this study is a standard test (Figure 7.5).

Then, to identify the test, required information such as well radius, net thickness and porosity must be entered. Reference time is the time when the first pressure reading is done.

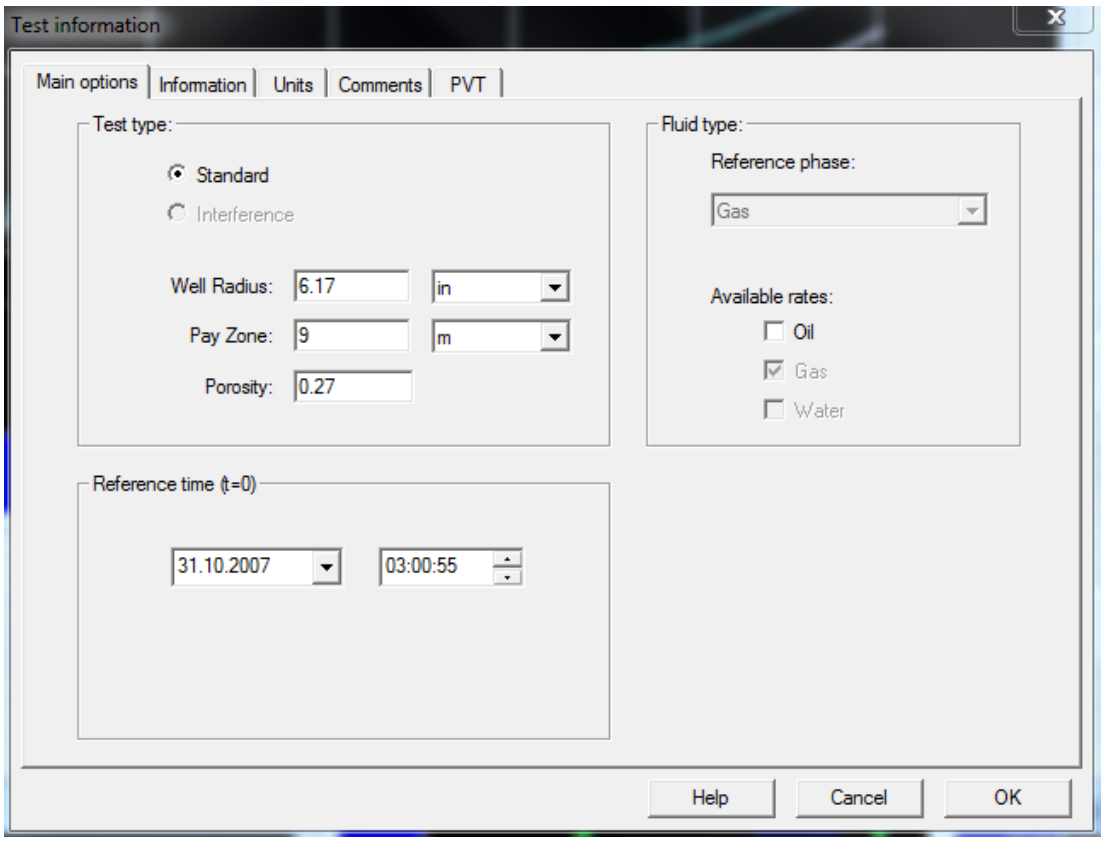

Figure 7.5 Reservoir Limit Test Information

Edition of the PVT parameters initially entered during the first startup process. For a slightly compressible fluid, only few properties are entered as a constant value such as viscosity, total compressibility and formation volume factor. For phase combinations, to calculate the pseudo pressure and pseudo time functions, correlations are required. To calculate this set of data, some fluid and rock properties and reservoir parameters have to be entered. For example, water saturation and formation compressibility is used while calculating the total compressibility (Figure 7.6).

Reservoir pressure and the reservoir temperature recorded from gauge are entered as reservoir parameters. In the reservoir, there are two types of fluid which are gas and residual water. Therefore dry gas and water are defined in the software (Figure 7.7).

After defining fluid types, gas composition is entered to calculate specific gravity and salinity is entered to calculate water density. Then, with the correlations for Z factor, viscosity, compressibility and formation volume factor of the fluids are determined (Figure 7.8 and Figure 7.9).

Determined fluid and petropysical properties in Chapter-6 and the data gathered during the test were entered for the initialization of well test interpretation.

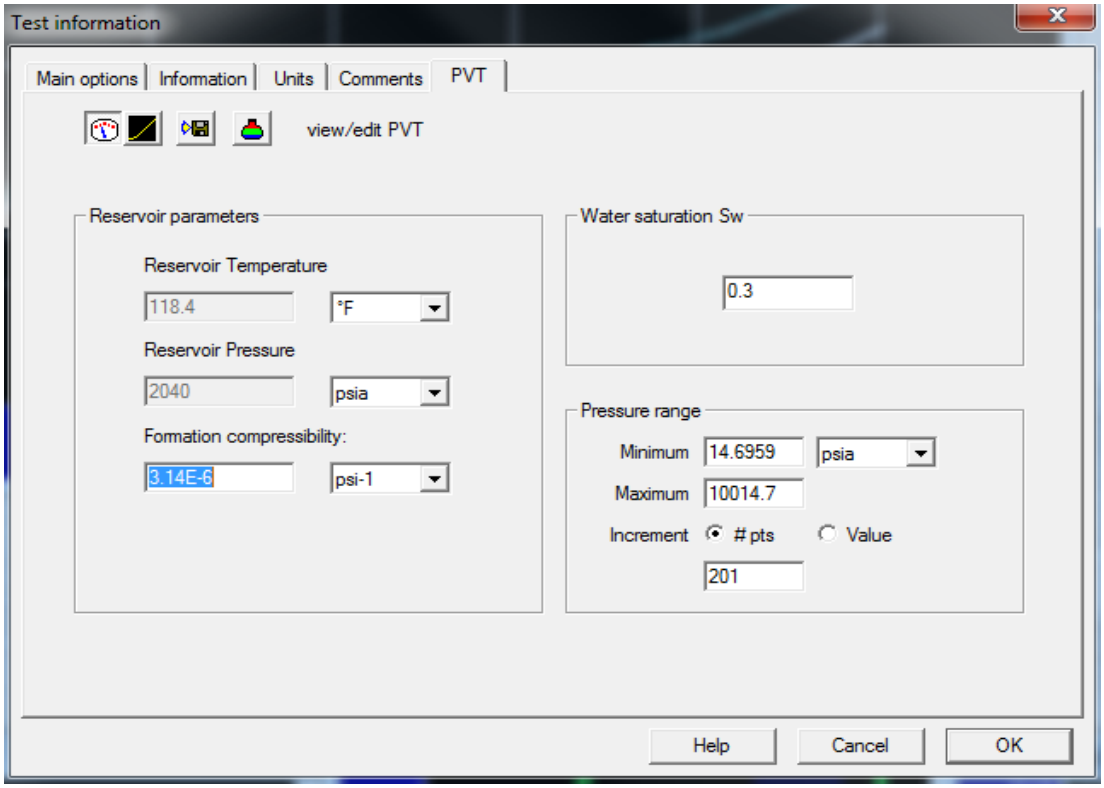

Figure 7.6 Defining Formation Compressibility and Water Saturation

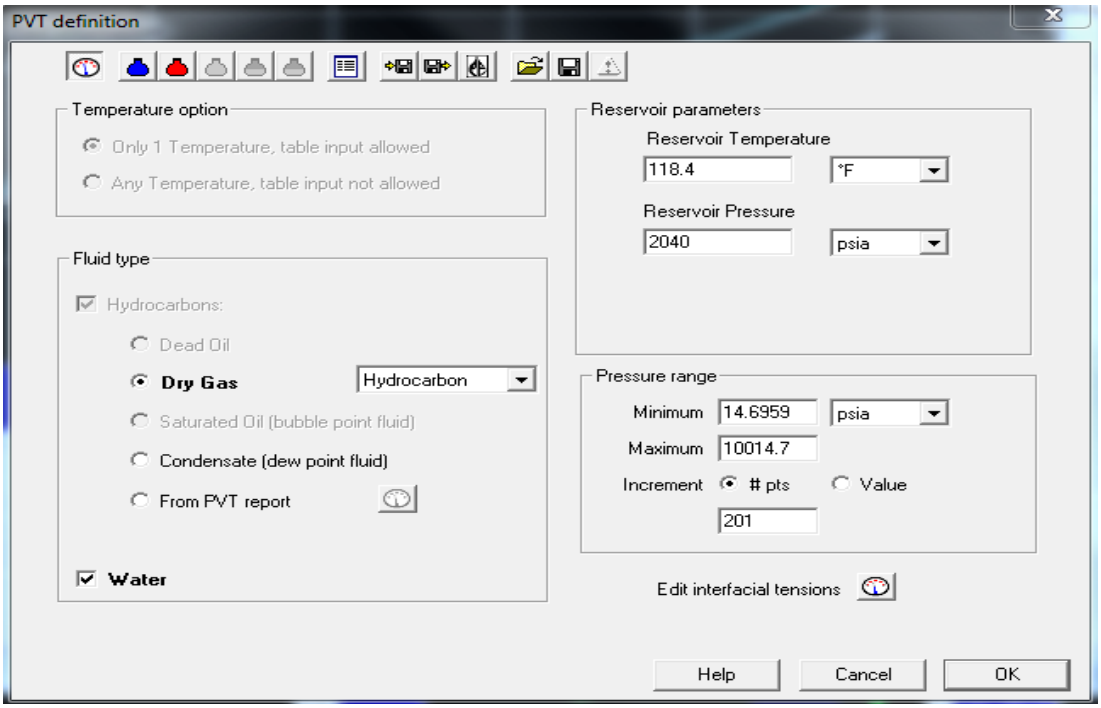

Figure 7.7 Defining fluid type and Reservoir Parameters

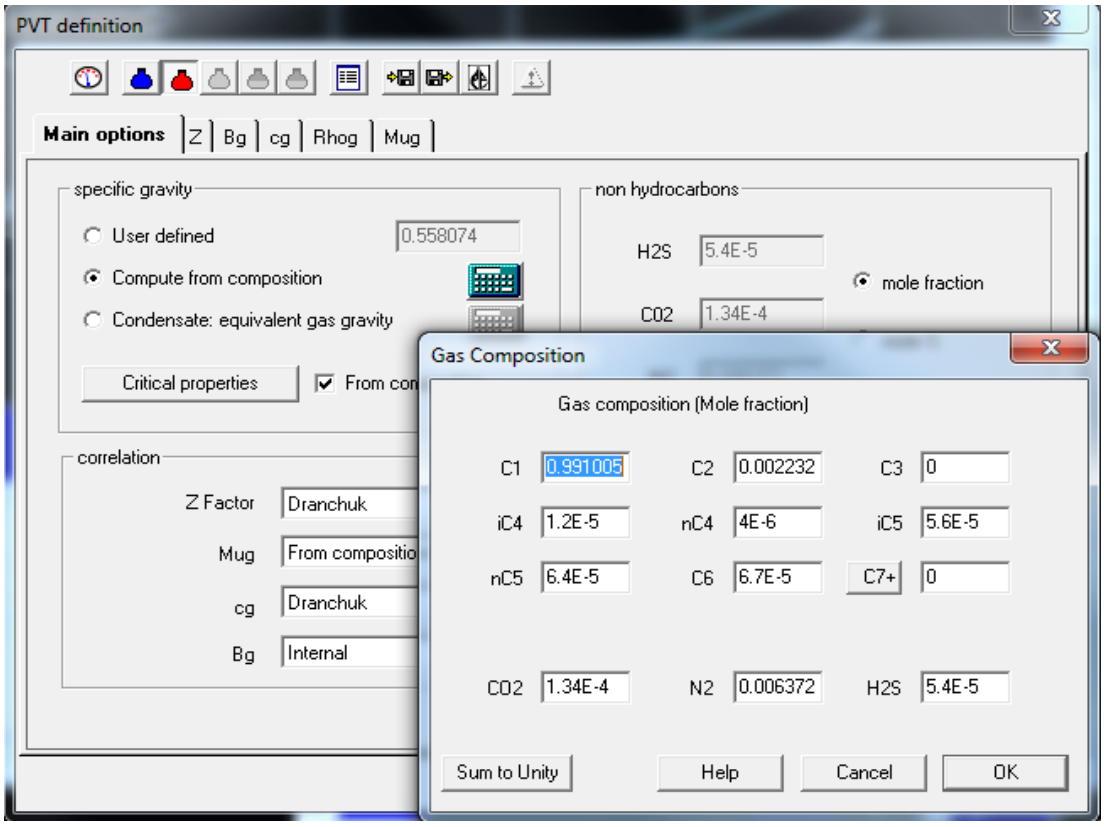

Figure 7.8 Gas Composition and the Correlations to Calculate PVT Properties of Gas

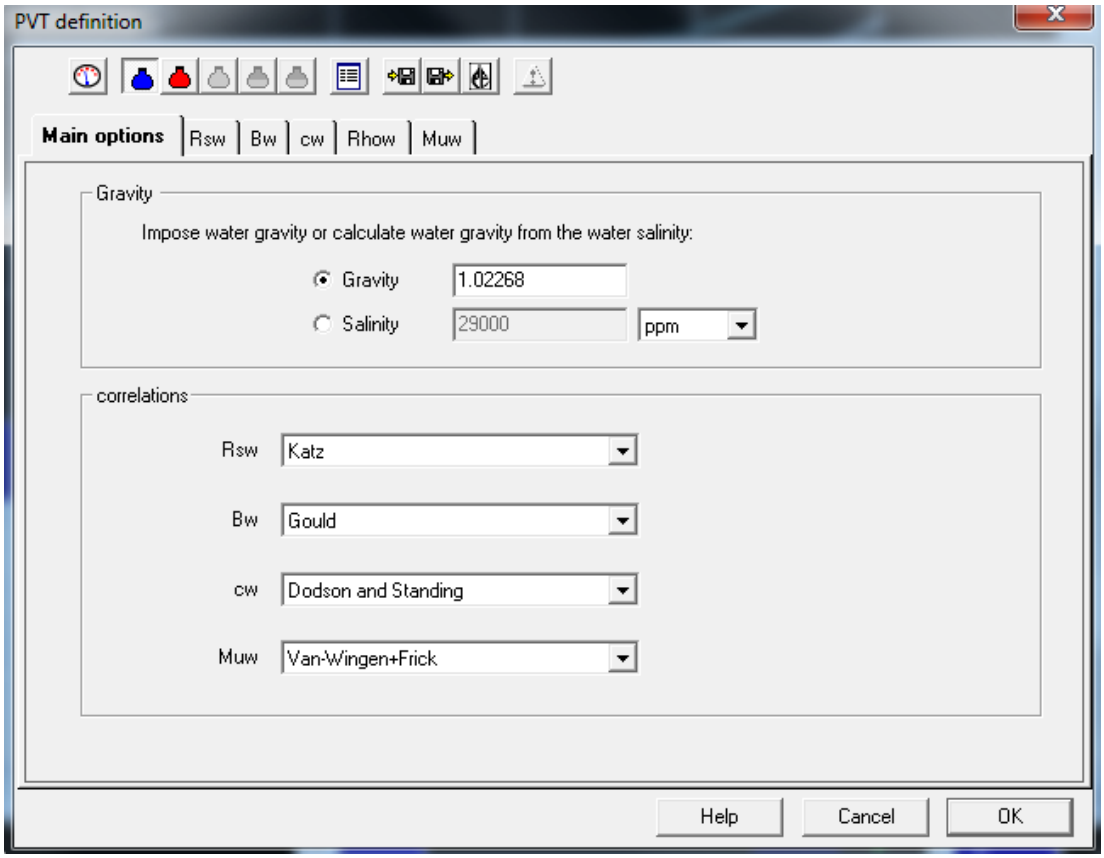

Figure 7.9 Water Salinity and Correlations to Calculate PVT Properties of Water

7.2.2 Loading Data

After initialization, all data acquired from all gauges during the well test was loaded without a filtered subset. Filtering should be applied later if it is necessary. There are three gauges used during reservoir limit test. All of the data from the gauges were loaded to the software. Comparing the data from the gauges is important for the quality assurance and quality control.

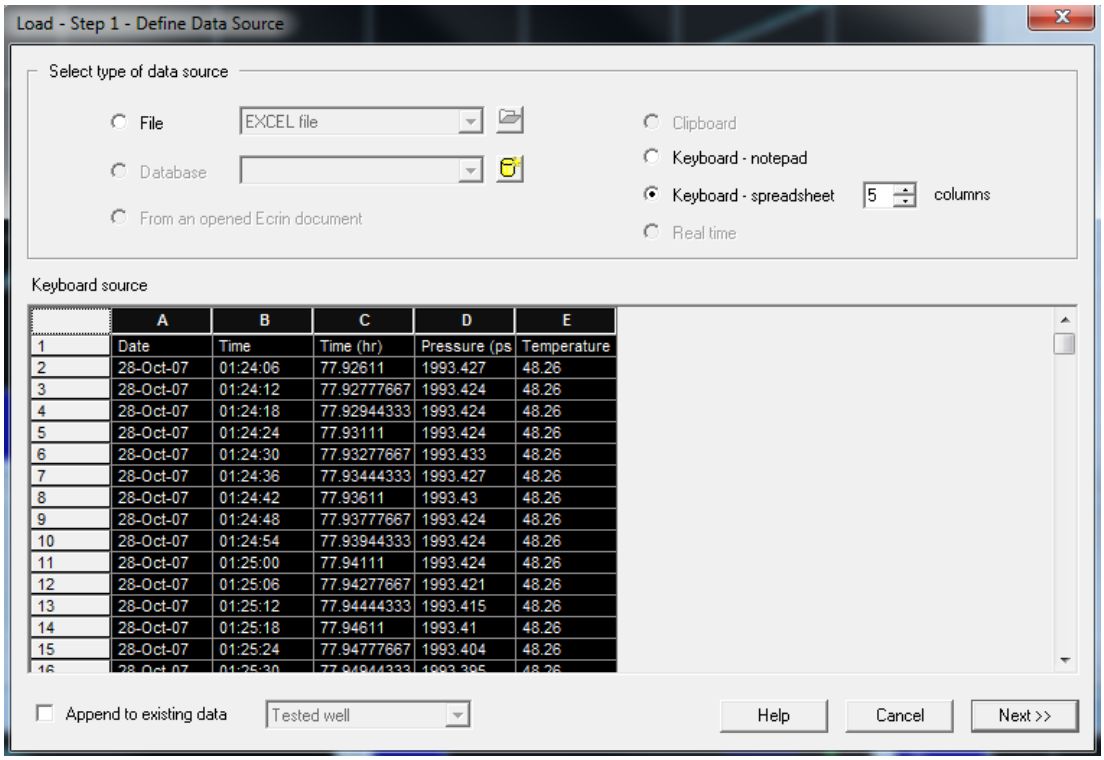

	A	B	C	D	E
1	Date	Time	Time (hr)	Pressure (ps	Temperature
2	28-Oct-07	01:24:06	77.92611	1993.427	48.26
3	28-Oct-07	01:24:12	77.92777667	1993.424	48.26
4	28-Oct-07	01:24:18	77.92944333	1993.424	48.26
5	28-Oct-07	01:24:24	77.93111	1993.424	48.26
6	28-Oct-07	01:24:30	77.93277667	1993.433	48.26
7	28-Oct-07	01:24:36	77.93444333	1993.427	48.26
8	28-Oct-07	01:24:42	77.93611	1993.43	48.26
9	28-Oct-07	01:24:48	77.93777667	1993.424	48.26
10	28-Oct-07	01:24:54	77.93944333	1993.424	48.26
11	28-Oct-07	01:25:00	77.94111	1993.424	48.26
12	28-Oct-07	01:25:06	77.94277667	1993.421	48.26
13	28-Oct-07	01:25:12	77.94444333	1993.415	48.26
14	28-Oct-07	01:25:18	77.94611	1993.41	48.26
15	28-Oct-07	01:25:24	77.94777667	1993.404	48.26

Figure 7.10 Loading the Recorded Pressure and Temperature Data by the Gauges

7.2.3 Quality Assurance and Quality Control

Quality control and quality assurance is the crucial part of the reservoir limit test interpretation and become a growing concern. It includes:

- Detection of failures, drift, clock failure and resolution
- Identification of operational problems
- Discrimination of wellbore effects

In Figure 7.11, recorded pressure by the gauges WTQR 1932, WTQR 2722 and WTQR 779 are drawn versus time to check their synchronization and coherence. Dynamic calculation of the difference between the gauges is an efficient diagnostic tool for quality check. There is not much difference between the recorded gauges except for the beginning of the first flow and end of the third build up as shown pressure differences versus time graph. Other differences can be ignored during well test interpretation. However noisy data part of the third builds up should not be taken into account while modeling because this part can affect the reservoir behavior and mask the behavior.

Except the beginning of the first flow and end of the third build up, small differences show that the absence of operational problems, gauge failure, gauge drift and clock failure.

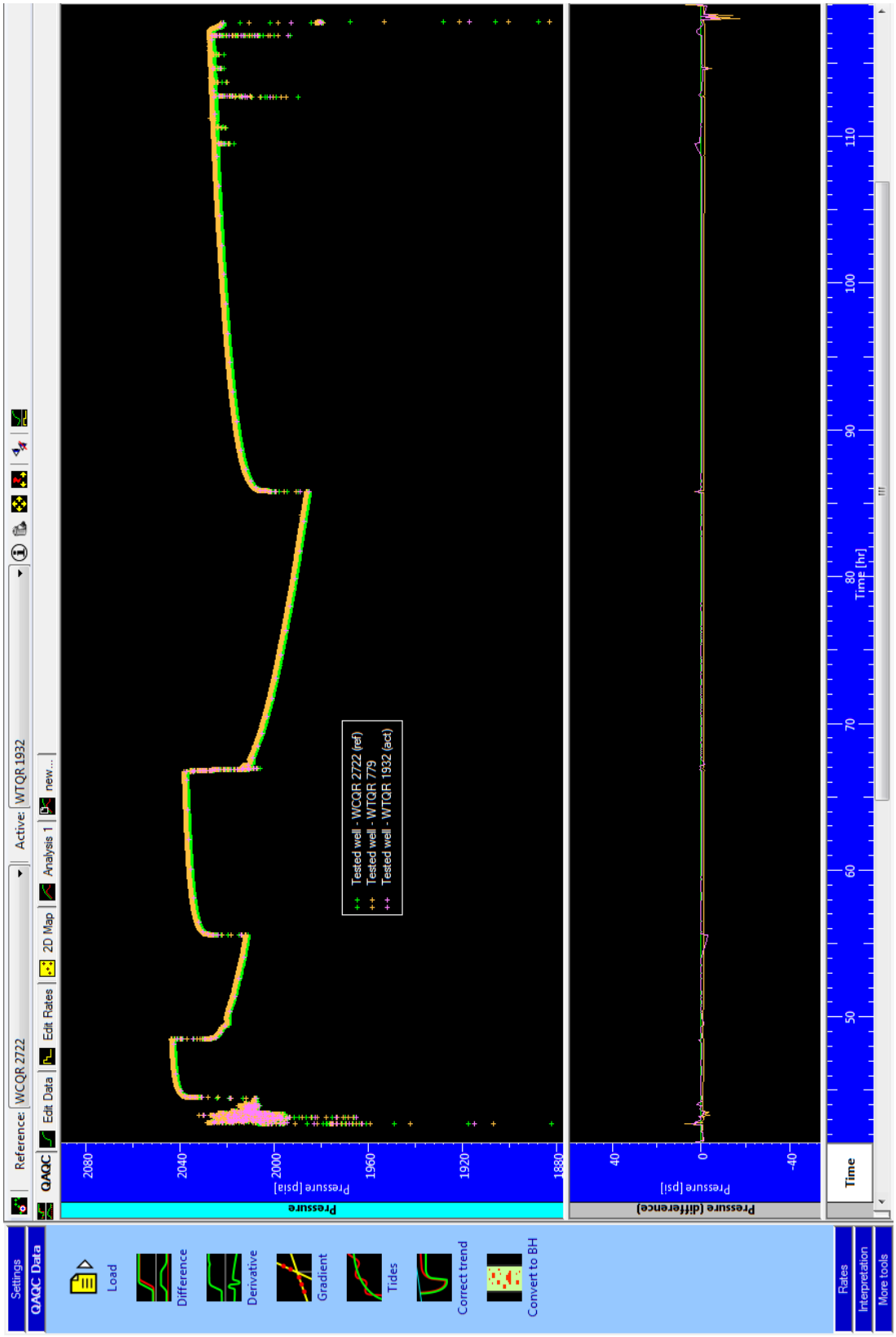

Figure 7.11 Quality Control and Quality Assurance with Triple Gauge

7.2.4 Editing Rate Data

Pressure is recorded from the downhole with memory gauges in real time while rates is still measured at surface with flowmeters and come from the well test report with a different time sampling. After removing of irrelevant and noisy data, time of the gas rate values and the pressure values are synchronized by getting the rate time to the pressure reference time to gather coherent data set.

Build up and shut in periods are identified and the rates are corrected from the cumulative volumes. Rate history is also simplified to reduce the CPU (Central Processing Unit) time required to run the cases.

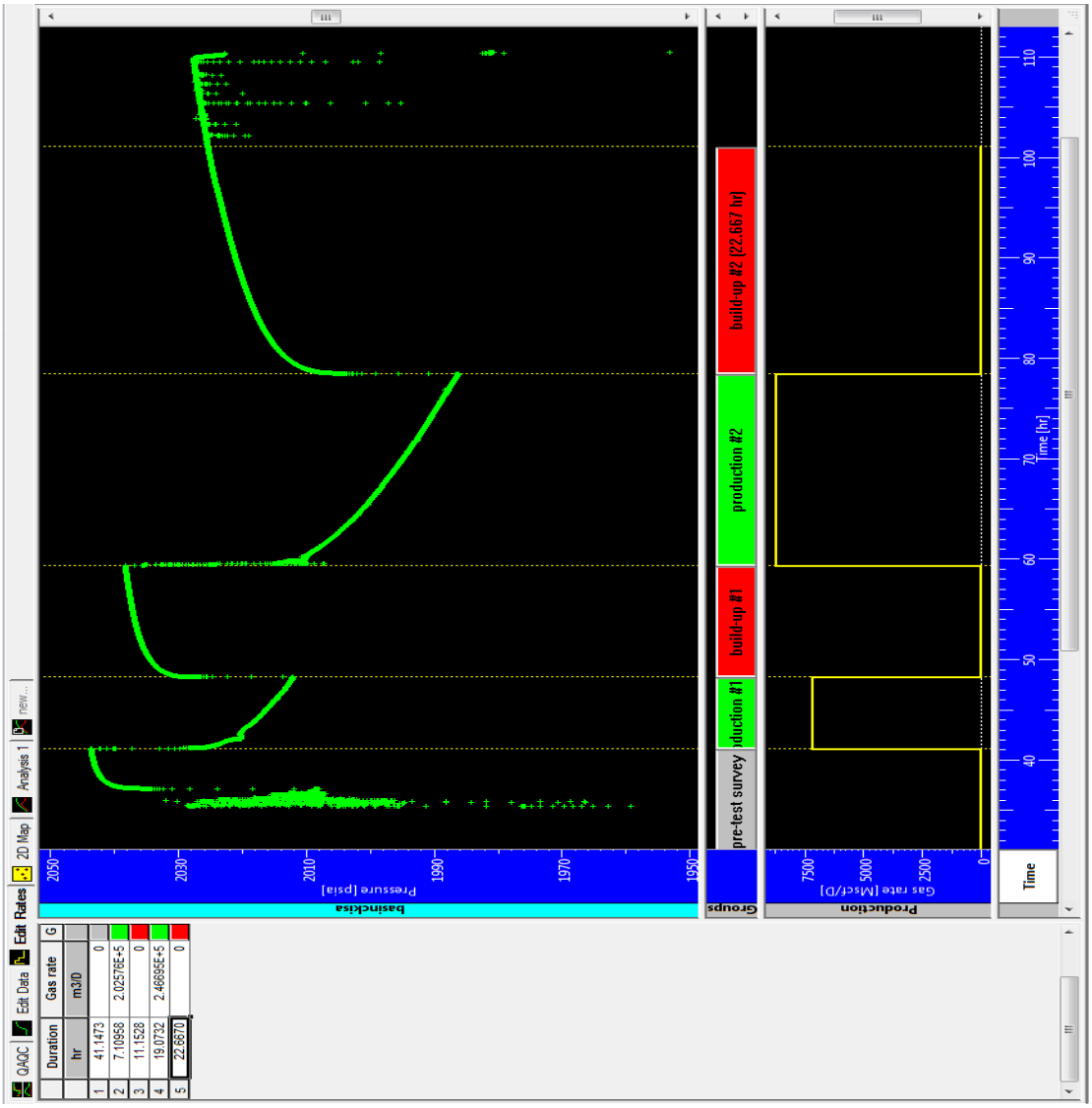

Figure 7.12 Pressure And Rate History Adjustment

7.2.5 Extraction

After pressure and rate data have been synchronized, log-log plots and semi-log plots of three build ups for gauge WCQR 779, WCQR 1932 and WCQR 2722 were extracted and overlaid respectively in Figure 7.13, Figure 7.14 and Figure 7.15. The last and the longest build up in pink color is the best for interpretation because it will give more information about the reservoir. The second and the third build up periods are analyzed in this study.

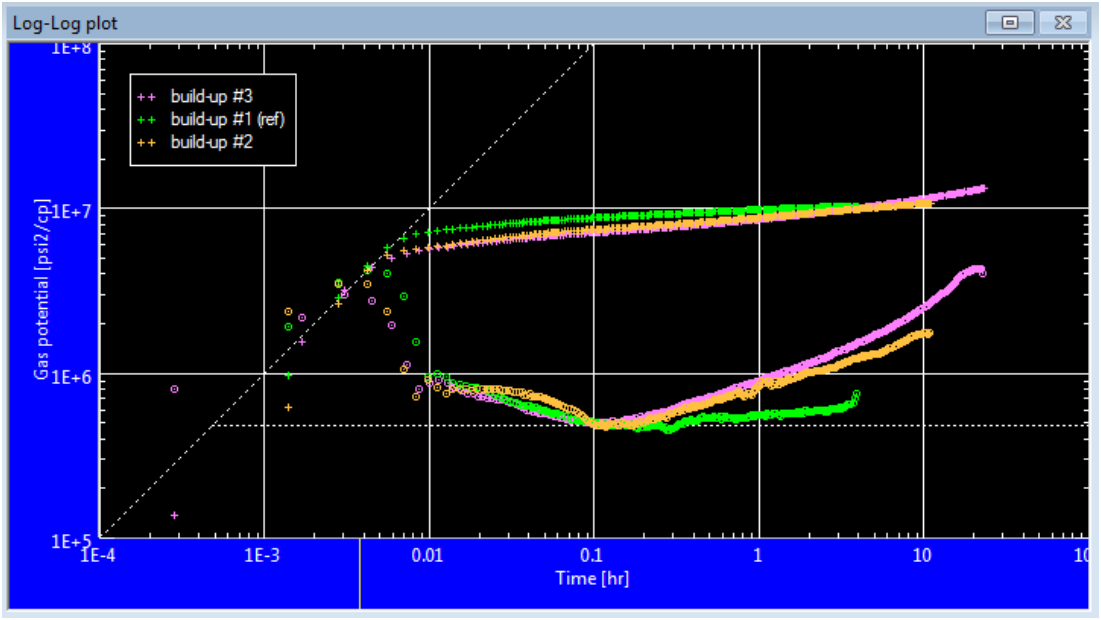

Figure 7.13 Log-log Plot of Three Build ups from Gauge WCQR 779

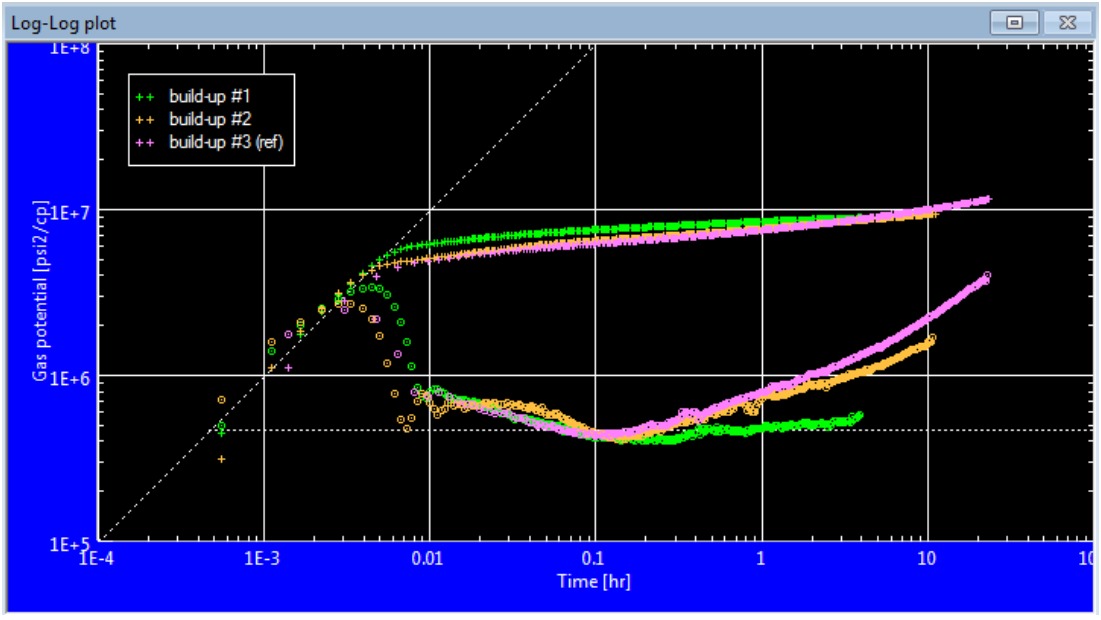

Figure 7.14 Log-log Plot of Three Build ups from Gauge WCQR 1932

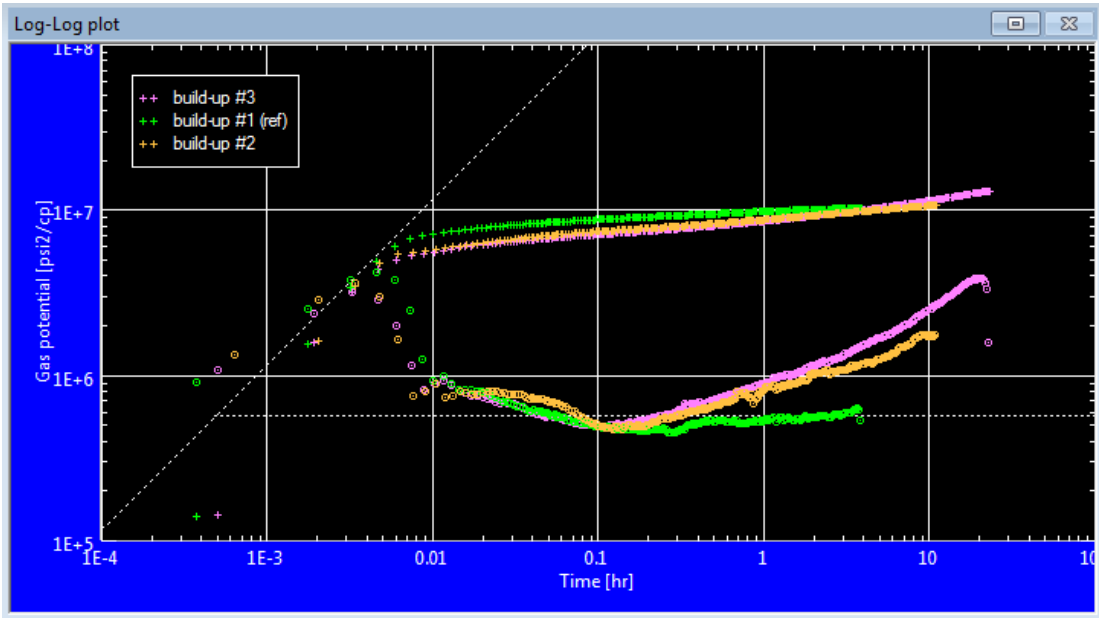

Figure 7.15 Log-log Plot of Three Build ups from Gauge WCQR 2722

To determine the gauge that should be focused on while interpretations, third build up of all gauges were overlaid in Figure 7.16. Log-log plot of gauge WCQR 779 and WCQR 2722 made a hump at the end of the build up, while Log-log plot of gauge WCQR 1932 behaved more straight. These hump may cause wrong interpretation, therefore gauge WCQR 1932 was chosen for well test analyze.

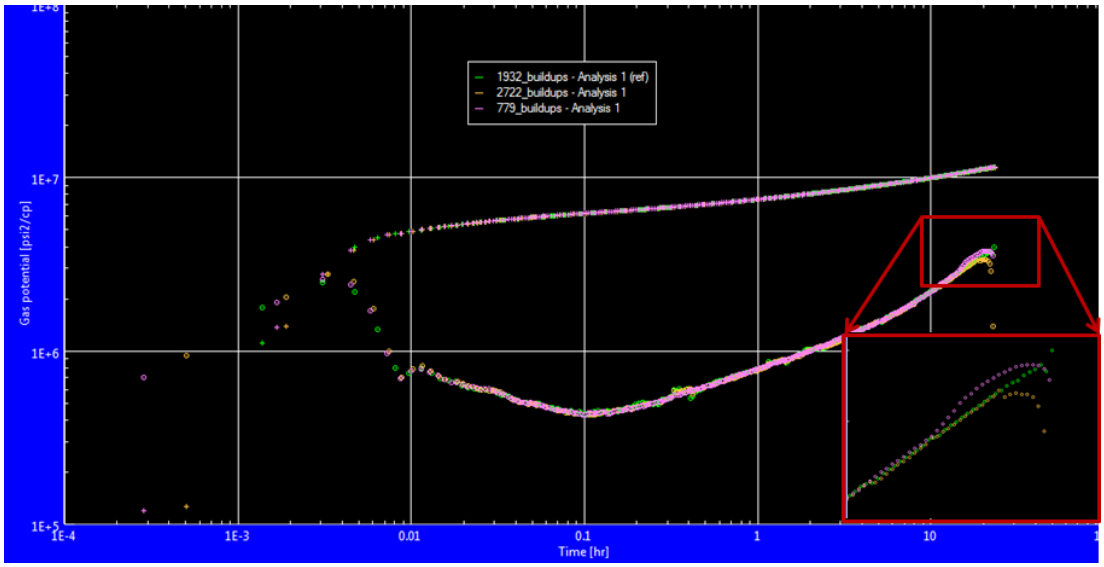

Figure 7.16 Log-Log Plot Of Third Build Up From All Gauges

7.2.6 Diagnostic

Extraction stage is followed by diagnostic stage. To diagnose the well test, first of all horizontal lines for Infinite Acting Radial Flow on Bourdet derivative and a unit slope line for wellbore storage on both pressure and Bourdet derivative must be positioned. The aim is to put these lines on the set of real data. This process provides a quick interpretation of the permeability thickness product and the wellbore storage. Different wellbore storage behaviors are shown in Figure 7.16. This is due to the gauges set at different depths. In other words, the volume between the perforated interval and the gauge is different.

Wellbore storage is an undesirable phenomenon which can delay the time to reach the Infinite Acting Radial Flow and sometimes may masks the Infinite Acting Radial flow behavior. In this test, although wellbore storage delayed the Infinite Acting Radial Flow behavior, the Infinite Acting Radial Flow behavior is not masked.

Infinite Acting Radial Flow is important because it is used to calculate the permeability. Infinite Acting Radial Flow straight line is also used to check the flow rates. Flow rate is a parameter used to calculate the reservoir permeability. The build up period elapsed time can give more information about the boundaries, however all build ups must give the one dignity for reservoir permeability. It can be possible in the event of positioning the Bourdet derivative of three build ups at the same level of Infinite Acting Radial flow. If one of the flow rates used for different build up periods is not correctly measured, Infinite Acting Radial Flow part of Bourdet derivative will take a position below or above the position of other derivatives extracted from other build ups.

In this test, the rate of first flow cannot be measured during the test, while rates of second and third flow were gathered from the flow meter. By guessing the first flow rate, derivative of the first build up was positioned at the derivative level of the second and the third build ups.

7.2.7 Model Generation

After diagnosing the pressure behavior, a model must be selected. The aim is matching the selected model to the pressure response. Wellbore, well test, reservoir and boundary model were selected for interpretation. For B.E Field, constant wellbore storage, vertical well, homogenous reservoir types were chosen (Figure 7.17). After IARF, pressure derivative curve converges up for all build ups. If curve exibits a unit slope, it means that all boundaries are detected and reservoir has a closed boundary. Even in the third build up, curve cannot reach unit slope line. This means the test time is inadequate for detecting the last boundary. That is why second and third build up was interpreted. To estimate the boundaries, deconvolution method was applied. Interpretations of the second and third build up and the deconvolved data will be explained in detail in Result and Discussion Chapter.

Estimated model parameters were input and the model is run. Finally simulated results are compared with the real pressure data in terms of both pressure and Bourdet derivative on the History plot, log-log plot and semi-log plot. To obtain best fit, the estimated parameters were altered and simulation was run again. While estimating parameters, straight lines for wellbore storage, IARF and closed systems were drawn on log-log plot, picking tool corresponding to signature part and trial and error for manual input approaches were used.

To get a good match, model parameters can be changed by manually however, Saphir Module has an "improve" option to fit the curves. Nonlinear Regression is used to refine the parameter estimates by minimizing an error function. All parameters are run manually than checked whether the errors of the match parameters are laerger than 10% or not by "improve" option. In Figure 7.18, the errors of the model parameters are shown. All error percentages of the parameters are below the 1.

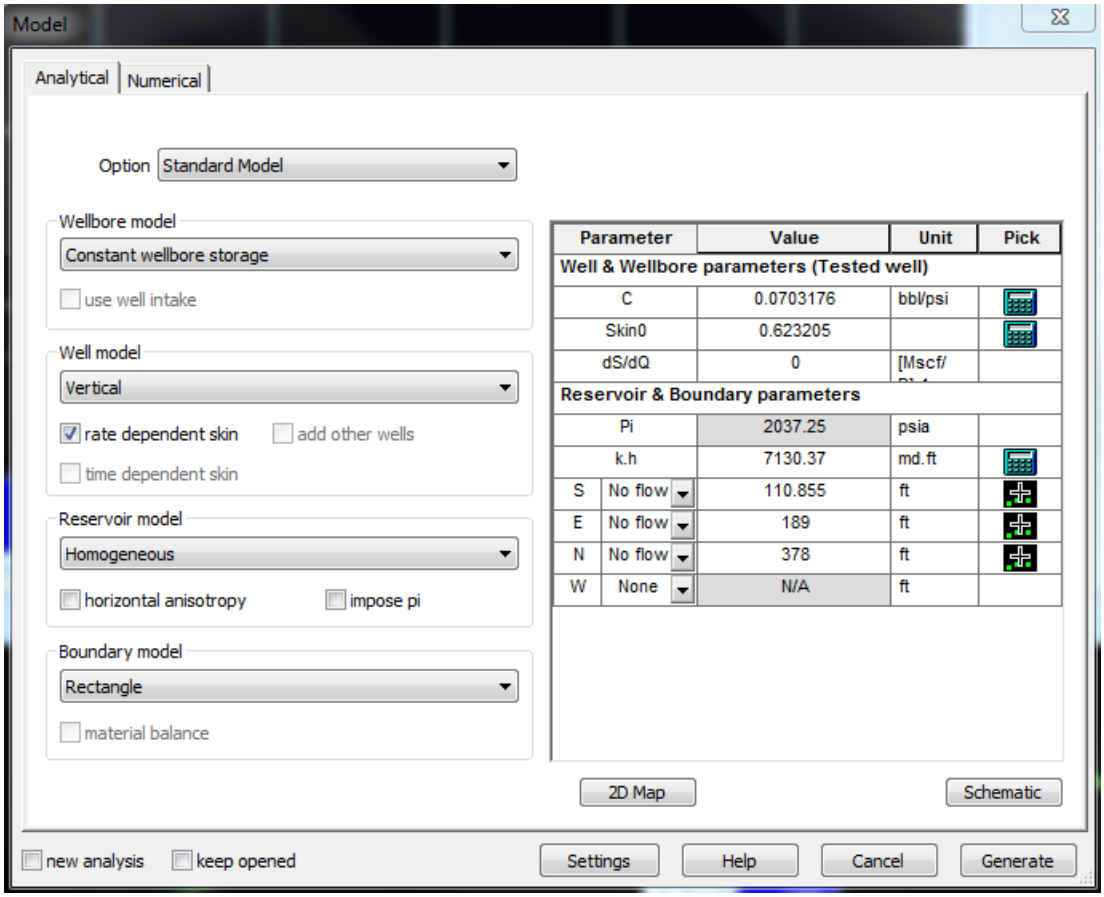

Figure 7.17 Model Selection For Wellbore, Well, Reservoir And Boundary

Parameter	Minimum	Value	Maximum	% Error
C	0.0986	0.0991	0.0996	0.47
Skin	2.13	2.14	2.14	0.11
k	268	269	269	0.13
S	124	125	126	0.52
E	389	391	393	0.51
N	293	294	295	0.3
W	5870	5900	5940	0.56

Figure 7.18 Error % of Model Parameters

After model of the well, wellbore, reservoir and boundary is selected, for all cases obtained from experimental design is run by changing the inputs. The same procedure explained above is applied to all cases.

7.3 Predictive Model Construction

After the runs and matching procedure, a predictive linear model is constructed for closed reservoir by using following equation.

$$y = g(x_1, x_2, \dots., x_k) + \varepsilon \tag{7.1}$$

ε is the error term. Error is assumed to be zero since the model parameters are obtained from the simulation runs instead of experiments. By using same inputs, same results are obtained for computer experiments while conducting experiments in laboratory can produce different results due to experimental set up.

Therefore, the model can be defined by the following equation, where $\vec{x}$ representing the input parameters, $\vec{a}$ representing coefficient matrix and n is the number of input parameters. The coefficients found by minimizing the sum of the squared deviations between the model parameters calculated from the equation and obtained from well test interpretation.

$$f(\vec{x}, \vec{a}) = a_0 + \ a_1 x_1 + \ a_2 x_2 + \ \dots\dots + \ a_n x_n \tag{7.2}$$

JMP software is used to construct the predictive model and sensitivity analyses are conducted from this predictive model.

CHAPTER-8

RESULTS AND DISCUSSION

8.1 Well Test Interpretation

With Saphir module of Kappa Software, 2nd and 3rd shut in periods of the test, namely pressure build up tests are analyzed by both type-curve matching and Horner analyses using the determined fluid and petrophysical properties listed in Figure 7.1. In these analyses, pseudo pressure values which give more accurate results for the gas wells are used. Finally, deconvolution is applied to the analyses in order to obtain the reservoir boundaries more accurately. After interpretation, input values of cases obtained from the experimental design were entered and cases were run to obtain all possible results.

8.1.1 Build-Up Analysis of 2nd Shut-In

The test model is taken as a constant wellbore storage and homogeneous reservoir with rectangle boundaries. Type-curve matching results for the model is given in Figure 8.1 and the Horner analysis is given in Figure 8.2. Specialized lines for well bore storage and IARF were positioned in Figure 8.1. Permeability-thickness product is found to be 8360 mD-ft, permeability is obtained as 283 mD (Table 8.1). Original reservoir pressure is 2040 psia. Only two boundary of the reservoir are seen in second build up. The curve obtained from the simulation result and the test values are shown in Figure 8.3.

Table 8.1 Pressure Build up Test Results of 2nd Shut-in

Model Parameters	**Results**
Reservoir pressure, Pi – psia	2040
Permeability – Thickness, kh – Md.ft	8360
Permeability, k – mD	283
Wellbore storage coefficient, C – bbl/psi	0.099
Skin factor, S	1.86
d1, ft	125
d2, ft	296

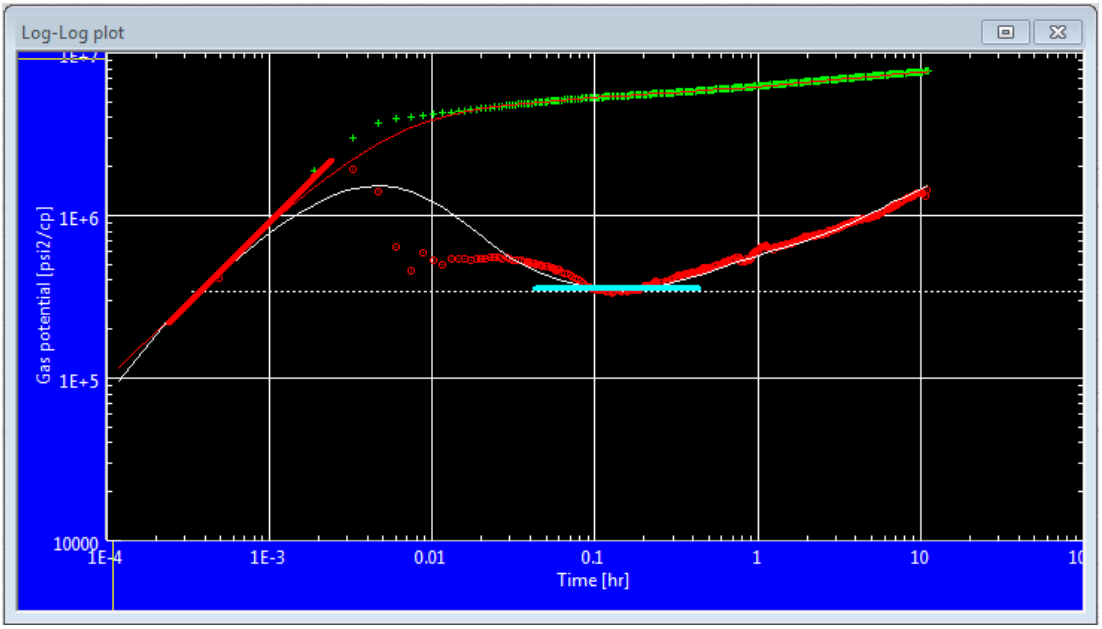

Figure 8.1 Type-Curve Matching of Build-up 2

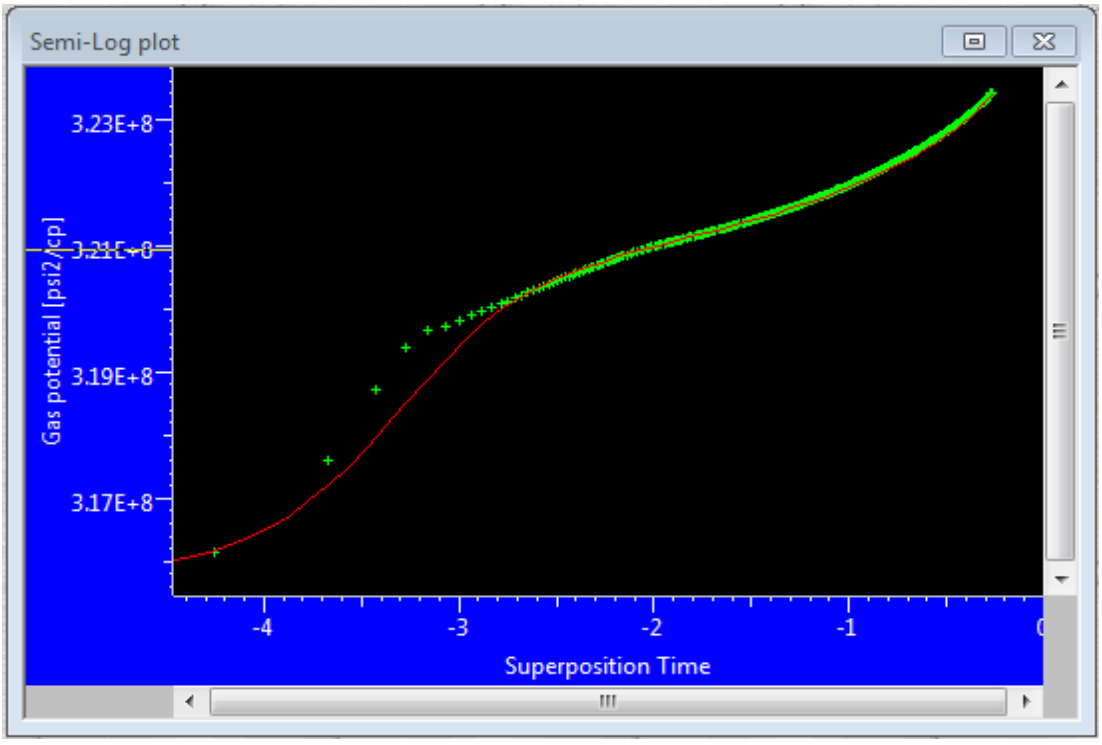

Figure 8.2 Horner Analysis of Build up-2

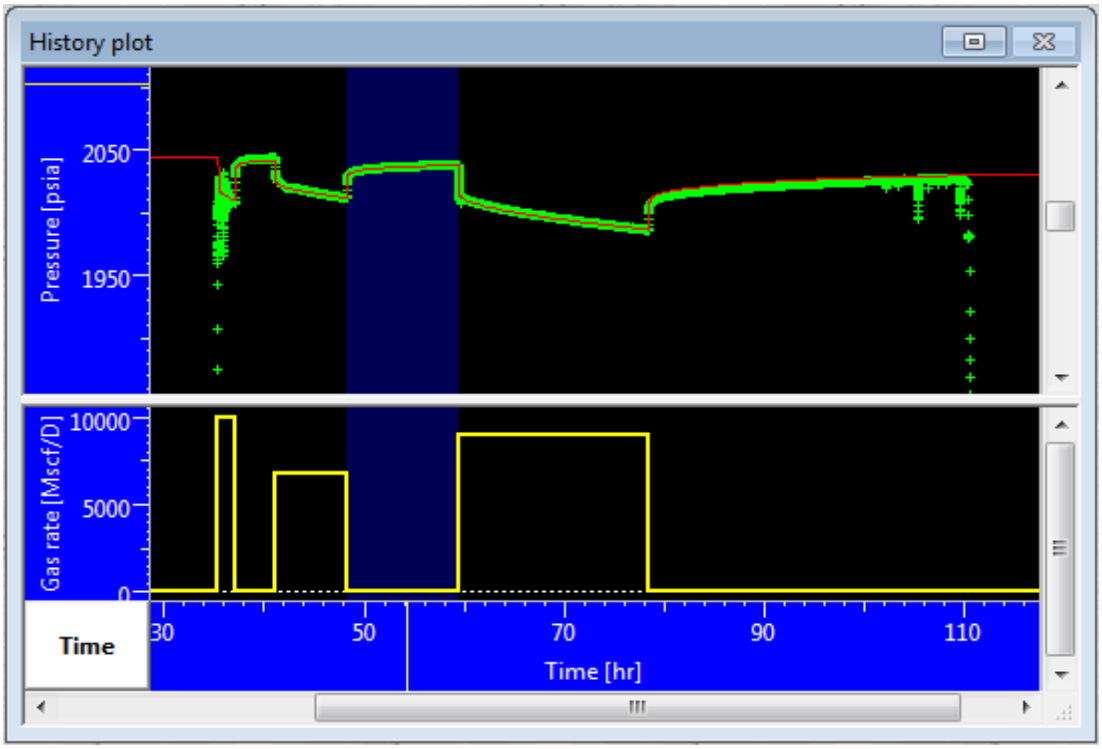

Figure 8.3 Simulation Result and the Test Values of Build-Up 2

8.1.2 Build-Up Analysis of 3rd Shut-In

The test model is taken same as model of the second build up. Type-curve matching for the model is given in Figure 8.4 and the Horner analysis is given in Figure 8.5. Specialized lines for well bore storage and IARF were positioned in Figure 8.4. For a closed system derivative curve shows a unit slopebehavior at the end. However in the 3rd build 3rd boundary is seen. Therefore curve could not act like a unit slope line. Permeability-thickness product is found to be 7970 mD-ft, permeability is obtained as 270 mD (Table 8.2).

Table 8.2 Pressure Build up Test Results of 3rd Shut-in

Model Parameters	**Results**
Reservoir pressure, Pi – psia	2042
Permeability – Thickness, kh – Md.ft	8140
Permeability, k – mD	270
Wellbore storage coefficient, C – bbl/psi	0.0772
Skin factor, S	0.918
d1, ft	126
d2, ft	257
d3, ft	432

Original reservoir pressure is 2042 psia. The curve obtained from the simulation result and the test values are shown in Figure 8.6. Late time of the model does not match the derivative of the test due to the superposition effects.

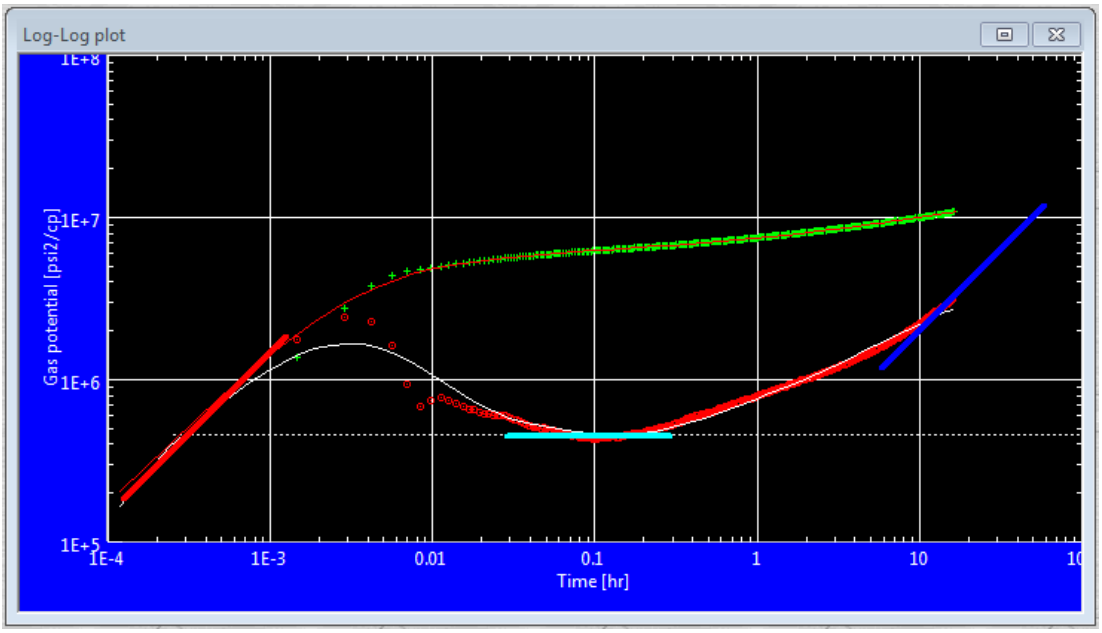

Figure 8.4 Type-Curve Matching of Build-up 3

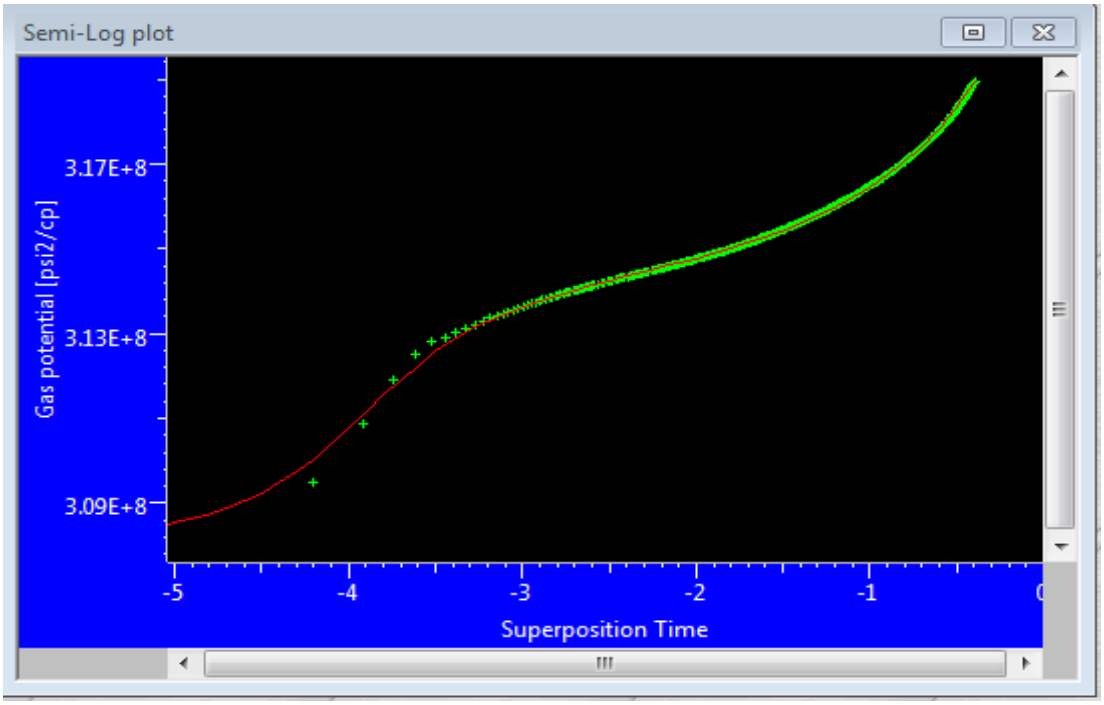

Figure 8.5 Horner Analysis of Build up-3

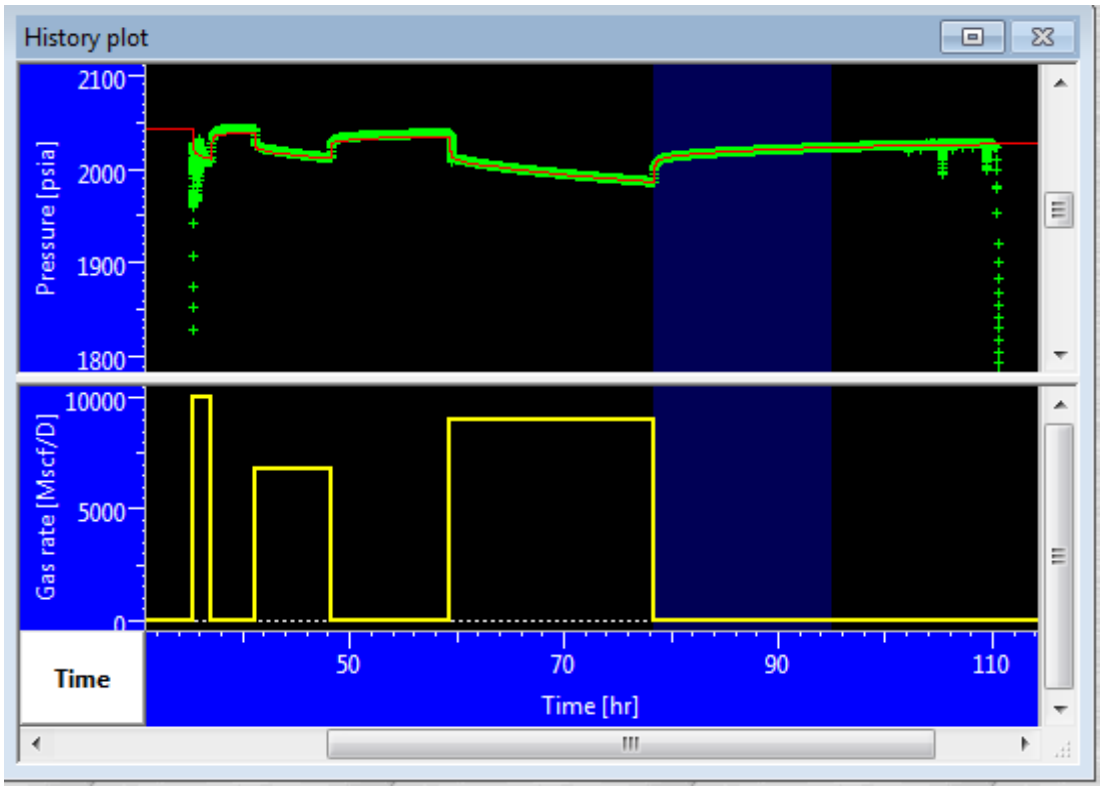

Figure 8.6 Simulation Result and the Test Values of Build-Up 3

8.1.3 Deconvolution Analaysis

Deconvolution is applied to the matched log-log plots of 2nd and 3rd shut-in periods in order to determine the original reservoir pressure before the test and the reservoir boundaries. To obtain the original reservoir pressure deconvoluted reservoir models chosen for these build-up periods should match together. By forcing initial reservoir pressure to 2047 psia for models of both 2nd and 3rd shut-in periods, deconvolution applications of these periods match (Figure 8.7). Thus it is concluded that the original reservoir pressure before the flow test is 2047 psia and material balance and absolute open flow potential calculations are performed using this value.

Deconvolution analysis gives a model of homogeneous reservoir with no-flow rectangle boundaries. Type-curve matching for the model is given in Figure 8.8 and the Horner analysis is given in Figure 8.9. Permeability-thickness product is found to be 7300 mD-ft, permeability is obtained as 247 mD (Table 8.3). Original reservoir pressure is 2047 psia. The curve obtained from the simulation result and the test values are shown in Figure 8.10. Sensitivity analysis is applied to the 4th reservoir boundary to determine the minimum reservoir extension thus the minimum boundary matching the model is chosen (Figure 8.11).

Table 8.3 Pressure Build up Test Results of Deconvolution of 3rd Shut-In

Model Parameters	**Results**
Reservoir pressure, Pi – psia	2047
Permeability – Thickness, kh – Md.ft	7300
Permeability, k – mD	247
Wellbore storage coefficient, C – bbl/psi	0.0995
Skin factor, S	2.17
d1, ft	124
d2, ft	295
d3, ft	390
d4, ft	5890

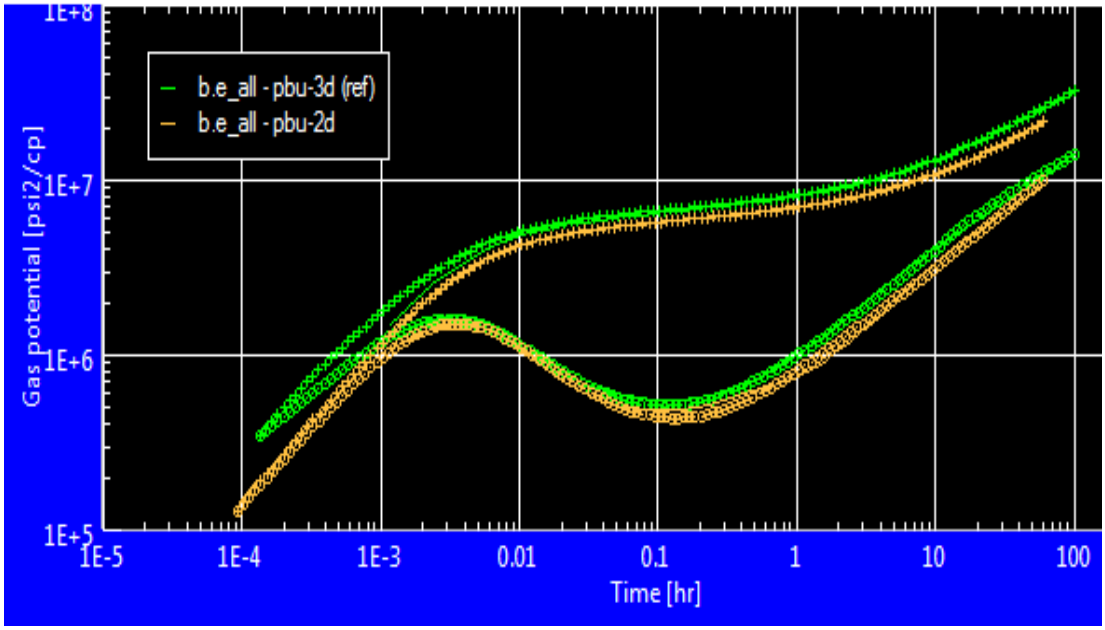

Figure 8.7 Deconvolution Match of Build-up 2 and Build up-3

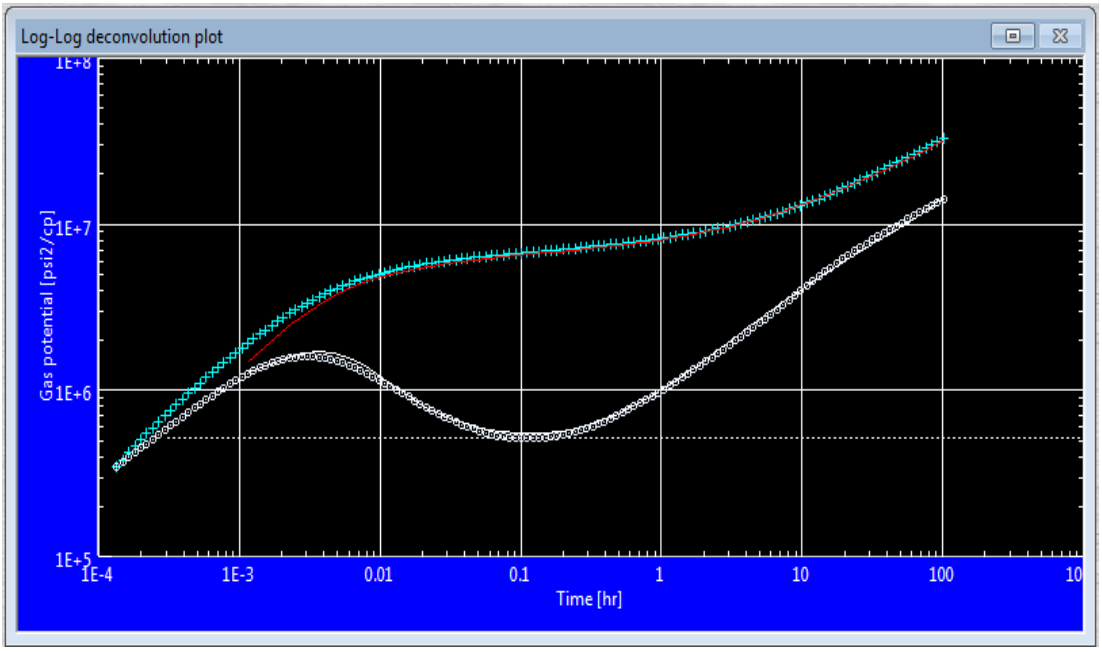

Figure 8.8 Deconvolution Analysis of Build-up-3

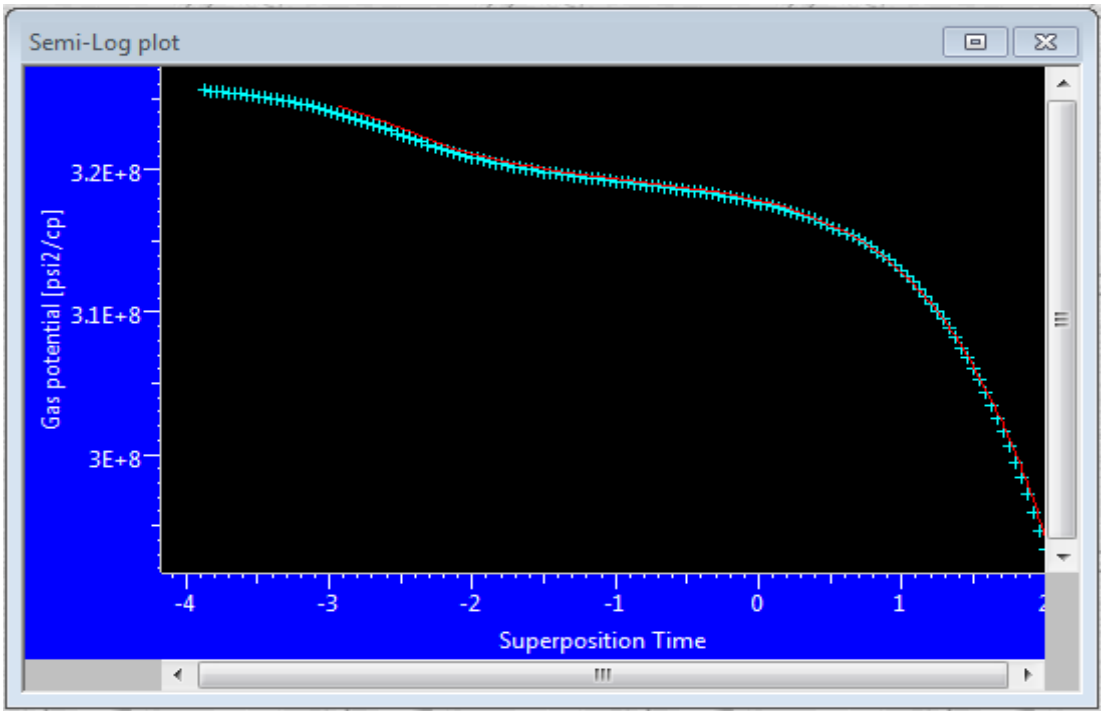

Figure 8.9 Horner Analysis of Build up-3

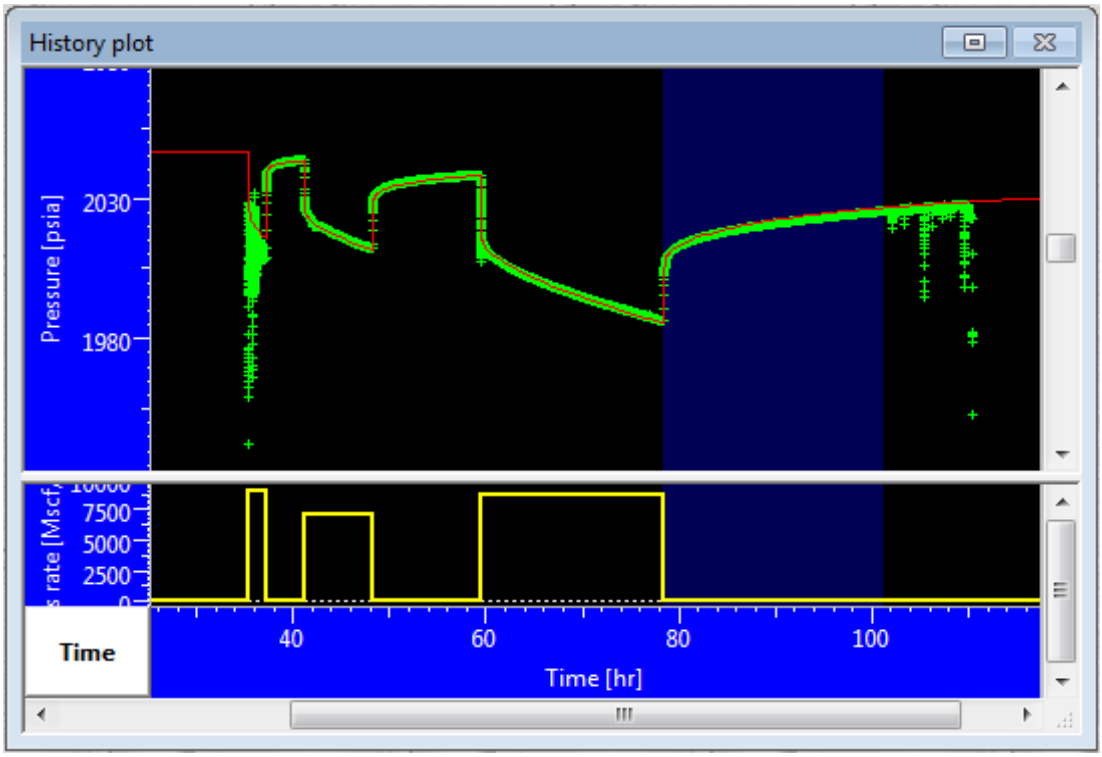

Figure 8.10 Simulation Result and the Test Values of Deconvolution

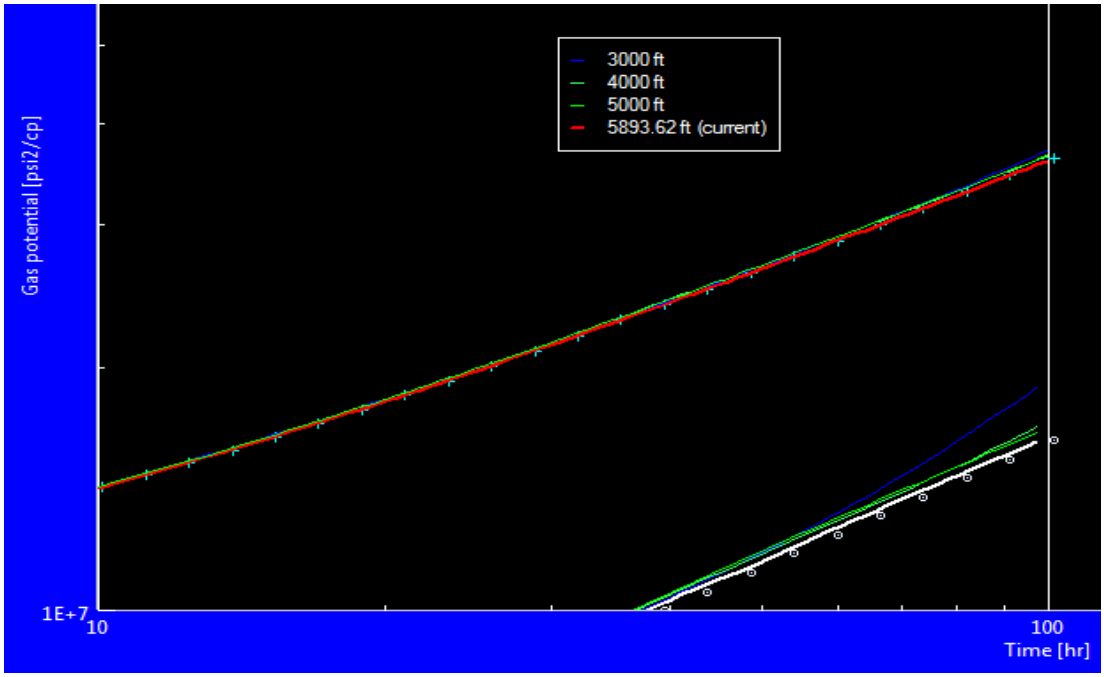

Figure 8.11 Sensitivity Analyze for 4th Boundary

Results of 2nd build up, 3rd build up and deconvolved data is given in Table 8.4.

Table 8.4 Results of 2nd Build up, 3rd Build up and Deconvolved data

Model Parameters	**Results of 2nd build up**	**Results of 3rd build up**	**Results of Deconvolution**
Reservoir pressure, Pi – psia	2040	2042	2047
Permeability – Thickness, kh – Md.ft	8360	8140	7300
Permeability, k – mD	283	270	247
Wellbore storage coefficient, C – bbl/psi	0.099	0.0772	0.0995
Skin factor, S	1.86	0.918	2.17
d1, ft	125	126	124
d2, ft	296	257	295
d3, ft		432	390
d4, ft			5890

8.2 Constructed Predictive Model and Sensitivity Analyses

After running all cases, a predictive model was constructed with the simulation results by using the JMP Software. While constructing predictive model Least Squares Method was used. The aim is minimizing the sum of the squared deviation between the model parameters obtained from simulation cases and the predictive equation. For each model parameter, an equation which includes the input parameters was obtained.

Finally, from the constructed predictive models for each model parameter sensitivity analyses were conducted to find the input parameter which has an impact on that model parameter. In order to analyze in detail, effect tests, scaled and sorted parameter estimations were conducted. Pareto plots and Leverage plots were drawn. Prediction profilers of the model parameters were developed.

8.2.1 Skin

Skin can be modeled by equivalent wellbore radius since it is related to wellbore radius. However for wellbore radius of B.E-1, 6.17" which is the inner diameter of the casing is the only dignity. If the test conducted in B.E-1 was an openhole test, skin would change according to openhole radius. Since it is a cased hole, skin is not expected to change. Skin mostly depends on wellbore radius, nonetheless it varies with porosity, net thickness and water saturation.

A linear predictive model constructed for skin is shown in Figure 8.12. Solid lines show the 45° line used to see how values obtained from predictive model coincides with values obtained from simulation. Dashed red lines show the 45° line used to see confidence intervals. RSq is the correlation coefficient and RMSE is the sum of the root mean squared

error. For predictive model of the skin, correlation coefficient is high and the sum of the root mean square is low. This means that the construction of linear predictive model to estimate skin is a representative model.

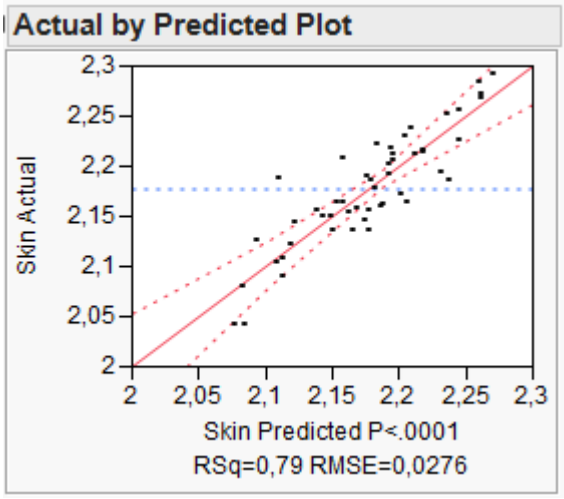

Figure 8.12 Linear Predictive Model Fit of Skin

Following equation belongs to the model of the skin. And the summary of the fit between the actual value of skin obtained from simulation and the equation is given in Table 8.4.

Prediction Expression

$$2{,}17717605784 + 0{,}05620274143236 * \left(\frac{(\text{Net Thickness} - 9)}{0{,}9}\right) + 0{,}04936309787091 * \left(\frac{(\text{Porosity} - 27)}{3{,}24}\right) - 0{,}0000837850197 * \left(\frac{(\text{Formation Compressibility} - 0{,}000003155)}{0{,}000000165}\right) + 0{,}00692942997633 * \left(\frac{(\text{Gas Density} - 0{,}583645)}{0{,}030045}\right) - 0{,}0050618679559 * \left(\frac{(\text{Water Salinity} - 29000)}{11000}\right) - 0{,}0425109312947 * \left(\frac{(\text{Water Saturation} - 30)}{7{,}5}\right)$$

Table 8.5 Statistical Parameters of Linear Predictive Model of Skin

Summary of Fit	
RSquare	0,78941
RSquare Adj	0,760025
Root Mean Square Error	0,027565
Mean of Response	2,177176
Observations (or Sum Wgts)	50

After model construction, sensitivity analysis is conducted to detect the effect of the input parameters on skin. In sorted parameter estimates, input parameters are sorted on the left side of Figure 8.13 according to the magnitude of their effect on skin. On the right side percent weight bars show the effects of each input parameter. Estimates of model parameters are shown in the first column. These values are the coefficients used in prediction formula. In other words, in this column input parameter estimates for the fitted least square model are listed. The input variables are sorted by the absolute value of t-ratio. The magnitude of t-ratio shows the most significant effect of the input parameter. The blue lines indicate the 0.05 significance level. Net thickness has the greatest impact on skin. While net thickness and porosity is directly proportional with skin, water saturation is inversely correlated with

skin. Water saturation is not directly related to skin. However saturations determine the total compressibility which has an effect on skin. Formation compressibility, water salinity and gas density are the input parameters that have less effect on skin.

Sorted Parameter Estimates

Term	Estimate	Std Error	t Ratio	Prob>|t|
Net Thickness(8,1,9,9)	0,0562027	0,006642	8,46	<,0001*
Porosity(23,76,30,24)	0,0493631	0,006695	7,37	<,0001*
Water Saturation(22,5,37,5)	-0,042511	0,006635	-6,41	<,0001*
Gas Density(0,5536,0,61369)	0,0069294	0,006625	1,05	0,3014
Water Salinity(18000,40000)	-0,005062	0,006644	-0,76	0,4503
Formation Compressibility(2,99e-6,3,32e-6)	-8,379e-5	0,006687	-0,01	0,9901

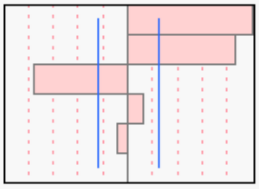

Figure 8.13 Sorted Parameter Estimates of Skin

In pareto plot, percent weigh bars show the magnitude of the effect on skin without considering inverse or direct effect. However it can be analyzed by Ortog Estimate column even if it is a negative or positive magnitude. On the left side, parameters are listed according to importance order. In addition to percent weight bars, cumulative weight line is drawn to show total effect on the left side.

Pareto Plot of Transformed Estimates

Term	Orthog Estimate
Net Thickness(8,1,9,9)	0,0315037
Porosity(23,76,30,24)	0,0281942
Water Saturation(22,5,37,5)	-0,0249776
Gas Density(0,5536,0,61369)	0,0043291
Water Salinity(18000,40000)	-0,0042707
Formation Compressibility(2,99e-6,3,32e-6)	-0,0011212

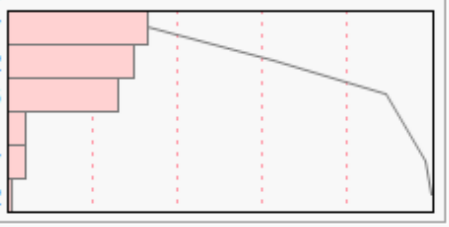

Figure 8.14 Pareto Plot of Skin

In addition to sorted parameter estimates and pareto plot, Leverage plots were drawn with the calculated skin from all ranges of input parameters to examine the each individual effect of input parameters on skin. The blue dashed line indicates skin obtained from the reference case. The skin value obtained from the reference case is the 2.17. Red line shows how skin is affected by each input parameter. Dashed red lines show the dispersion of the data. Skin values obtained from equation vs. all input parameter within the error range are in Figures 8.15. Skin values vary between 2.05 and 2.30.

If net thickness increases, skin of the formation also increases. Thickness is not directly related to skin. However thickness is related to permeability and if net thickness increases for a given production, permeability decreases. If permeability of the formation decreases, skin of the formation increases. Porosity is another input parameter affect the skin of the formation. If porosity increases, skin of the formation increase. Water saturation is the third parameter mostly affects the formation skin. Water saturation is used to determine the total compressibility. With the increase of the water saturation, total compressibility decrease and

the skin of the formation decrease. Formation compressibility, gas density and water salinity have less effect on skin.

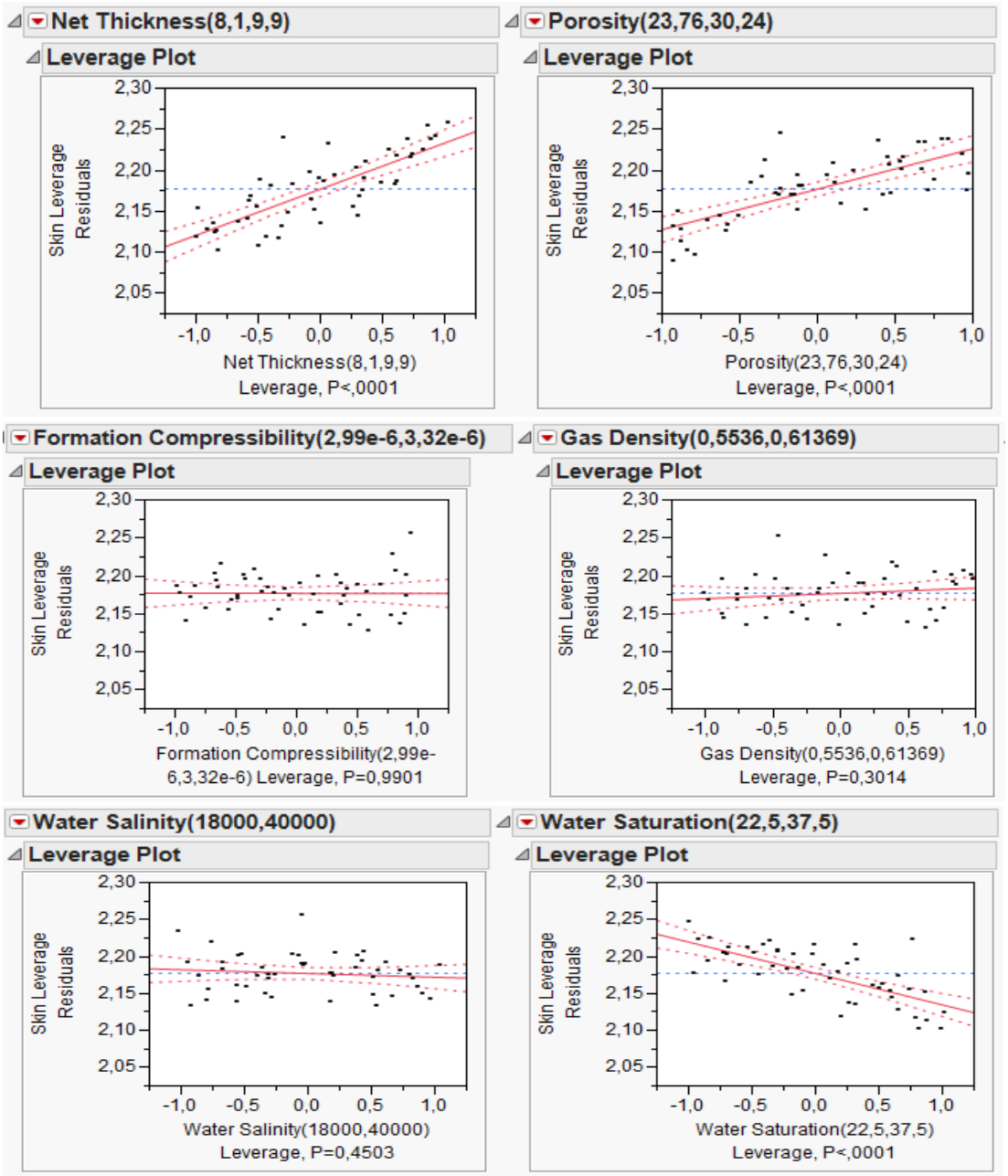

Figure 8.15 Leverage plots, Skin vs. Input Parameters

8.2.2 Wellbore Storage Coefficient

Van Everdingen and Hurst (1949) represented wellbore storage by compressibility of fluid c_w in the wellbore volume V_w. Earlougher (1977) defined wellbore storage which is related to the rise of the fluid level in the wellbore. Therefore wellbore storage is directly related to gas compressibility calculated with the Dranchuk's correlation by using the gas density. It is expected that wellbore storage coefficient is affected by changing of gas density since other

parameters are related to the reservoir rather that wellbore, they should not affect the wellbore storage.

A linear predictive model constructed for wellbore storage is shown in Figure 8.16. For predictive model of the wellbore storage, correlation coefficient is high (0.99) and the sum of the root mean square is low (0.001). This means that the construction of linear predictive model to estimate wellbore storage coefficient is a representative model.

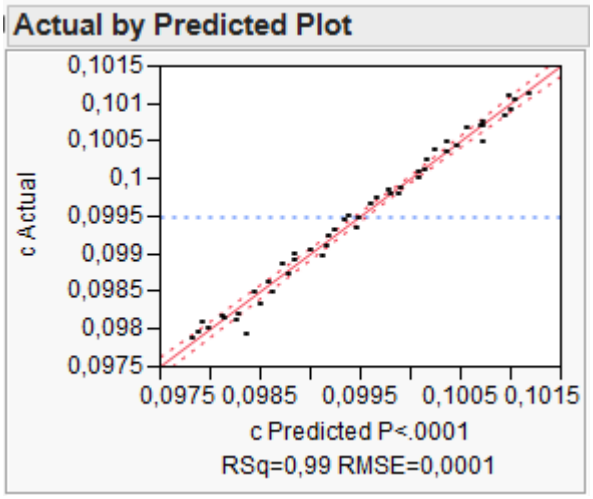

Figure 8.16 Linear Predictive Model Fit of Wellbore Storage Coefficient

Following equation belongs to the model of the wellbore storage coefficient. And the summary of the fit between the actual value of wellbore storage coefficient obtained from simulation and the equation is given in Table 8.5.

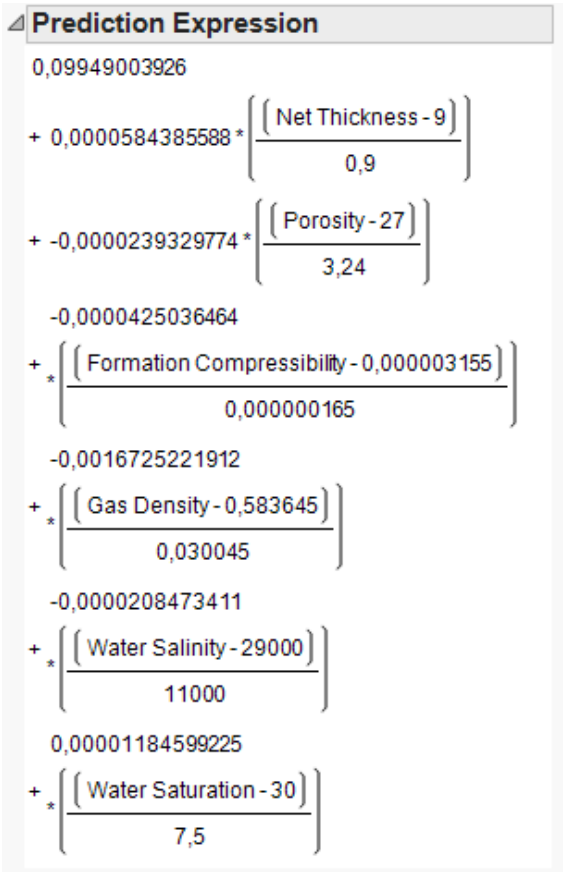

Table 8.6 Statistical Parameters of Linear Predictive Model of Wellbore Storage Coefficient

Summary of Fit	
RSquare	0,988191
RSquare Adj	0,986543
Root Mean Square Error	0,000116
Mean of Response	0,09949
Observations (or Sum Wgts)	50

After model construction, sensitivity analysis is conducted to detect the effect of the input parameters on wellbore storage coefficient. In sorted parameter estimates, input parameters are sorted on the left side of Figure 8.17 according to the magnitude of their effect on wellbore storage coefficient. On the right side percent weight bars show the effects of each input parameter. Gas density has the greatest impact on wellbore storage coefficient. Gas density is inversely related to wellbore storage coefficient. Net thickness, porosity, water saturation, formation compressibility and water salinity are the input parameters that have less effect on wellbore storage coefficient.

Sorted Parameter Estimates

Term	Estimate	Std Error	t Ratio	Prob>|t|
Gas Density(0,5536,0,61369)	-0,001673	0,000028	-59,91	<,0001*
Net Thickness(8,1,9,9)	5,8439e-5	0,000028	2,09	0,0428*
Formation Compressibility(2,99e-6,3,32e-6)	-4,25e-5	2,818e-5	-1,51	0,1388
Porosity(23,76,30,24)	-0,000024	2,822e-5	-0,85	0,4010
Water Salinity(18000,40000)	-2,085e-5	0,000028	-0,74	0,4606
Water Saturation(22,5,37,5)	1,1846e-5	0,000028	0,42	0,6739

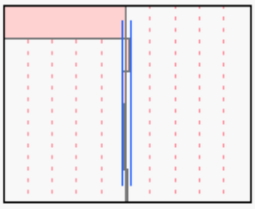

Figure 8.17 Sorted Parameter Estimates of Wellbore Storage Coefficient

In pareto plot (Figure 8.18), percent weigh bar of the gas density shows that it has the greatest effect on wellbore storage coefficient. The other input parameters are less effective.

Pareto Plot of Transformed Estimates

Term	Orthog Estimate
Gas Density(0,5536,0,61369)	-0,0009842
Net Thickness(8,1,9,9)	0,0000395
Porosity(23,76,30,24)	0,0000258
Water Salinity(18000,40000)	-0,0000119
Formation Compressibility(2,99e-6,3,32e-6)	-0,0000091
Water Saturation(22,5,37,5)	0,0000070

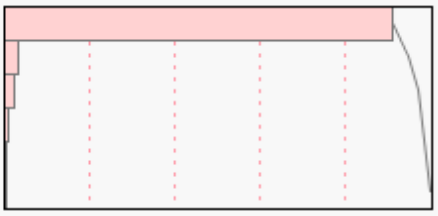

Figure 8.18 Pareto Plot of Wellbore Coefficient

In addition to sorted parameter estimates and pareto plot, Leverage plots were drawn with the calculated wellbore storage coefficient from all ranges of input parameters to examine the each individual effect of input parameters on wellbore storage coefficient. The blue dashed line indicates wellbore storage coefficient obtained from the reference case. The wellbore storage coefficient value obtained from the reference case is the 0.0995 1/psi. Red line shows how wellbore storage coefficient is affected by each input parameter. Dashed red lines show the dispersion of the data. Wellbore storage coefficient values obtained from equation vs. all input parameter within the error range are in Figures 8.19. Wellbore storage coefficient values vary between 0.0975 1/psi and 0.1015 1/psi.

While gas density increases, wellbore storage coefficient decreases since the gas compressibility decreases. P values of the graphs shows that gas density is the single input parameter that affect the wellbore storage coefficient.

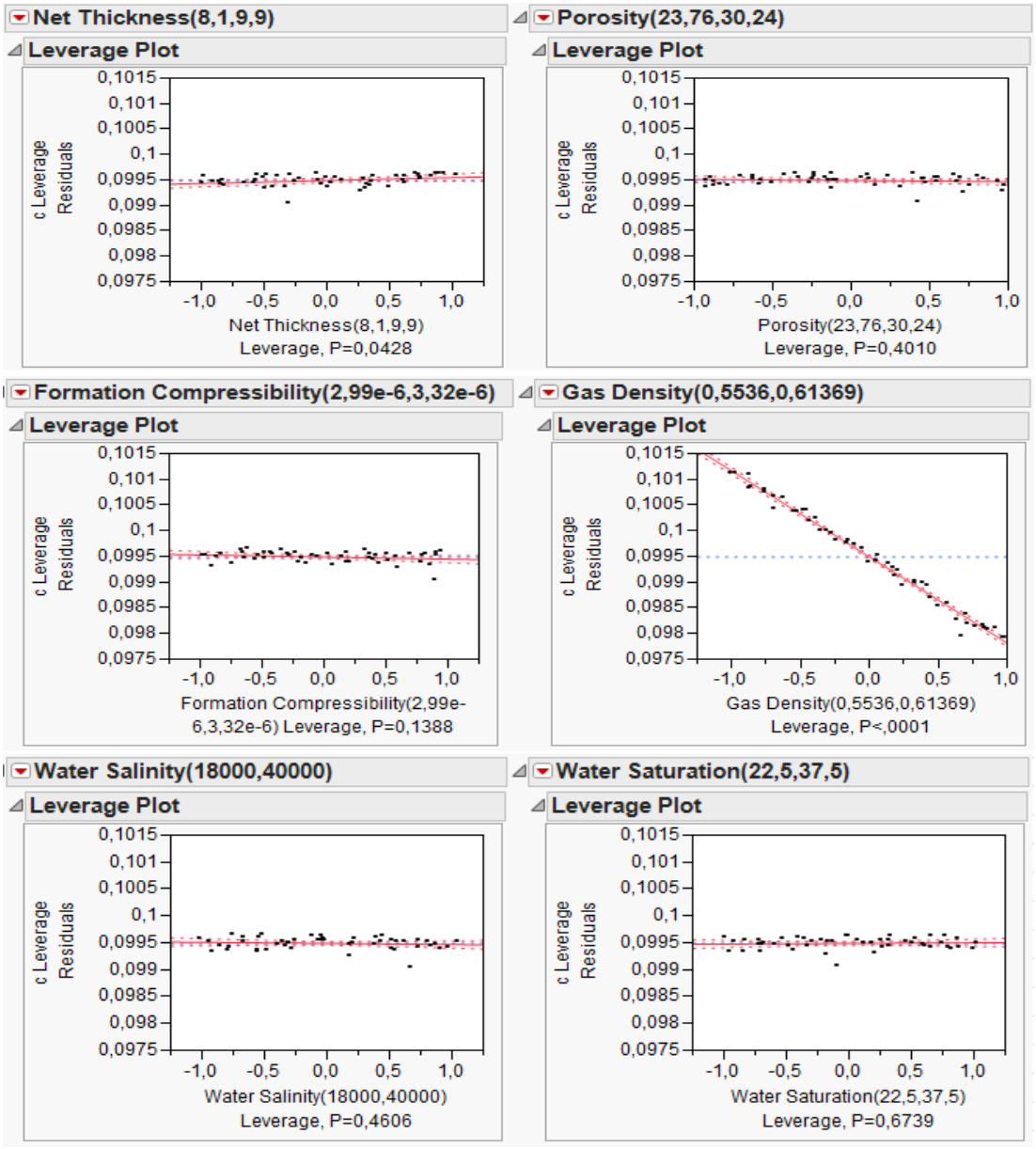

Figure 8.19 Leverage Plots, Wellbore Storage Coefficient vs. Input Parameters

8.2.3 Permeability

The end of the wellbore storage time from straight line positioned on the infinite acting radial flow, the reservoir permeability thickness is estimated. Net thickness and gas rate at given net thickness are the other two parameters used to calculate permeability. Gas rates are measured by flow meters and checked by superposing IARF of the tree build up derivatives. Net thickness obtained from density neutron log is the main parameter that is expected to affect the permeability.

A linear predictive model constructed for permeability is shown in Figure 8.20. For predictive model of the permeability, correlation coefficient is high (0.97) and the sum of the

root mean square is low (2.73). This means that the construction of linear predictive model to estimate wellbore storage coefficient is a representative model.

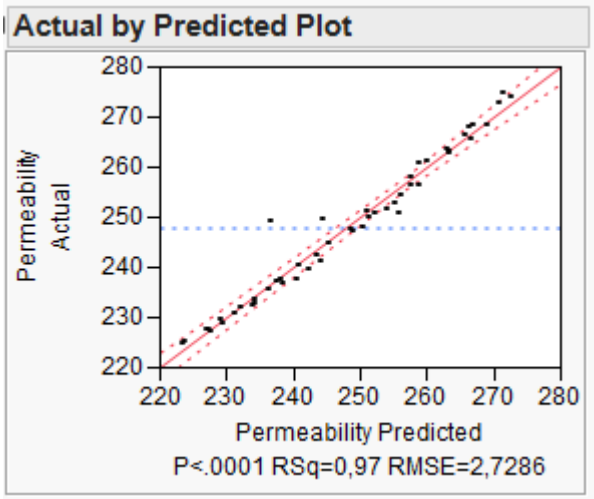

Figure 8.20 Linear Predictive Model Fit of Permeability

Following equation belongs to the model of the permeability. The summary of the fit between the actual value of wellbore storage coefficient obtained from simulation and the equation is given in Table 8.6.

Table 8.7 Statistical Parameters of Linear Predictive Model of Permeability

Summary of Fit	
RSquare	0,969112
RSquare Adj	0,964802
Root Mean Square Error	2,728623
Mean of Response	247,8174
Observations (or Sum Wgts)	50

Prediction Expression

$$
\begin{aligned}
&247{,}817416308 \\
&+ -23{,}994595657109 * \left(\frac{(\text{Net Thickness} - 9)}{0{,}9} \right) \\
&+ 0{,}05350971696079 * \left(\frac{(\text{Porosity} - 27)}{3{,}24} \right) \\
&0{,}41001848690933 \\
&+ * \left(\frac{(\text{Formation Compressibility} - 0{,}000003155)}{0{,}000000165} \right) \\
&-1{,}4629635689345 \\
&+ * \left(\frac{(\text{Gas Density} - 0{,}583645)}{0{,}030045} \right) \\
&0{,}51175359297096 \\
&+ * \left(\frac{(\text{Water Salinity} - 29000)}{11000} \right) \\
&0{,}36744882184091 \\
&+ * \left(\frac{(\text{Water Saturation} - 30)}{7{,}5} \right)
\end{aligned}
$$

After model construction, sensitivity analysis is conducted to detect the effect of the input parameters on permeability. In sorted parameter estimates, input parameters are sorted on the left side of Figure 8.21 according to the magnitude of their effect on permeability. On the right side percent weight bars show the effects of each input parameter. Net thickness has the greatest impact on permeability. Net thickness is inversely related to permeability. Porosity, water saturation, formation compressibility, gas density and water salinity have less effect on permeability.

Sorted Parameter Estimates

Term	Estimate	Std Error	t Ratio	Prob>|t|
Net Thickness(8,1,9,9)	-23,9946	0,657483	-36,49	<,0001*
Gas Density(0,5536,0,61369)	-1,462964	0,655753	-2,23	0,0310*
Water Salinity(18000,40000)	0,5117536	0,657677	0,78	0,4408
Formation Compressibility(2,99e-6,3,32e-6)	0,4100185	0,661917	0,62	0,5389
Water Saturation(22,5,37,5)	0,3674488	0,656764	0,56	0,5787
Porosity(23,76,30,24)	0,0535097	0,662769	0,08	0,9360

Figure 8.21 Sorted Parameter Estimates of Permeability

In pareto plot (Figure 8.22), percent weigh bar of the net thickness shows that it has the greatest effect on wellbore storage coefficient. Gas density is the second input that affects the

permeability since viscosity is the parameter used to calculate the permeability. Gas density has a less effect on permeability. The other input parameters have almost no effect.

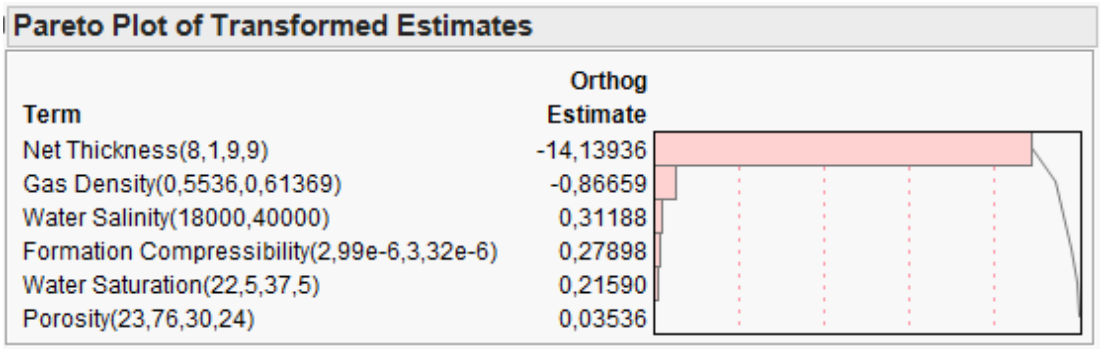

Figure 8.22 Pareto Plot of Permeability

In addition to sorted parameter estimates and pareto plot, Leverage plots were drawn with the calculated permeability from all ranges of input parameters to examine the each individual effect of input parameters on permeability. The blue dashed line indicates permeability obtained from the reference case. The permeability obtained from the reference case is 247 mD. Red line shows how permeability is affected by each input parameter. Dashed red lines show the dispersion of the data. Permeability values obtained from equation vs. all input parameter within the error range are in Figures 8.23. Permeability values vary between 220 mD and 280 mD. Increase in net thickness leads to decrease in permeability since the gas rate stays the same for an increasing net thickness. Low P value of the net thickness vs. permeability graph shows that it is the single input parameter that affects the permeability.

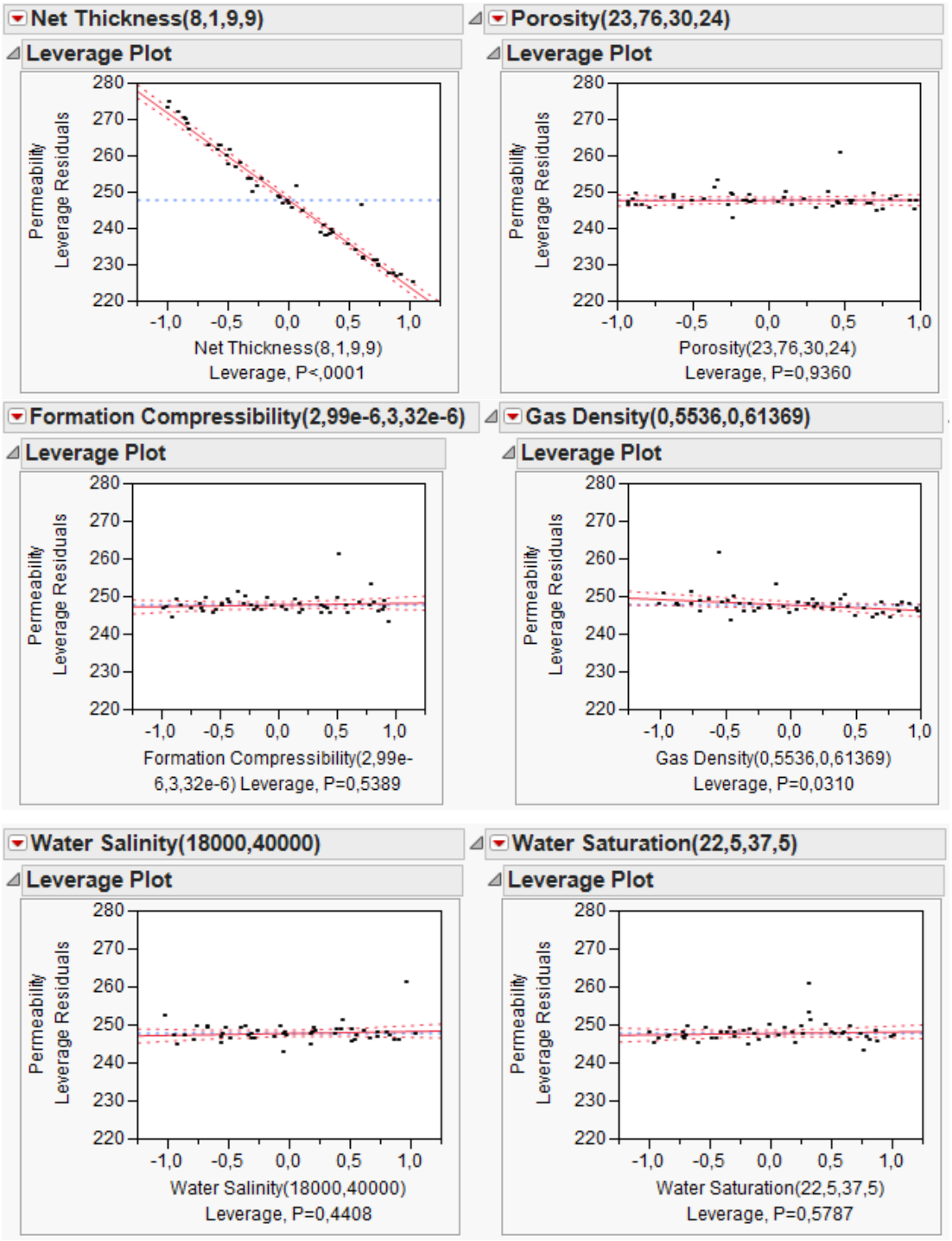

Figure 8.23 Leverage Plots, Permeability vs. Input Parameters

8.2.4 Distances to the Boundaries

S, E, N and W represents the distances to south, east, north and west boundaries or first, second, third and fourth boundaries respectively. Distances of the boundaries are very important since they are used in the calculation of reservoir volume. Distance to boundary is directly proportional with the square root of permeability and time and inversely proportion with square root of porosity, total compressibility and viscosity. Therefore it is expected that it increases with increasing permeability and decreases with increasing porosity, viscosity and total compressibility. Since permeability is inversely proportional with net thickness, distances to boundaries decrease due to increase in net thickness. Since water saturation is inversely proportional with total compressibility, distances to boundaries increase due to increase in water saturation.

Linear predictive models constructed for distances to the first, second, third and fourth boundaries are shown in Figure 8.24, 8.25, 8.26 and 8.27. For predictive model of distances to the boundaries, correlation coefficients are 0.91, 0.95, 0.95 and 0.75 respectively and the sum of the root mean squares are 2, 5, 4 and 173. The correlation coefficients are high and sum of the root mean squares are low except for the fourth distance to boundaries. However the sum of the root mean square, 173 ft, is a small value when it is compared with fourth distance, 5890 ft. In addition to that model of the fourth boundary has 0.75 as correlation coefficient which is acceptable for the most uncertain boundary. The constructed linear predictive models to estimate distances to boundaries are representative models.

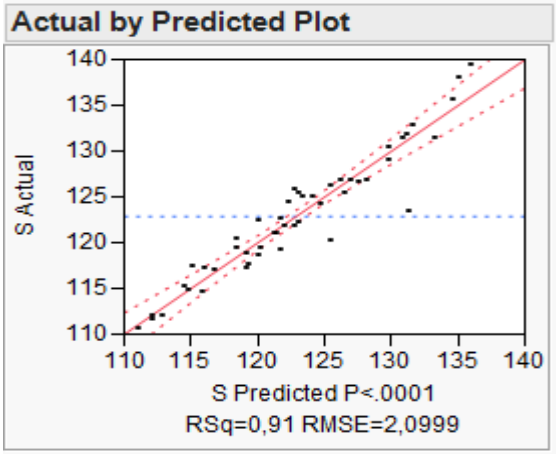

Figure 8.24 Linear Predictive Model Fit of First Boundary

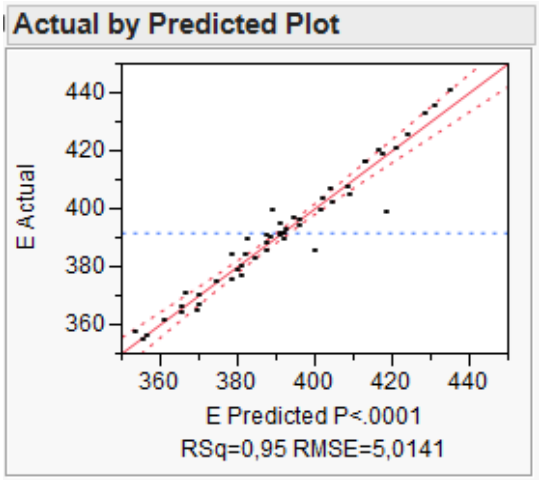

Figure 8.25 Linear Predictive Model Fit of Second Boundary

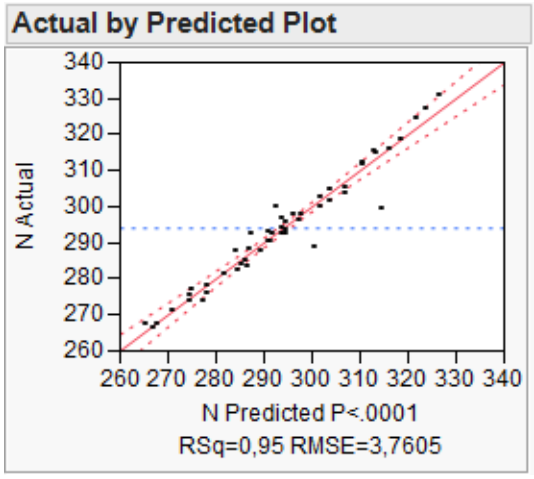

Figure 8.26 Linear Predictive Model Fit of Third Boundary

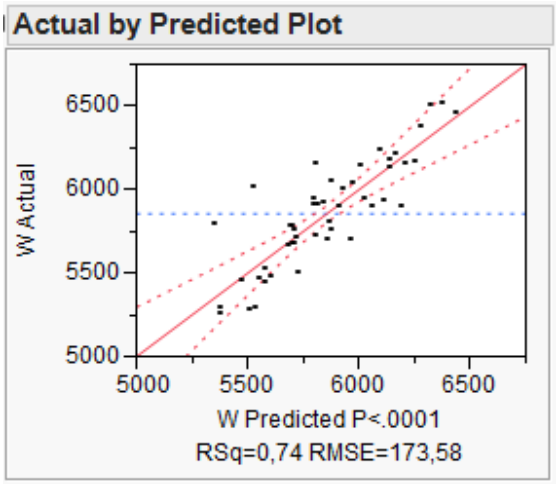

Figure 8.27 Linear Predictive Model Fit of Third Boundary

Following equations belongs to the predictive linear models of the first, second, third and fourth distances to boundaries respectively.

Response S

Prediction Expression

122,8846903

+ -6,494832373519 * ((Net Thickness - 9) / 0,9)

+ -6,6811157946637 * ((Porosity - 27) / 3,24)

-0,2859967705678

+ * ((Formation Compressibility - 0,000003155) / 0,000000165)

-0,8492289633961

+ * ((Gas Density - 0,583645) / 0,030045)

0,74647600550497

+ * ((Water Salinity - 29000) / 11000)

5,70151574002661

+ * ((Water Saturation - 30) / 7,5)

Response E

Prediction Expression

391,56561578

+ -19,41334313257 * ((Net Thickness - 9) / 0,9)

+ -22,375047198387 * ((Porosity - 27) / 3,24)

-1,8887824420652

+ * ((Formation Compressibility - 0,000003155) / 0,000000165)

-3,0492844071251

+ * ((Gas Density - 0,583645) / 0,030045)

2,28633188319582

+ * ((Water Salinity - 29000) / 11000)

19,1890322839663

+ * ((Water Saturation - 30) / 7,5)

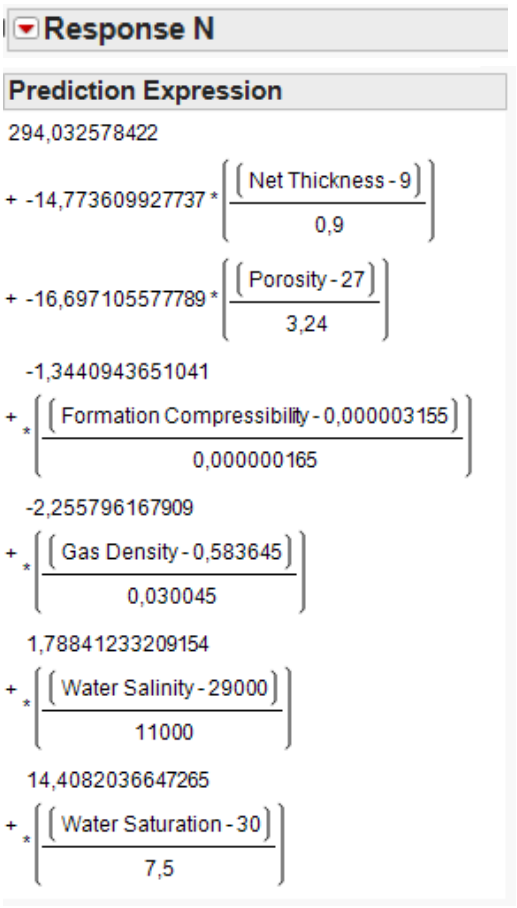

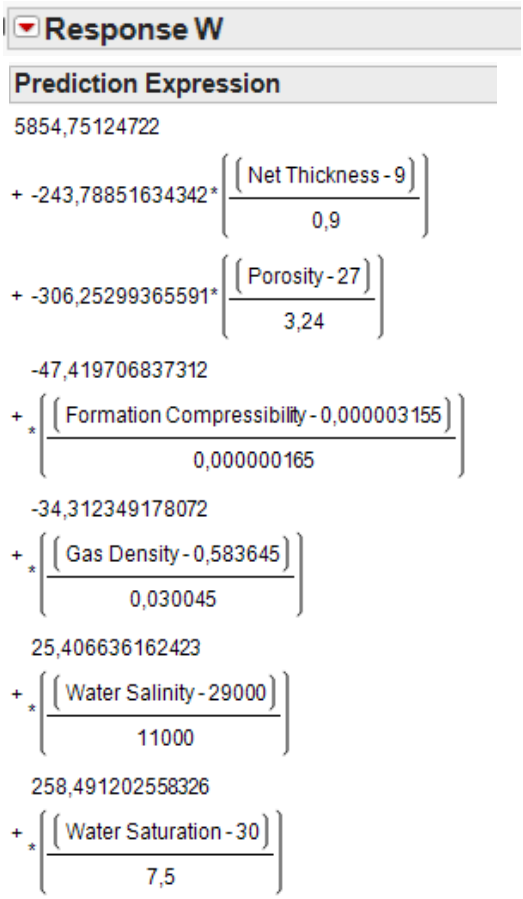

And the summary of the fit between the actual value of distances to boundaries obtained from simulation and the equation is given in Table 8.7, 8.8, 8.9 and 8.10.

Table 8.8 Statistical Parameters of Linear Predictive Model of First Boundary

Summary of Fit	
RSquare	0,912138
RSquare Adj	0,899879
Root Mean Square Error	2,099891
Mean of Response	122,8847
Observations (or Sum Wgts)	50

Table 8.9 Statistical Parameters of Linear Predictive Model of Second Boundary

Summary of Fit	
RSquare	0,949907
RSquare Adj	0,942917
Root Mean Square Error	5,01415
Mean of Response	391,5656
Observations (or Sum Wgts)	50

Table 8.10 Statistical Parameters of Linear Predictive Model of Third Boundary

Summary of Fit	
RSquare	0,950217
RSquare Adj	0,94327
Root Mean Square Error	3,760495
Mean of Response	294,0326
Observations (or Sum Wgts)	50

Table 8.11 Statistical Parameters of Linear Predictive Model of Fourth Boundary

Summary of Fit	
RSquare	0,735374
RSquare Adj	0,698449
Root Mean Square Error	173,5824
Mean of Response	5854,751
Observations (or Sum Wgts)	50

After model construction, sensitivity analysis is conducted to detect the effect of the input parameters on distances to boundaries. In sorted parameter estimates, input parameters are sorted on the left side of Figure 8.28, 8.29, 8.30 and 8.31 according to the magnitude of their effect on distances to boundaries. On the right side percent weight bars show the effects of each input parameter. Porosity, net thickness and saturation are the most effective input parameters. Porosity has the greatest impact on distances to boundaries. As porosity and net thickness increase, pressure response reaches boundaries faster. Thus makes the distances to boundaries decrease. The third input that is directly proportional to distance to boundaries is water saturation. Increase in water saturation leads to increase in distances to boundaries. Formation compressibility, gas density and water salinity are the input parameters have less effect on distances to boundaries.

Sorted Parameter Estimates

Term	Estimate	Std Error	t Ratio	Prob>|t|
Porosity(23,76,30,24)	-6,681116	0,510053	-13,10	<,0001*
Net Thickness(8,1,9,9)	-6,494832	0,505985	-12,84	<,0001*
Water Saturation(22,5,37,5)	5,7015157	0,505431	11,28	<,0001*
Gas Density(0,5536,0,61369)	-0,849229	0,504654	-1,68	0,0997
Water Salinity(18000,40000)	0,746476	0,506134	1,47	0,1475
Formation Compressibility(2,99e-6,3,32e-6)	-0,285997	0,509397	-0,56	0,5774

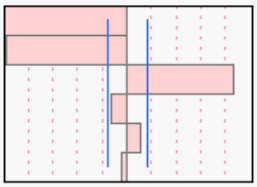

Figure 8.28 Sorted Parameter Estimates of First Distance to Boundaries

Sorted Parameter Estimates

Term	Estimate	Std Error	t Ratio	Prob>|t|
Porosity(23,76,30,24)	-22,37505	1,217912	-18,37	<,0001*
Net Thickness(8,1,9,9)	-19,41334	1,208198	-16,07	<,0001*
Water Saturation(22,5,37,5)	19,189032	1,206876	15,90	<,0001*
Gas Density(0,5536,0,61369)	-3,049284	1,205019	-2,53	0,0151*
Water Salinity(18000,40000)	2,2863319	1,208555	1,89	0,0653
Formation Compressibility(2,99e-6,3,32e-6)	-1,888782	1,216345	-1,55	0,1278

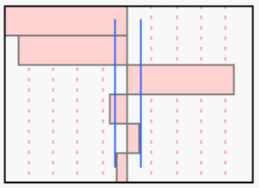

Figure 8.29 Sorted Parameter Estimates of Second Distance to Boundaries

Sorted Parameter Estimates

Term	Estimate	Std Error	t Ratio	Prob>|t|
Porosity(23,76,30,24)	-16,69711	0,913406	-18,28	<,0001*
Net Thickness(8,1,9,9)	-14,77361	0,90612	-16,30	<,0001*
Water Saturation(22,5,37,5)	14,408204	0,905129	15,92	<,0001*
Gas Density(0,5536,0,61369)	-2,255796	0,903736	-2,50	0,0165*
Water Salinity(18000,40000)	1,7884123	0,906388	1,97	0,0549
Formation Compressibility(2,99e-6,3,32e-6)	-1,344094	0,912231	-1,47	0,1479

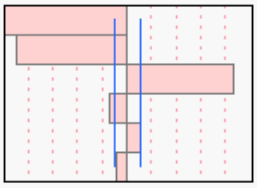

Figure 8.30 Sorted Parameter Estimates of Third Distance to Boundaries

Estimate, standard error and t ratio values which show the magnitude of the effect are similar for porosity, net thickness and water saturation. For the fourth boundary, effect of the water saturation is a bit more than net thickness different from the first, second and third boundaries. The reason is that the linear predictive model constructed for the fourth distance to boundary is 0.75 which is less than the correlation coefficient of the other boundaries. Since magnitude of the responses of water saturation and net thickness on the all distances to boundaries are so close, it is an acceptable error.

Sorted Parameter Estimates

Term	Estimate	Std Error	t Ratio	Prob>|t|
Porosity(23,76,30,24)	-306,253	42,16231	-7,26	<,0001*
Water Saturation(22,5,37,5)	258,4912	41,78027	6,19	<,0001*
Net Thickness(8,1,9,9)	-243,7885	41,82601	-5,83	<,0001*
Formation Compressibility(2,99e-6,3,32e-6)	-47,41971	42,10808	-1,13	0,2664
Gas Density(0,5536,0,61369)	-34,31235	41,71596	-0,82	0,4153
Water Salinity(18000,40000)	25,406636	41,83838	0,61	0,5469

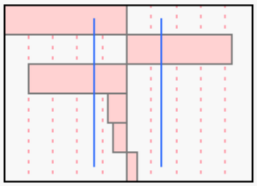

Figure 8.31 Sorted Parameter Estimates of Fourth Distance to Boundaries

In pareto plots (Figure 8.32, 8.33, 8.34, 8.35), percent weigh bar of the porosity shows that it has the greatest effect on distances to boundaries. Net thickness and the water saturation are

the other parameters have effect on distances to boundaries. The other input parameters have less effect.

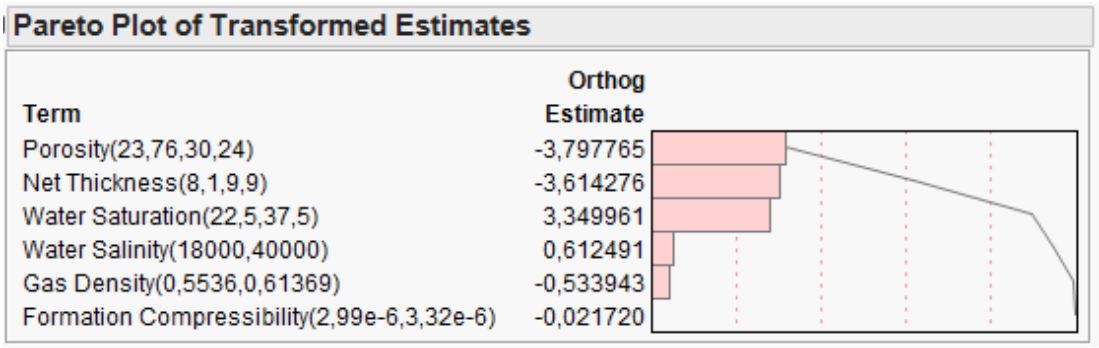

Figure 8.32 Pareto Plot of First Distance to Boundaries

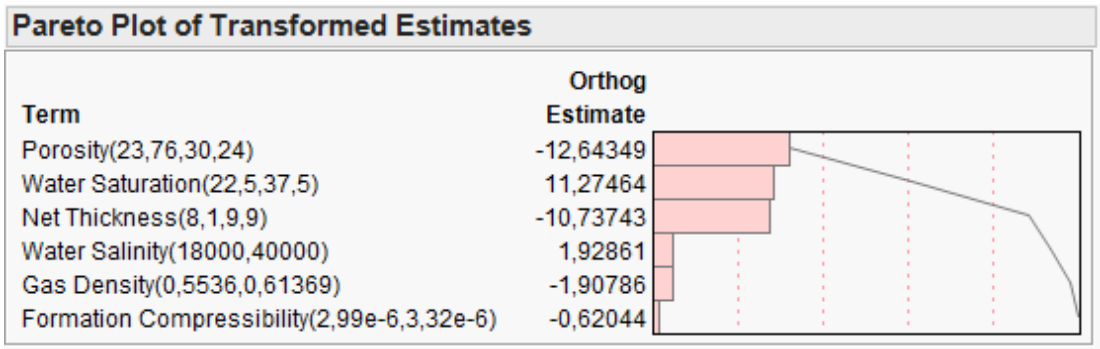

Figure 8.33 Pareto Plot of Second Distance to Boundaries

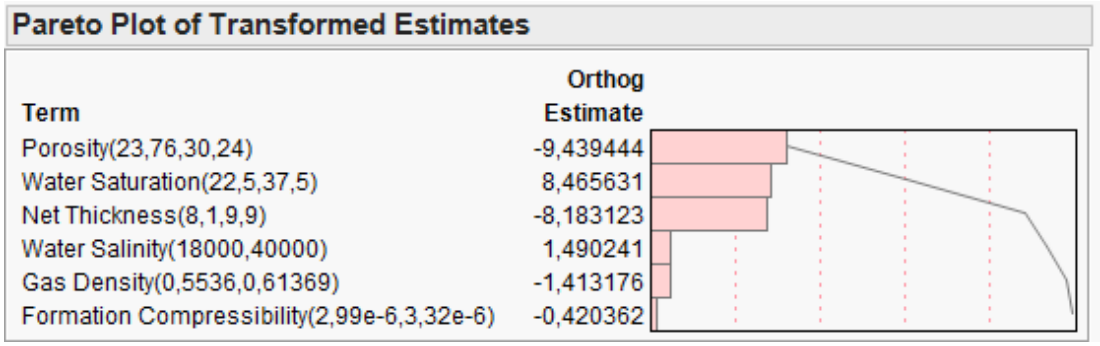

Figure 8.34 Pareto Plot of Third Distance to Boundaries

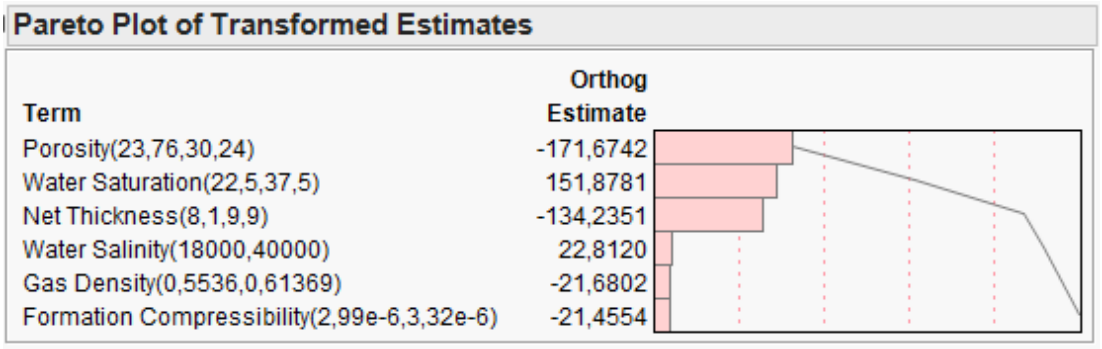

Figure 8.35 Pareto Plot of Fourth Distance to Boundaries

In addition to sorted parameter estimates and pareto plot, Leverage plots were drawn with the calculated distances to boundaries from all ranges of input parameters to examine the each individual effect of input parameters on distances to boundaries. The blue dashed line indicates distances to boundaries obtained from the reference case. First, second, third and fourth distances to boundaries obtained from the reference case are 124 ft, 390 ft, 295 ft and 5890 ft. Red line shows how distances are affected by each input parameter. Dashed red lines show the dispersion of the data. First, second, third and fourth distances to boundaries obtained from equation vs. all input parameter within the error range are in Figures 8.36, 8.37, 8.38 and 8.39.

First distance to boundaries varies between 110 ft. and 140 ft. Increasing in porosity and net thickness leads to decreases in distances to boundaries. All distances to boundaries increase with increasing water saturation. Formation compressibility, water salinity and gas density have almost no effect on distances to boundaries.

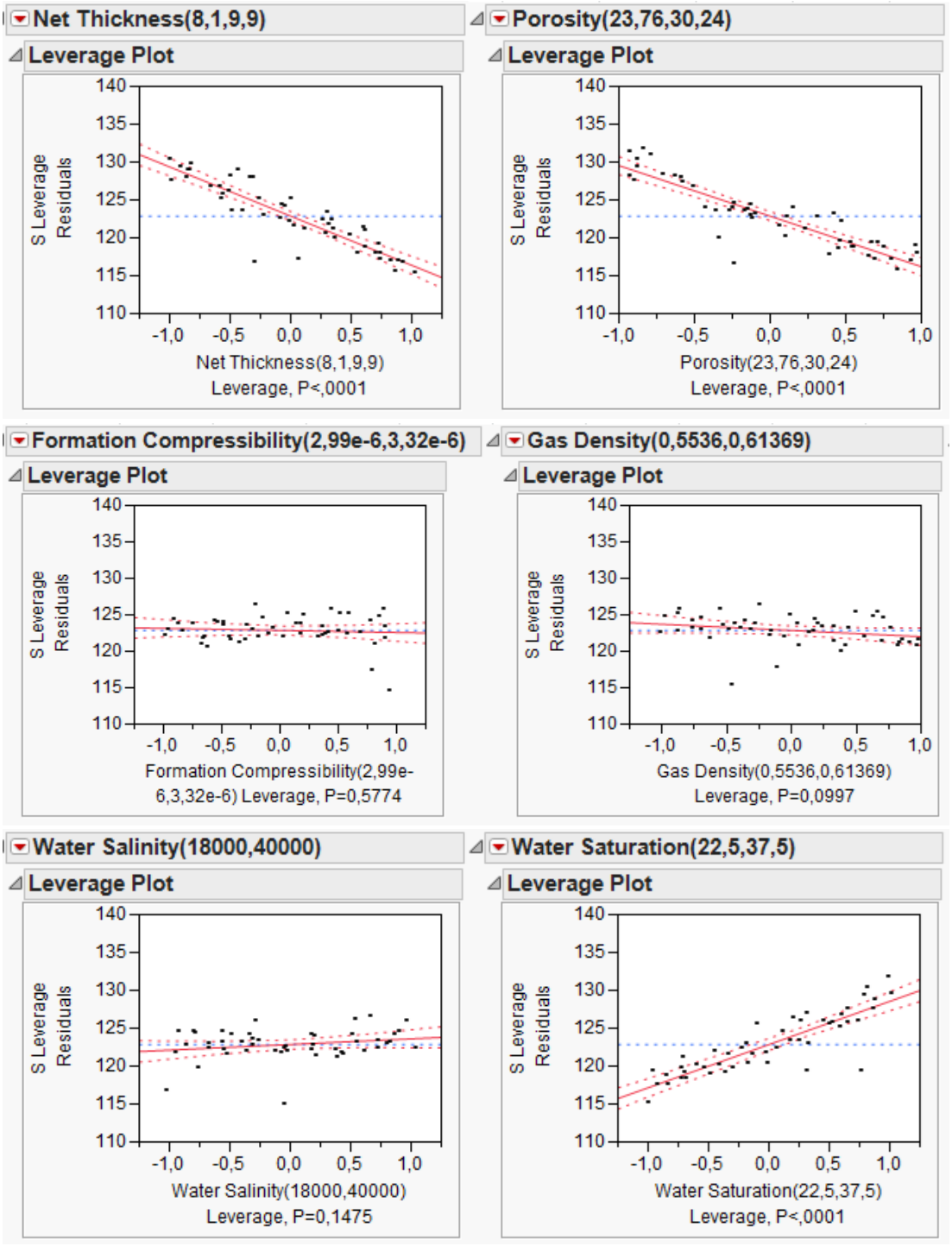

Figure 8.36 Leverage Plots, First Distance to Boundaries vs. Input Parameters

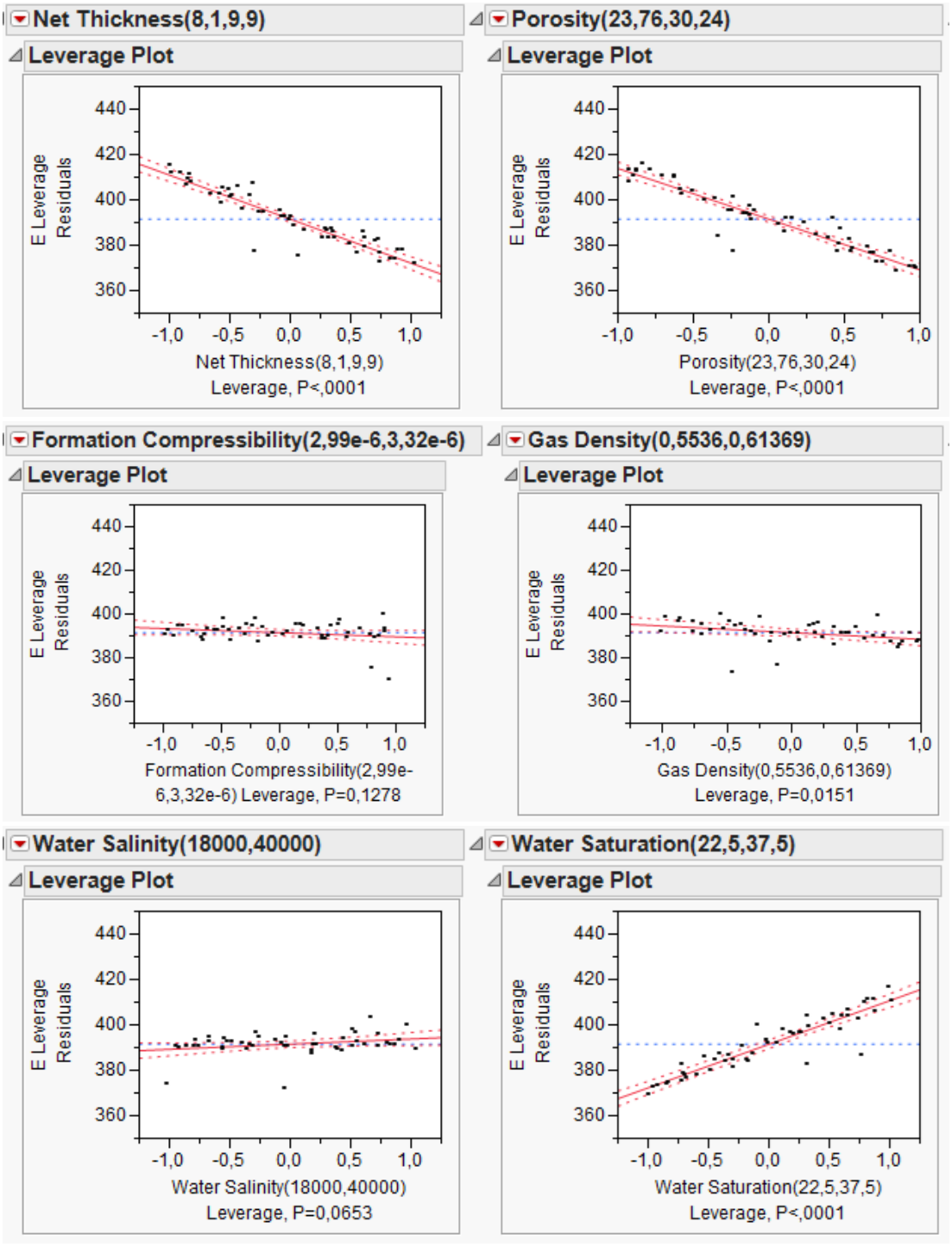

Figure 8.37 Leverage Plots, Second Distance to Boundaries vs. Input Parameters

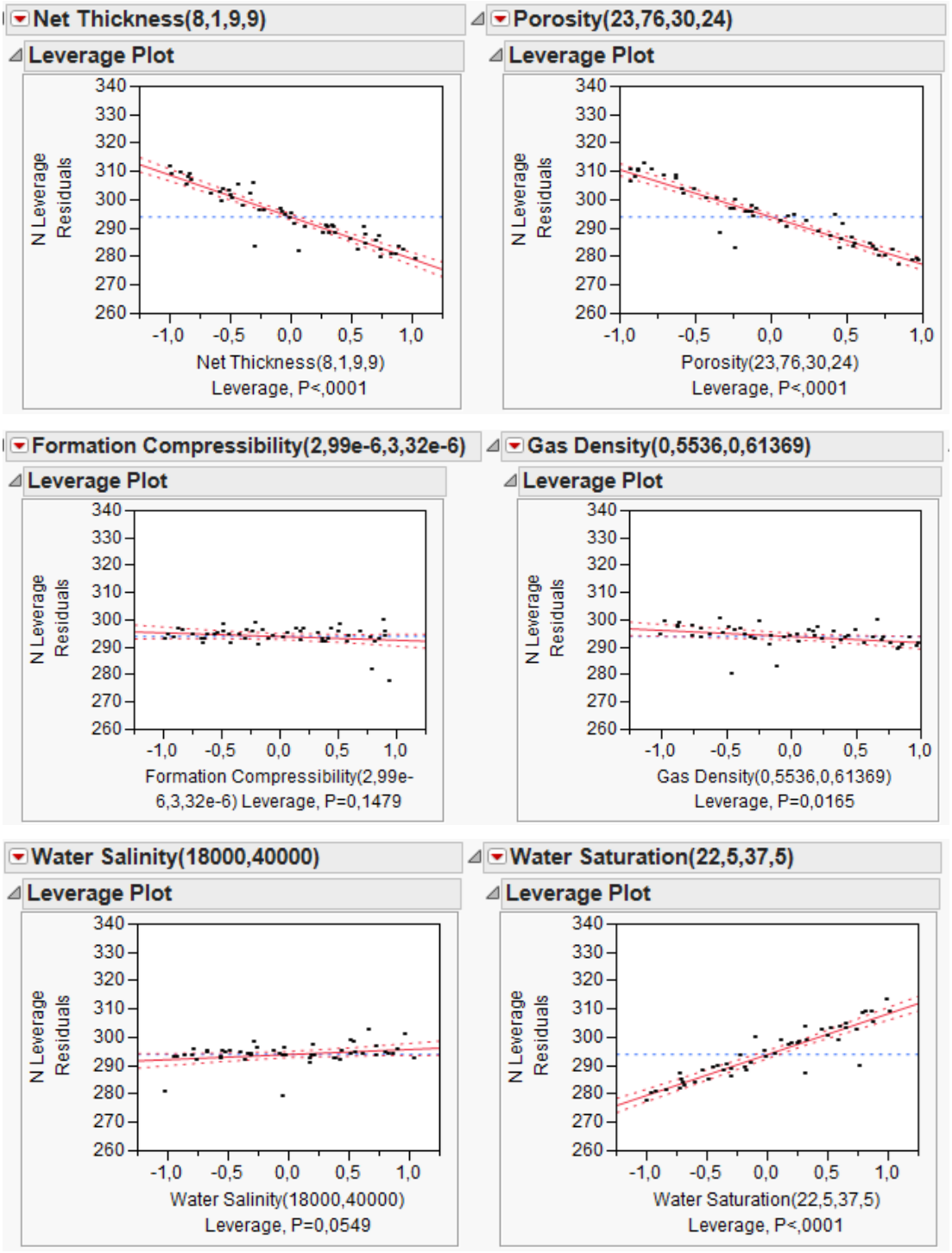

Figure 8.38 Leverage Plots, Third Distance to Boundaries vs. Input Parameters

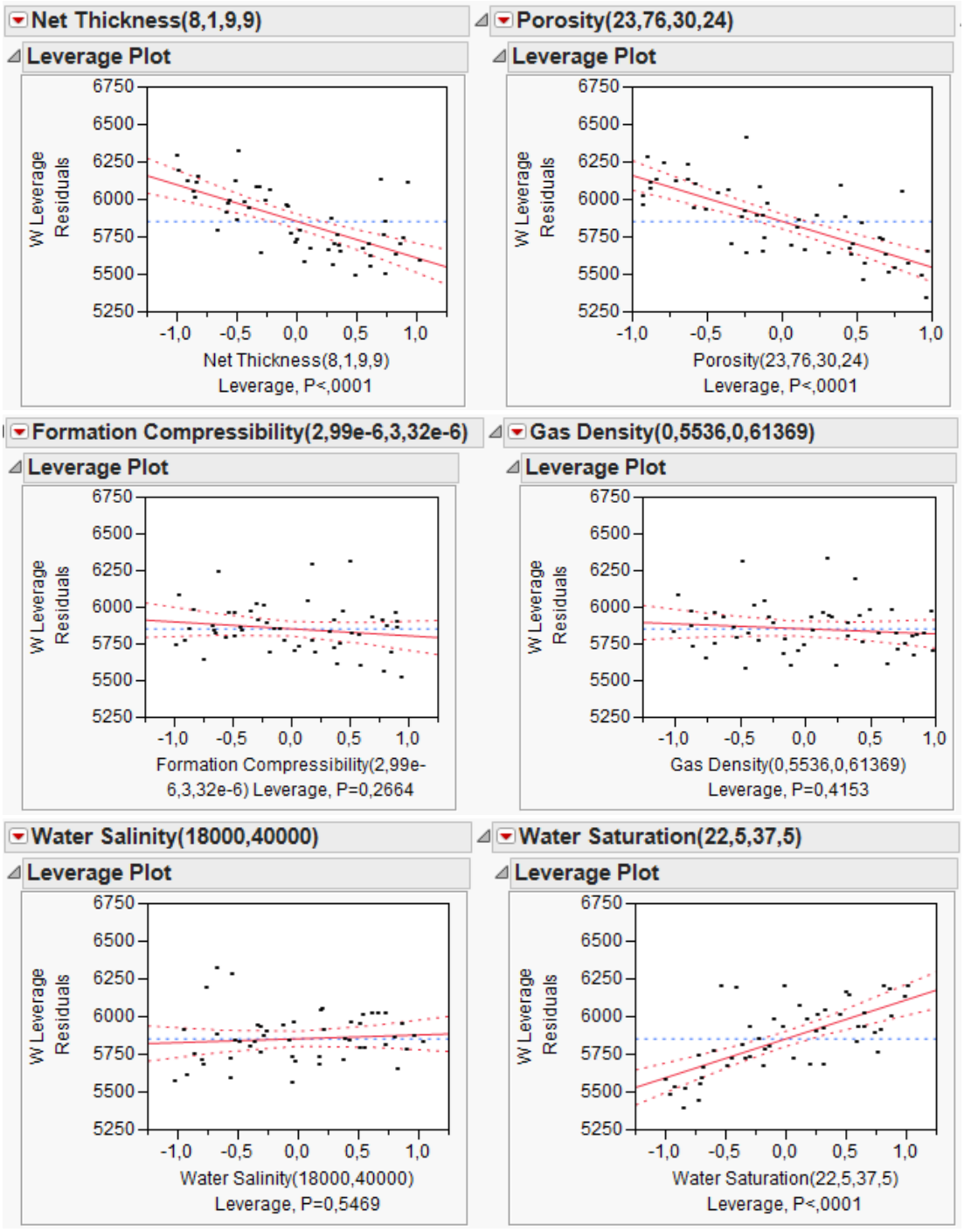

Figure 8.39 Leverage Plots, Fourth Distance to Boundaries vs. Input Parameters

8.2.5 Pore Volume

Tested volume is the connected pore volume limited by the radius of investigation. Pore volume is the product of porosity, net thickness and area. Therefore it is expected that porosity and net thickness are the two input parameters which affect the pore volume. While porosity and net thickness increase, distances decrease and make the product constant. For this reason porosity and net thickness do not affect the pore volume. For such pressure and given input parameters reservoir volume is constant. With increasing water saturation, tested volume increases to keep the reservoir volume constant.

A linear predictive model constructed for pore volume is shown in Figure 8.40. For predictive model of the pore volume, correlation coefficient is high (0.97) and the sum of the root mean square is low (4.07). This means that the construction of linear predictive model to estimate wellbore storage coefficient is a representative model.

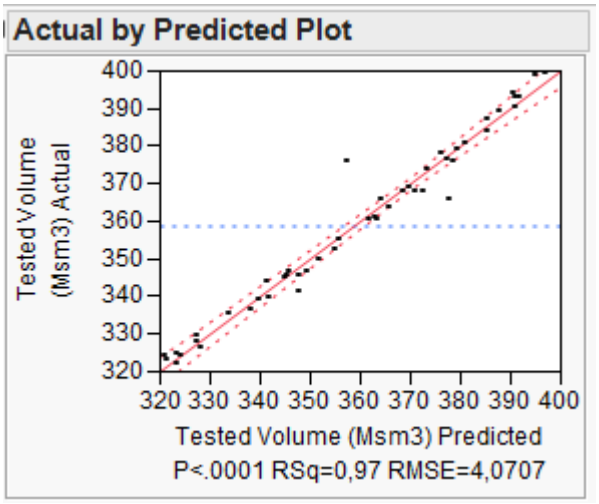

Figure 8.40 Linear Predictive Model Fit of Pore Volume

Following equation belongs to the model of the pore volume. And the summary of the fit between the actual value of pore volume obtained from simulation and the equation is given in Table 8.6.

Prediction Expression

$$
\begin{aligned}
&358{,}70932 \\
&+ -1{,}3639418279094 * \left(\frac{(\text{Net Thickness} - 9)}{0{,}9} \right) \\
&+ 1{,}44949445172414 * \left(\frac{(\text{Porosity} - 27)}{3{,}24} \right) \\
&\quad 0{,}87894102873899 \\
&+ * \left(\frac{(\text{Formation Compressibility} - 0{,}000003155)}{0{,}000000165} \right) \\
&\quad -4{,}8356890742068 \\
&+ * \left(\frac{(\text{Gas Density} - 0{,}583645)}{0{,}030045} \right) \\
&\quad 0{,}73751267439342 \\
&+ * \left(\frac{(\text{Water Salinity} - 29000)}{11000} \right) \\
&\quad 37{,}4789673062483 \\
&+ * \left(\frac{(\text{Water Saturation} - 30)}{7{,}5} \right)
\end{aligned}
$$

Table 8.12 Statistical Parameters of Linear Predictive Model of Pore Volume

Summary of Fit	
RSquare	0,972407
RSquare Adj	0,968557
Root Mean Square Error	4,070651
Mean of Response	358,7093
Observations (or Sum Wgts)	50

After model construction, sensitivity analysis is conducted to detect the effect of the input parameters on pore volume. In sorted parameter estimates, input parameters are sorted on the left side of Figure 8.41 according to the magnitude of their effect on pore volume. On the right side percent weight bars show the effects of each input parameter. Saturation has the greatest impact on permeability. Net thickness, porosity, water saturation, formation compressibility, gas density and water salinity are the input parameters have almost no effect on pore volume.

Sorted Parameter Estimates

Term	Estimate	Std Error	t Ratio	Prob>|t|
Water Saturation(22,5,37,5)	37,478967	0,979782	38,25	<,0001*
Gas Density(0,5536,0,61369)	-4,835689	0,978274	-4,94	<,0001*
Porosity(23,76,30,24)	1,4494945	0,988741	1,47	0,1499
Net Thickness(8,1,9,9)	-1,363942	0,980855	-1,39	0,1715
Formation Compressibility(2,99e-6,3,32e-6)	0,878941	0,987469	0,89	0,3784
Water Salinity(18000,40000)	0,7375127	0,981145	0,75	0,4563

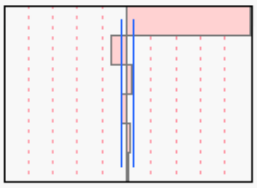

Figure 8.41 Sorted Parameter Estimates of Pore Volume

In pareto plot (Figure 8.42), percent weigh bar of the saturation shows that it has the greatest effect on pore volume. Gas density is the second parameter has an effect on pore volume. However it has less effect than water saturation. The other input parameters have almost no effect.

Pareto Plot of Transformed Estimates

Term	Orthog Estimate
Water Saturation(22,5,37,5)	22,02100
Gas Density(0,5536,0,61369)	-3,03989
Water Salinity(18000,40000)	1,57654
Porosity(23,76,30,24)	1,50541
Formation Compressibility(2,99e-6,3,32e-6)	1,31549
Net Thickness(8,1,9,9)	-1,24764

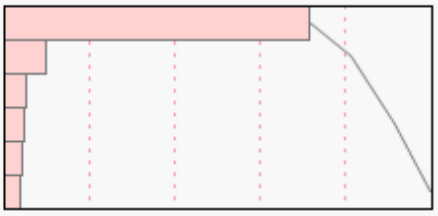

Figure 8.42 Pareto Plot of Pore Volume

In addition to sorted parameter estimates and pareto plot, Leverage plots were drawn with the calculated pore volume from all ranges of input parameters to examine the each individual effect of input parameters on pore volume. The blue dashed line indicates permeability obtained from the reference case. The tested pore volume obtained from the reference case is 360 Msm^3. Red line shows how pore volume is affected by each input parameter. Dashed red lines show the dispersion of the data. Tested pore volumes obtained from equation vs. all input parameter within the error range are in Figures 8.43. Pore volumes vary between 320 Msm^3 and 410 Msm^3. Increase in water saturation leads to increase in pore volume. While gas density decrease tested pore volume increase since Bg decrease with increasing gas density.

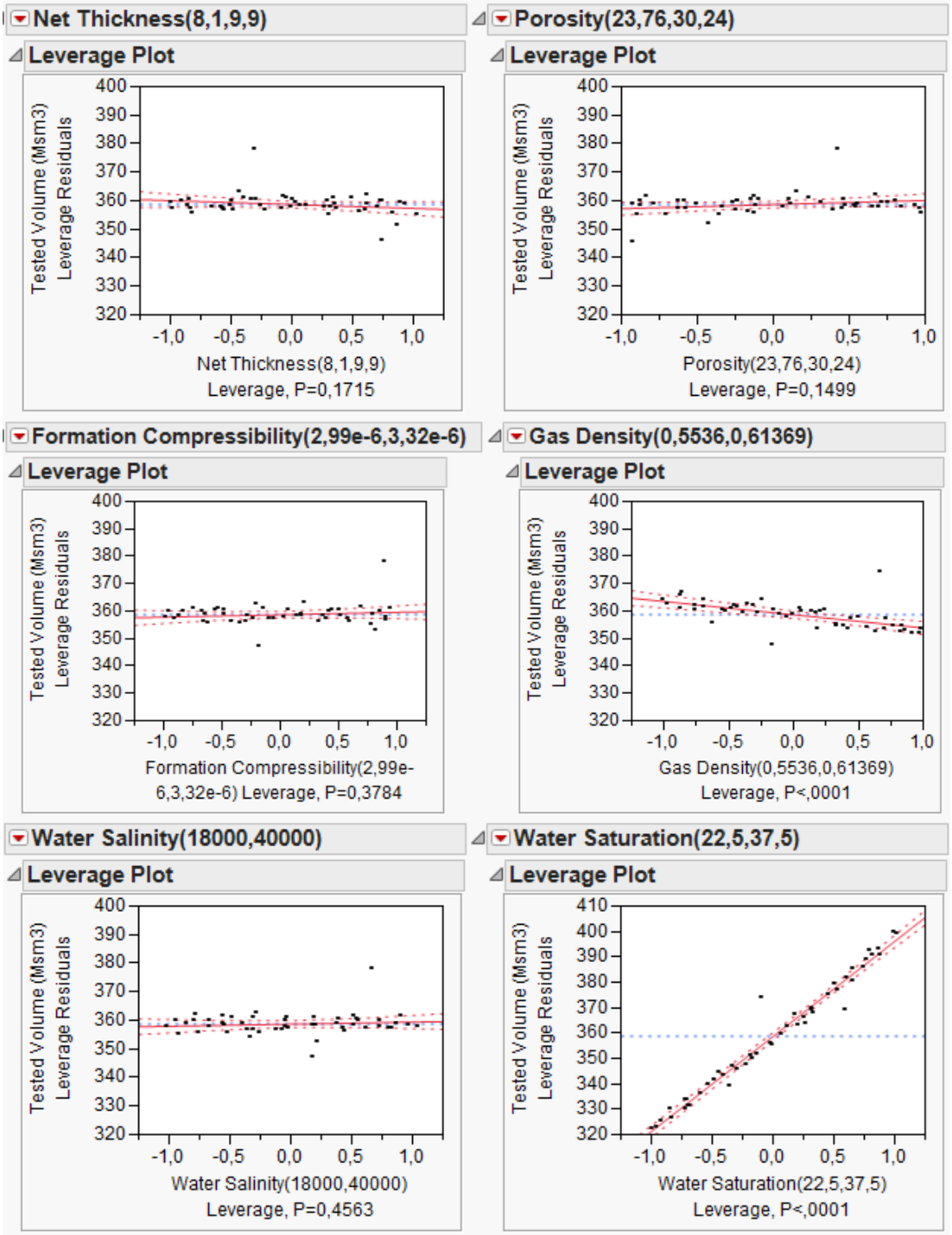

Figure 8.43 Leverage Plots, Tested Pore Volume vs. Input Parameters

In the following Figure 8.44, Prediction profile plots of the sensitivity analysis are shown. Prediction profiler provides to show how changes in input parameters affect the test results. Black values written on the y axis are predicted results that calculated by applying %5 error margins. In other means, values in black written on the y axis are the value of dashed lines which are 95% confidence intervals on the mean responses. Red values written on the x and y axis are the input parameters of base case and corresponding results of the base case. Red dashed lines show input parameters of the base case and the corresponding results. Blue lines show the relation even results are correlated with input parameters directly or inversely. If blue lines are nearly horizontal, results are independent of the input variables.

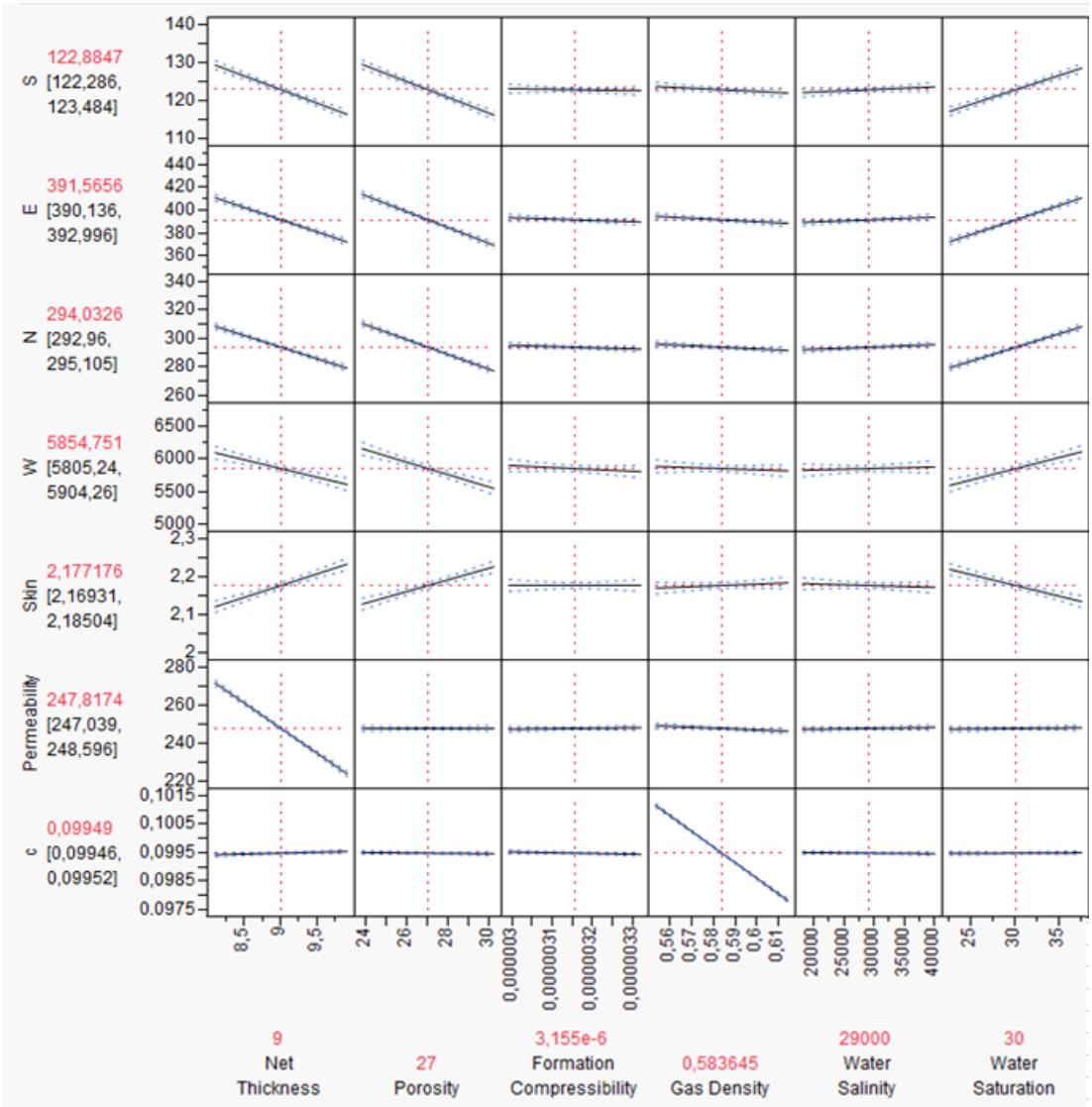

Figure 8.44 Prediction Profile Plot

CHAPTER-9

CONCLUSION

This study emphasizes the effect of input parameters on uncertainties in reservoir limit test results since all input parameters bring their own error in the reservoir limit test results. To find the cause of the error and error ranges of the petrophysical parameters, fluid parameters and the recorded pressure and rates, literature is reviewed.

From logs, porosity, net thickness, water saturation and formation compressibility are determined as 27%, 9 m, 30%, 3.14E-5 1/psi respectively. From gas sample, gas density is determined as 0.5579. Analogy from the nearest fields is conducted to approach the range of the formation water salinity. Average value of the salinities of the nearest fields is 29,000 ppm. These input parameters constitute the base case.

By applying error ranges to B.E field data, the intervals of the input parameters used for well test interpretation is determined. Latin Hypercube Space Filling Design is constructed with the intervals of the 6 input parameters to obtain 50 cases in JMP software.

Reservoir limit test is interpreted in Saphir Module of Ecrin Software after B.E recorded test data and determined field data is loaded. Best match is obtained when the test model is taken as a constant wellbore storage and homogeneous reservoir with rectangle boundaries for B.E. field. However the last distance to boundaries could not be detected from the interpretation of second and third build ups. Deconvolution method is applied to detect the last distance to boundaries. For the base case, permeability, wellbore storage coefficient and skin are 247 mD, 0.0995 1/psi and 2,17 respectively. Distances to boundaries are 124 ft, 295 ft, 390 ft and 5800 ft.

After model selection, 50 cases are run. Results are used to construct linear predictive model by using Least Squares Method. Sensitivity analyses are conducted on this linear predictive model to understand the effect of each input variable on the reservoir limit test results. From sensitivity analysis, following concluding remarks are obtained;

Net thickness has the greatest impact on skin. While net thickness and porosity is directly proportional with skin, water saturation is inversely correlated with skin. As net thickness and porosity increase, skin is also increases. Increase in water saturation leads to decrease in skin. Formation compressibility, water salinity and gas density are the input parameters have

less effect on skin. Skin is found to be 2.17 for the base case. However it varies between 2.10 and 2.25 when all cases run. Skin is the least uncertain result of the reservoir limit test.

The most effective parameter on wellbore storage coefficient is found to be gas density. Gas density is inversely related to wellbore storage coefficient. Wellbore storage coefficient decreases with increasing gas density. Other parameters have almost no effect on wellbore storage coefficient. Wellbore storage coefficient is 0.995 for the base case. Results of the 50 cases vary between 0.0975 1/psi and 0.1015 1/psi. Wellbore storage coefficient is one of the less uncertain results.

Net thickness which is inversely related to permeability has much more effect than other input parameters. As net thickness increases, permeability decreases. Other parameters have not much effect on permeability. Permeability of the B.E. reservoir is 247 mD according to base case. Results obtained from 50 different case gives a range that alters between 220 mD and 280 mD. Permeability is more uncertain compare to than skin and wellbore storage coefficient.

Porosity, net thickness and saturation are the most effective input parameters while determining the distances to boundaries. Porosity has the greatest impact on distances to boundaries. As porosity and net thickness increase, pressure response reaches boundaries faster. Thus making the distances to boundaries decrease. The third input that is directly proportional to distance to boundaries is water saturation. Increase in water saturation leads to increase in distances to boundaries. Formation compressibility, gas density and water salinity are the input parameters that have less effect on distances to boundaries. While distances to boundaries are found to be 124 ft, 295 ft, 390 ft and 5800 ft for the base case, after applying different cases distances to boundaries vary between 115 ft and 135 ft, 270 ft and 310 ft, 360 ft and 420 ft, 5250 ft and 6250 ft respectively. Although the deconvolution method is applied, the most uncertain result of the reservoir limit test is the fourth boundary.

Since tested volume is the connected pore volume, the main effective input parameter is water saturation. For the base case tested volume is found to be 360 Msm3. Results of the 50 cases vary between 320 Msm^3 and 410 Msm^3. Tested volume is uncertain as the distances to boundaries

CHAPTER-10

RECOMMENDATIONS

Most of the studies related to uncertainty in well test interpretation are related to model match with different choices. Uncertainty of the reservoir model should not be evaluated without uncertainty in input parameters. If for a field more than one model can match the pressure derivative, results of the well test interpretation are not unique. Although distances to boundaries are reported with a resolution of a tenth of foot, permeability less than 100 mD with 0.1 resolutions and skin with two decimal units, uncertainty range are much bigger than that resolution.

To overcome such dilemma, uncertainties of the input parameters should be defined very well and the possible range of the input parameters determined before the reservoir limit tests interpretation. An experimental design which includes good coverage of all input data space should be constructed. Results of the cases obtained from experimental design are used to construct predictive model. Predictive model make possible to compare results of the limit test for cases by putting forth the different analysis.

REFERENCES

Ahmed, T. (2006). *Reservoir engineering handbook*: Access Online via Elsevier.

Aly, A. M., Hunt, E. R., Pursell, D. A., & McCain, W. D. J. (1997). *Application of Multi-Well Normalization of Open Hole Logs in Integrated Reservoir Studies*. Paper presented at the SPE Western Regional Meeting, Long Beach, California.

Archer, R. A., Merad, M. B., & Blasingame, T. A. (2002). *Effects on Well Test Analysis of Pressure and Flowrate Noise*. Paper presented at the SPE Annual Technical Conference and Exhibition, San Antonio, Texas.

Azi, A. C., Gbo, A., & Gringarten, A. C. (2008). *Evaluation of Confidence Intervals in Well Test Interpretation Results*. Paper presented at the Europec/EAGE Conference and Exhibition, Rome, Italy.

Bateman, R. M. (1986). Openhole log analysis and formation evaluation.

Bourdet. (2002). *Well Test Analaysis the Use of Advanced Interpretation Models* (Vol. 3): Elsevier Science.

Bourdet, D., Whittle, T., Douglas, A., & Pirard, Y. (1983). A new set of type curves simplifies well test analysis. *World Oil, 196*(6), 95-106.

Brons, F., & Marting, V. (1961). The effect of restricted fluid entry on well productivity. *Journal of Petroleum Technology, 13*(2), 172-174.

Cioppa, T. M., & Lucas, T. W. (2007). Efficient nearly orthogonal and space-filling Latin hypercubes. *Technometrics, 49*(1).

Danesh, A. (1998). *PVT and phase behaviour of petroleum reservoir fluids* (Vol. 47): Elsevier.

Earlougher, R. C. (1977). *Advances in well test analysis*: Henry L. Doherty Memorial Fund of AIME New York.

El-Hawary, A. M., Mahgoub, I. S., & Sayyouh, M. H. (1999). *Improving Transient Testing Results Using Data Management*. Paper presented at the Middle East Oil Show and Conference, Bahrain.

Gringarten, A., Burgess, T., Viturat, D., Pelissier, J., & Aubry, M. (1981). *Evaluating fissured formation geometry from well test data: a field example.* Paper presented at the SPE Annual Technical Conference and Exhibition.

Gringarten, A. C. (2008). From Straight Lines to Deconvolution: The Evolution of the State of the Art in Well Test Analysis. *SPE Reservoir Evaluation & Engineering, 11*(1), pp. 41-62. doi: 10.2118/102079-pa

Hall, H. (1953). Compressibility of reservoir rocks. *Journal of Petroleum Technology, 5*(1), 17-19.

Horne, R. N. (1994). *Uncertainty in Well Test Interpretation*. Paper presented at the University of Tulsa Centennial Petroleum Engineering Symposium, Tulsa, Oklahoma.

Horner, D. (1951). *Pressure build-up in wells.* Paper presented at the 3rd World Petroleum Congress.

Houze, O., Viturat, D., & Fjaere, S. O. (2011). Dynamic Data Analaysis. In KAPPAENG (Ed.), *The Theory and Practice of Pressure Transient and Production Analysis, Well Performance Analysis, Production Logging and The Use of data from Permanent Downhole Gauges.*

Institute, S. (2008). *Jmp 8 Statistics and Graphics Guide*: SAS Institute.

Khasanov, M., Khabibullin, R., & Krasnov, V. (2004). *Interactive Visualization of Uncertainty in Well Test Interpretation*. Paper presented at the SPE Asia Pacific Oil and Gas Conference and Exhibition, Perth, Australia.

Larsen, L. (1983). *Limitations on the use of single-and multiple-rate Horner, Miller-Dyes-Hutchinson, and Matthews-Brons-Hazebroek analysis.* Paper presented at the SPE Annual Technical Conference and Exhibition.

Lee, A., González, M., & Eakin, B. (1966). The viscosity of natural gases. *Journal of Petroleum Technology, 18*(8), 997-1000.

Lee, J., Rollins, J. B., & Spivey, J. P. (2003). *Pressure transient testing*: Richardson, Tex.: Henry L. Doherty Memorial Fund of AIME, Society of Petroleum Engineers.

Lee, W. J. (1982). *Well testing*: Society of petroleum engineers of AIME Dallas TX.

Mahgoub, S. S. E., Daoud, A. M., & El-Tayeb, E.-S. A. M. (2008). *Development of Water Saturation Error Analysis Charts for Different Shaly Sand Models for Uncertainty Quantification of Volumetric In-Place Estimate*. Paper presented at the SPE Russian Oil and Gas Technical Conference and Exhibition, Moscow, Russia.

Matthews, C. S., & Russell, D. G. (1967). *Pressure buildup and flow tests in wells* (Vol. 1): Society of petroleum engineers of AIME Dallas, TX.

McCain Jr., W. D. (1991). Reservoir-Fluid Property Correlations-State of the Art (includes associated papers 23583 and 23594). *SPE Reservoir Engineering, 6*(2), 266-272. doi: 10.2118/18571-pa

McCain, W. (1990). *The properties of petroleum fluids*: PennWell Books.

McCain, W. D., Voneiff, G. W., Hunt, E. R., & Semmelbeck, M. E. (1993). *A Tight Gas Field Study: Carthage (Cotton Valley) Field*. Paper presented at the SPE Gas Technology Symposium, Calgary, Alberta, Canada.

McCoy, D. D., Jr., H. R. W., & Fisher, T. E. (1997). Water-Salinity Variations in the Ivishak and Sag River Reservoirs at Prudhoe Bay. *SPE Reservoir Engineering, 12*(1), 37-44. doi: 10.2118/28577-pa

McKay, M., Beckman, R., & Conover, W. (1979). A comparison of three methods for selecting values of input variables in the analysis of output from a computer code. *Technometrics, 42*(1), 55-61.

Miller, C. C., Dyes, A. B., & Jr., C. A. H. (1950). *The Estimation of Permeability and Reservoir Pressure From Bottom Hole Pressure Build-Up Characteristics*.

Newman, G. H. (1973). Pore-Volume Compressibility of Consolidated, Friable, and Unconsolidated Reservoir Rocks Under Hydrostatic Loading. *Journal of Petroleum Technology, 25*(2), 129-134. doi: 10.2118/3835-pa

Osif, T. (1988). The effects of salt, gas, temperature, and pressure on the compressibility of water. *SPE Reservoir Engineering, 3*(1), 175-181.

Pickett, G. (1966). A review of current techniques for determination of water saturation from logs. *Journal of Petroleum Technology, 18*(11), 1425-1433.

Piper, L., WD, M., & Corredor, J. (1993). *Compressibility Factors for Naturally Occurring Petroleum Gases (1993 version).* Paper presented at the SPE Annual Technical Conference and Exhibition.

Ramey Jr, H. (1970). Short-time well test data interpretation in the presence of skin effect and wellbore storage. *J. Pet. Tech, 22*, 97-104.

Rosepiler, M. J. (1982). *Calculation and Significance of Water Saturations In Low Porosity Shaly Gas Sands.* Paper presented at the SPE Cotton Valley Symposium, Tyler, Texas.

Ryan, T. P. (2008). *Modern regression methods* (Vol. 655): Wiley-Interscience.

Santner, T. J., Williams, B. J., & Notz, W. I. (2003). *The design and analysis of computer experiments*: Springer Verlag.

Siemek, J., & Nagy, S. (2004). Estimation of uncertainles in gas--condensate systems reserves by Monte Carlo simulation. *Acta Montanistica Slovaca, 9*(3), 289-293.

Siomina, I., & Ahlinder, S. (2008). Lean optimization using supersaturated experimental design. *Applied numerical mathematics, 58*(1), 1-15.

Spivey, J. P., & Pursell, D. A. (1998). *Errors in Input Data and the Effect on Well-Test Interpretation Results*. Paper presented at the SPE Permian Basin Oil and Gas Recovery Conference, Midland, Texas.

Standing, M. B., & Katz, D. L. (1942). *Density of Natural Gases*.

Stoin, E., & Sullivan, J. T. (1965). *Theorical Calculation And Emprical Evaluation of the Specific Gravity of Seperator Gas*.

Van Everdingen, A., & Hurst, W. (1949). The application of the Laplace transformation to flow problems in reservoirs. *Journal of Petroleum Technology, 1*(12), 305-324.

von Schroeter, T., Hollaender, F., & Gringarten, A. C. (2004). Deconvolution of well-test data as a nonlinear total least-squares problem. *SPE journal, 9*(4), 375-390.

Waxman, M. H., & Smits, L. J. M. (1968). 1863-A-Electrical Conductivities in Oil-Bearing Shaly Sands. *Old SPE Journal, 8*(2), 107-122.

Waxman, M. H., & Thomas, E. C. (1974). Electrical conductivities in shaly sands-I. The relation between hydrocarbon saturation and resistivity index; II. The temperature coefficient of electrical conductivity. *Journal of Petroleum Technology, 26*(2), 213-225.

Wyss, G. D., & Jorgensen, K. H. (1998). A user's guide to LHS: Sandia's Latin hypercube sampling software. *SAND98-0210, Sandia National Laboratories, Albuquerque, NM*.

Zabalza-Mezghani, I., Manceau, E., Feraille, M., & Jourdan, A. (2004). Uncertainty management: From geological scenarios to production scheme optimization. *Journal of Petroleum Science and Engineering, 44*(1), 11-25.

Zahoor, M. K., & Khan, A. (2012). Impact of Uncertainties in Formation Thickness on Parameters Estimated from Well Testing Part 1: Gas Reservoirs. *Life Science Journal, 9*(4).

APPENDIX A

DISTRIBUTION OF INPUT VARIABLES

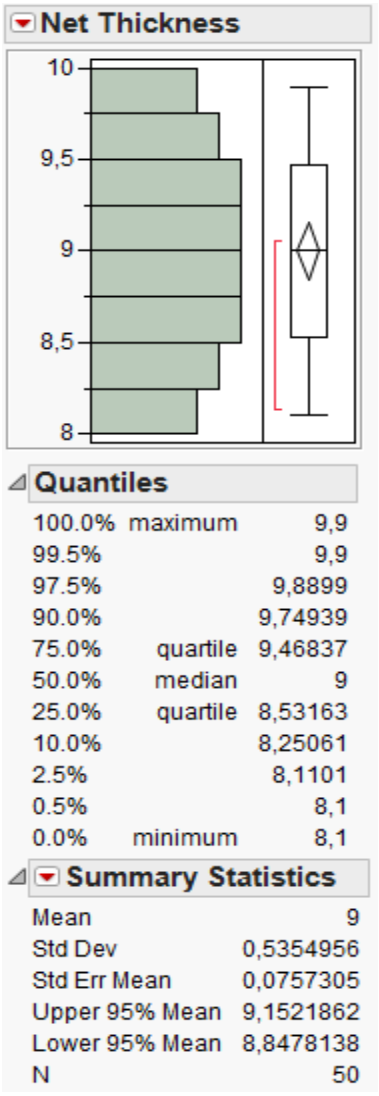

Figure A. 1 Net Thickness Distribution

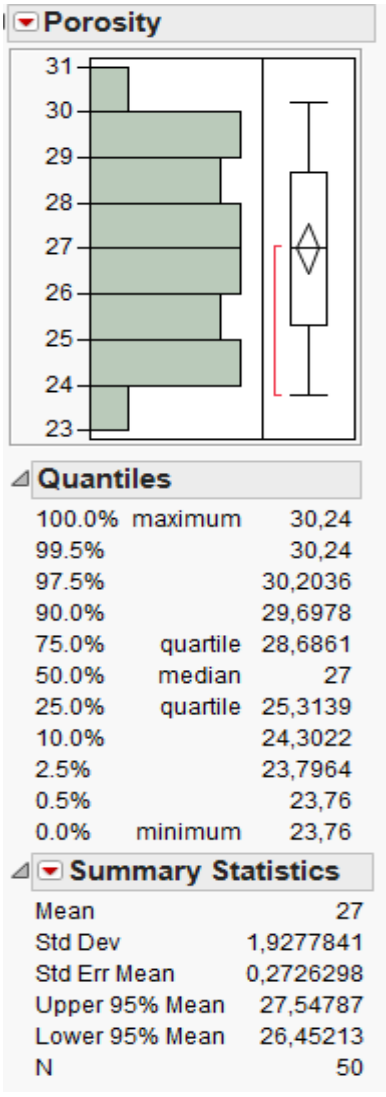

Figure A. 2 Porosity Distribution

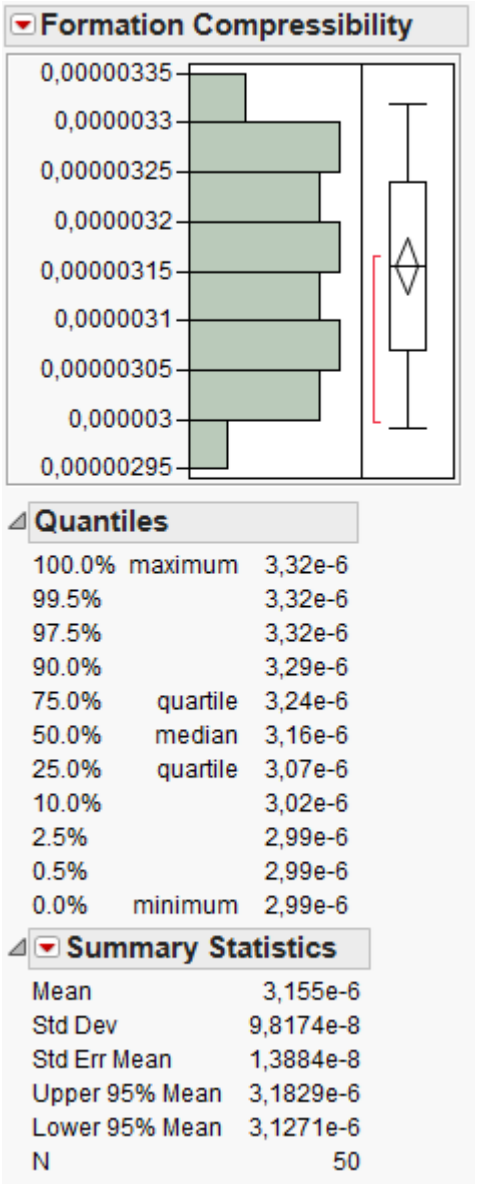

Figure A. 3 Formation Compressibility Distribution

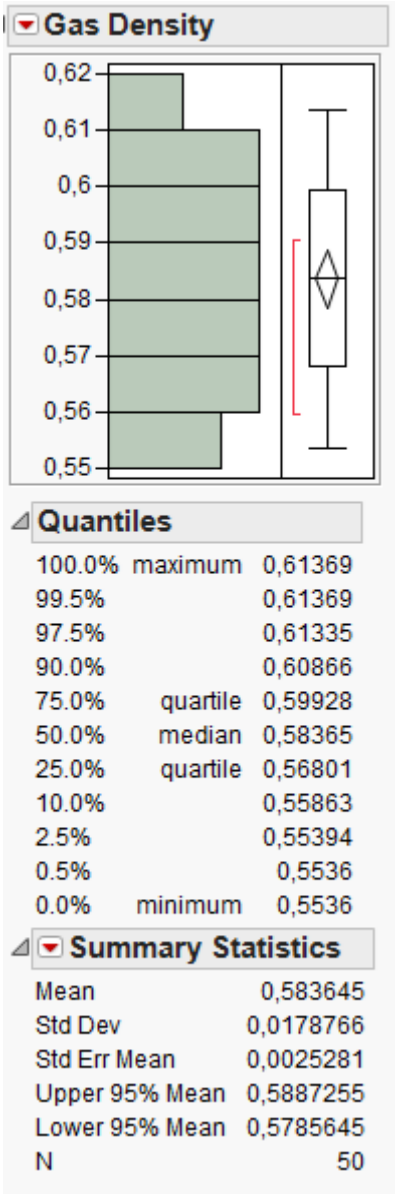

Figure A. 4 Gas Density Distribution

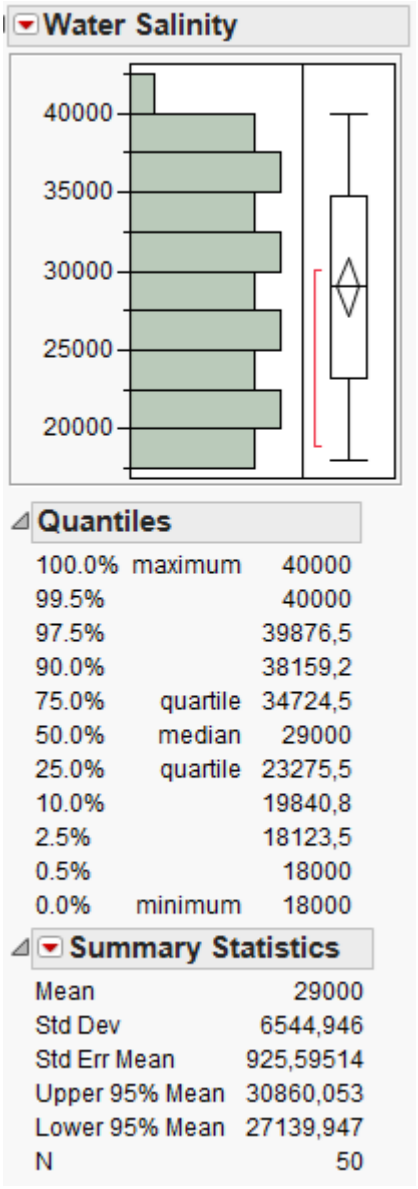

Figure A. 5 Water Salinity Distribution

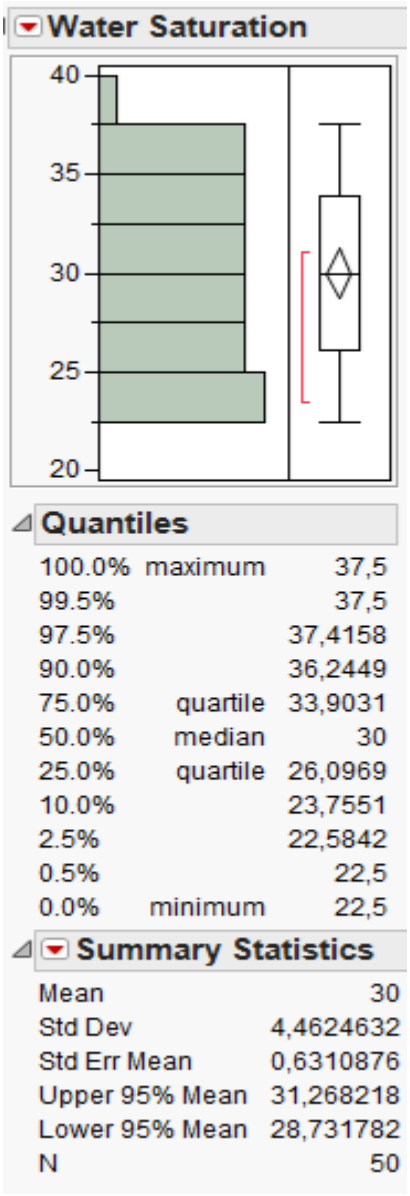

Figure A. 6 Water Saturation Distribution

APPENDIX B

PROJECTED DISTRIBUTION OF DESIGN POINTS

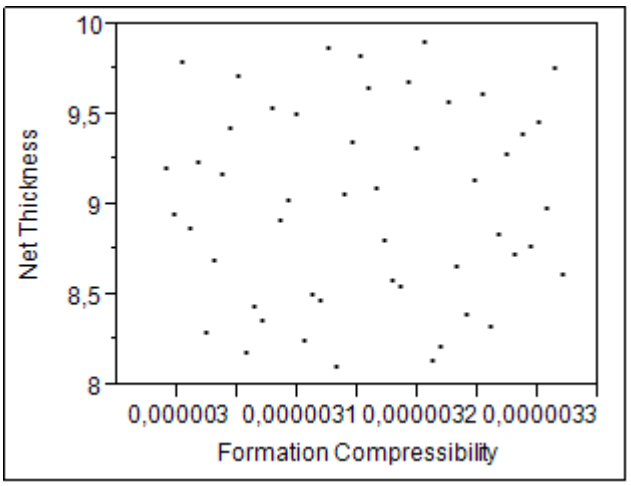

Figure B. 1 Net Thickness vs. Formation Compressibility

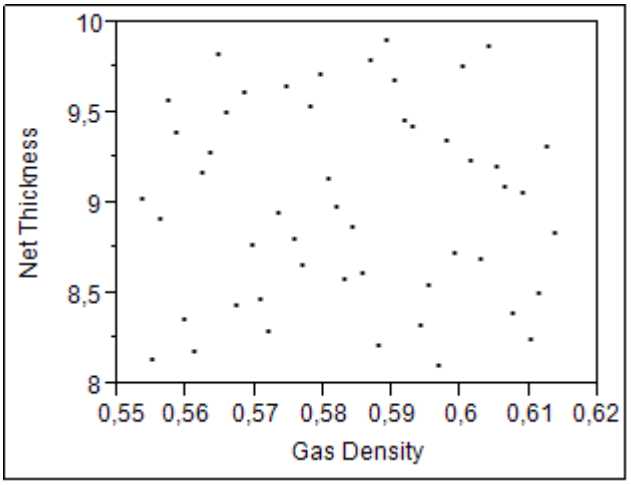

Figure B. 2 Net Thickness vs. Gas Density

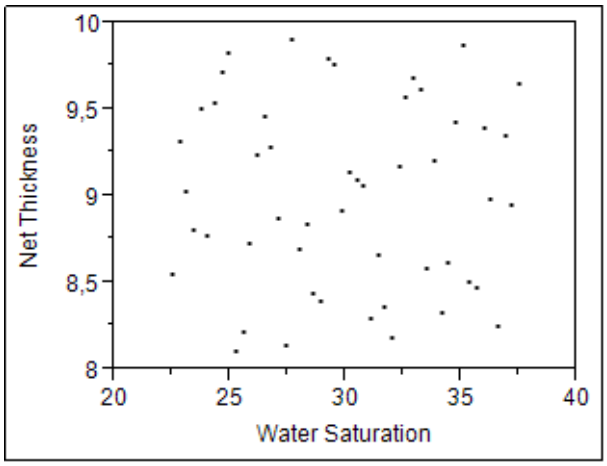

Figure B. 3 Net Thickness vs. Water Saturation

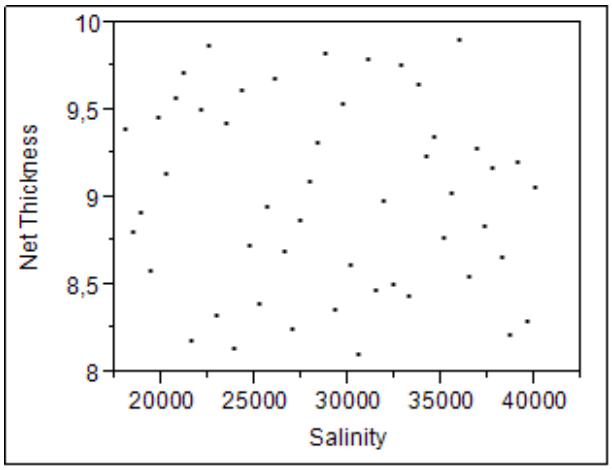

Figure B. 4 Net Thickness vs. Salinity

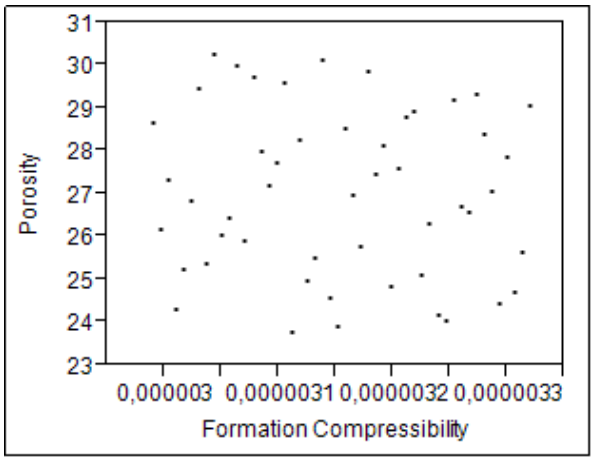

Figure B. 5 Porosity vs. Formation Compressibility

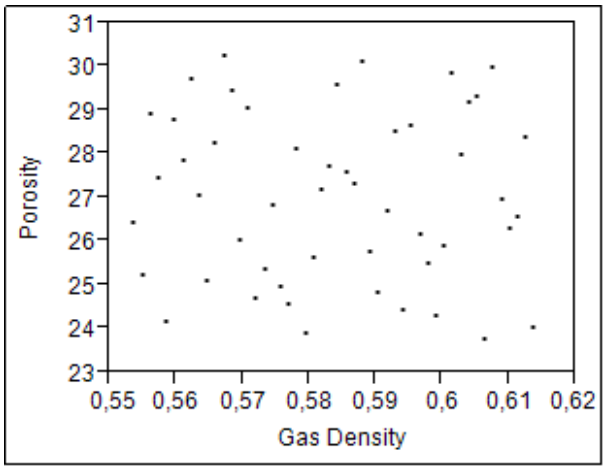

Figure B. 6 Porosity vs. Gas Density

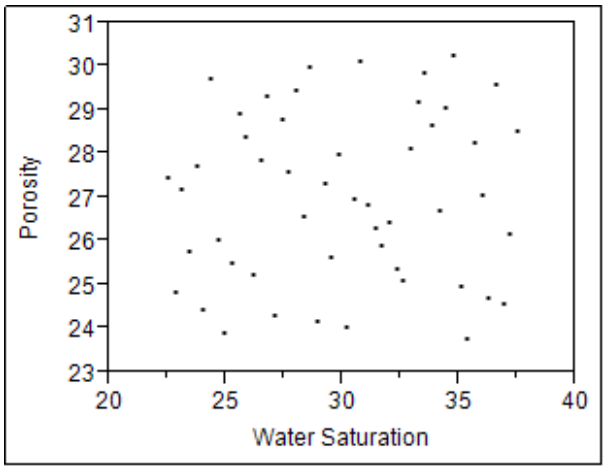

Figure B. 7 Porosity vs. Water Saturation

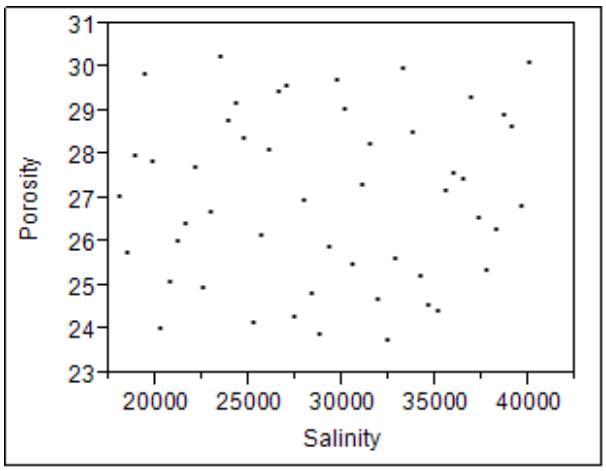

Figure B. 8 Porosity vs. Salinity

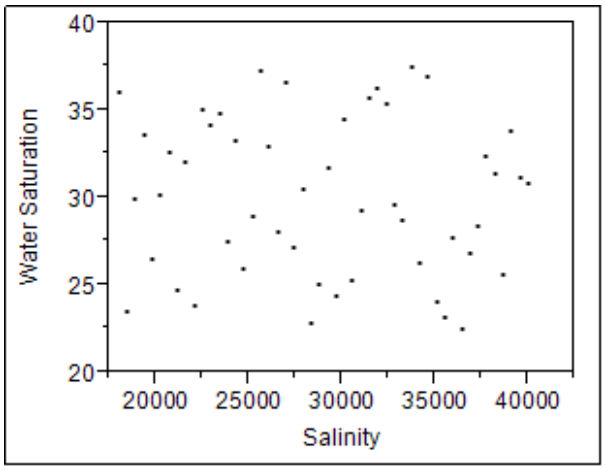

Figure B. 9 Water Saturation vs. Salinity

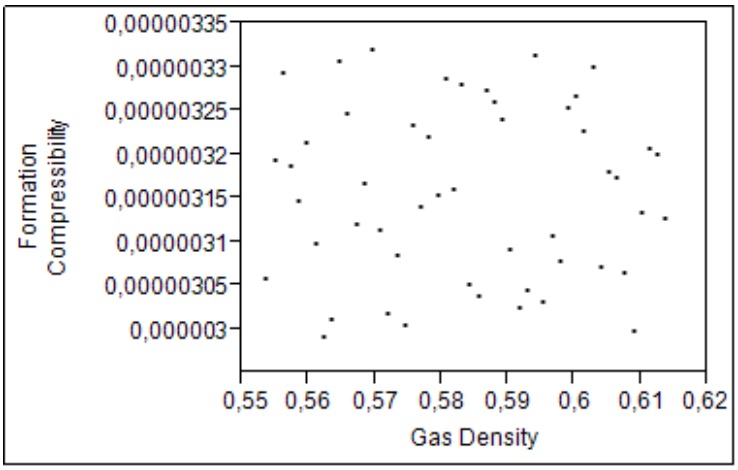

Figure B. 10 Formation Compressibility vs. Gas Density

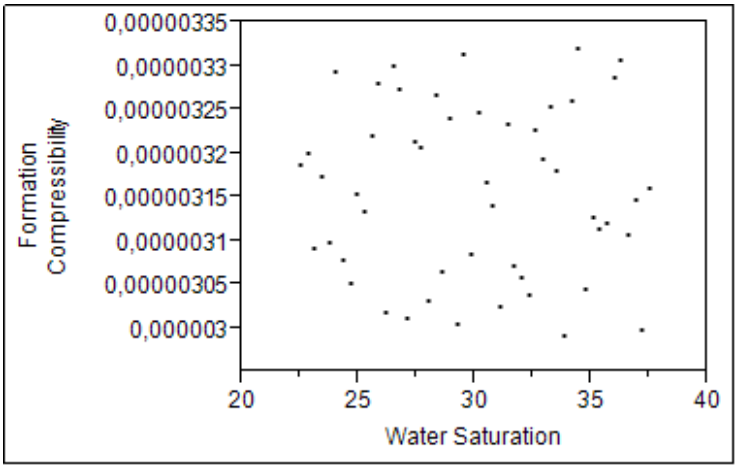

Figure B. 11 Formation Compressibility vs. Water Saturation

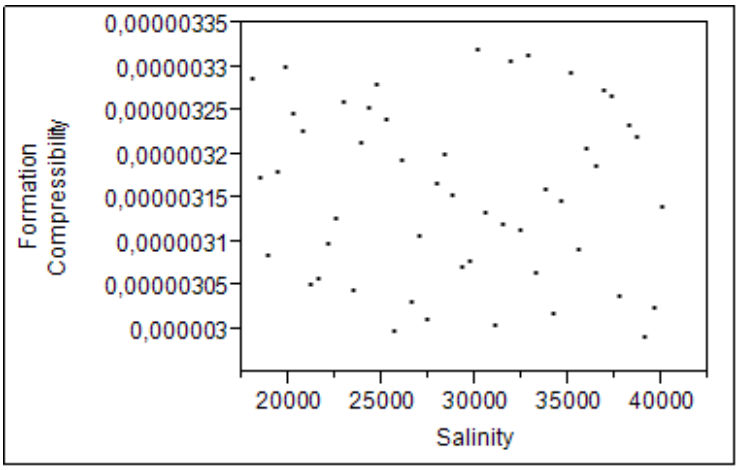

Figure B. 12 Formation Compressibility vs. Salinity

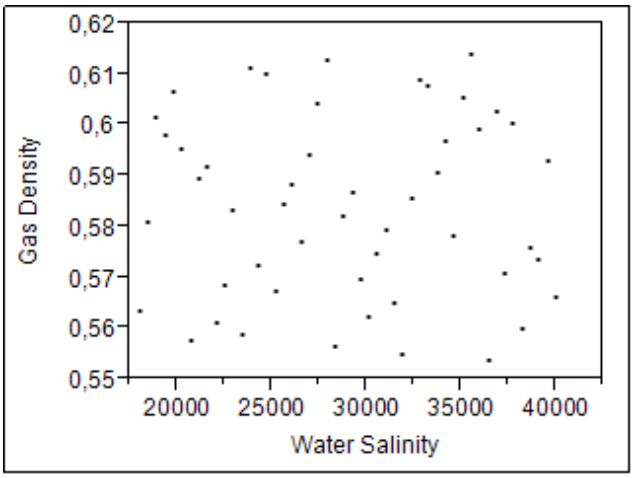

Figure B. 13 Gas Density vs. Water Salinity

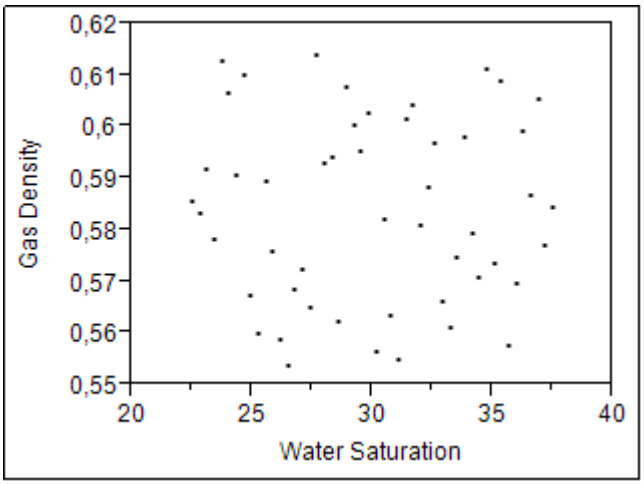

Figure B. 14 Gas Density vs. Water Saturation

APPENDIX-C

SPACE FILLING LATIN HYPERCUBE DESIGN

Table C. 1 Space Filling Latin Hypercube Design Points

Run No:	Net Thickness (m)	Porosity (%)	Formation Compressibility (1/psi)	Gas Density	Water Salinity (ppm)	Water Saturation (%)
1	8.21	30.11	3.26E-06	0.588	26082	32.30
2	9.68	24.82	3.09E-06	0.590	33714	24.34
3	9.42	28.52	3.04E-06	0.593	39551	28.01
4	8.47	29.05	3.11E-06	0.571	37306	34.44
5	8.91	28.92	3.29E-06	0.556	28327	30.15
6	9.13	25.61	3.29E-06	0.581	18449	31.99
7	8.76	26.01	3.32E-06	0.570	29673	35.97
8	9.50	28.26	3.25E-06	0.566	40000	32.91
9	8.32	24.42	3.31E-06	0.594	26980	28.32
10	8.25	26.27	3.13E-06	0.610	24735	24.64
11	8.98	27.20	3.16E-06	0.582	28776	30.46
12	9.46	26.67	3.02E-06	0.592	21592	23.11
13	9.39	24.16	3.14E-06	0.559	23388	26.17
14	8.50	26.54	3.21E-06	0.611	23837	34.74
15	8.69	27.99	3.30E-06	0.603	36857	29.85
16	8.54	28.65	3.03E-06	0.595	20245	29.54
17	9.75	25.88	3.27E-06	0.600	37755	29.23
18	8.39	29.98	3.06E-06	0.608	33265	28.93
19	8.94	25.35	3.08E-06	0.573	39102	35.05
20	8.61	27.60	3.04E-06	0.585	32367	22.50
21	9.20	29.31	3.18E-06	0.605	35061	36.89
22	9.53	28.12	3.22E-06	0.578	34612	23.42
23	9.31	28.39	3.20E-06	0.612	27878	23.72
24	9.02	26.40	3.06E-06	0.554	36408	26.48
25	8.14	25.21	3.19E-06	0.555	31918	31.07
26	9.06	26.93	3.00E-06	0.609	32816	35.36
27	8.87	29.58	3.05E-06	0.584	25633	37.50
28	9.79	27.33	3.27E-06	0.587	29224	36.58
29	8.80	24.95	3.23E-06	0.576	38653	25.87
30	9.83	25.08	3.31E-06	0.565	31469	27.40
31	9.24	29.84	3.23E-06	0.601	18898	31.38
32	9.35	25.48	3.08E-06	0.598	19347	33.83
33	8.65	24.55	3.14E-06	0.577	26531	37.19
34	9.57	27.46	3.19E-06	0.557	20694	35.66

Table C. 1 Space Filling Latin Hypercube Design Points (Continued)

35	8.36	28.79	3.21E-06	0.560	38204	25.26
36	8.43	30.24	3.12E-06	0.567	25184	24.95
37	8.83	24.02	3.12E-06	0.614	35510	27.70
38	9.61	29.45	3.17E-06	0.568	22490	26.79
39	9.64	26.80	3.00E-06	0.574	30571	33.52
40	8.72	24.29	3.25E-06	0.599	35959	36.28
41	9.90	25.74	3.24E-06	0.589	21143	25.56
42	8.17	27.86	3.10E-06	0.561	22041	33.21
43	8.10	26.14	3.10E-06	0.597	34163	32.60
44	8.28	24.69	3.02E-06	0.572	24286	27.09
45	8.58	27.73	3.28E-06	0.583	22939	22.81
46	9.86	29.18	3.07E-06	0.604	27429	31.68
47	9.28	27.07	3.01E-06	0.563	18000	30.77
48	9.72	23.89	3.15E-06	0.579	31020	34.13
49	9.17	29.71	2.99E-06	0.562	30122	28.62
50	9.09	23.76	3.17E-06	0.606	19796	24.03